STABILIZING POWER OSCILLATION WITH THE NEW PHASE MODULATION METHOD FOR SYNTHETIC LOADING OF INDUCTION MOTORS

STABILIZING POWER OSCILLATION WITH THE NEW PHASE MODULATION METHOD FOR SYNTHETIC LOADING OF INDUCTION MOTORS

By
MANY PEUNG, B. ENG. AND MGMT.

A Thesis
Submitted to the School of Graduate Studies
In Fulfillment of the Requirements
For the Degree
Master of Applied Science

McMASTER UNIVERSITY
December 2006

MASTER OF APPLIED SCIENCE (2006) McMaster University

(Electrical and Computer Engineering) Hamilton, Ontario

TITLE: Stabilizing Power Oscillation with the New Phase Modulation Method for Synthetic Loading of Induction Motors

AUTHOR: Many Peung, B. Eng. and Mgmt.

SUPERVISOR: Professor Dr. Barna Szabados

NUMBER OF PAGES: x, 104

SCOPE OF CONTENTS: Simulation of the machine system was developed, and experiments were designed and conducted in order to determine the viability of different techniques for suppressing power oscillation in the new phase modulation method for synthetic loading of induction motors. Results were used in case studies performed to identify the machine parameters responsible for causing power imbalance in the machine system.

ABSTRACT

Conventional method for testing the total power loss and internal temperature rise of induction motors under full load can often be a complex and costly process. The new phase modulation method for synthetic full-load testing of induction machines has been proven viable, provided the power oscillation in this method can be minimized. This thesis explores two techniques for stabilizing power fluctuation in the new method, and determines the test system's power sensitivities to parameter changes in the equivalent circuit of the induction motors under test.

A computer simulation representing the test system used in the new phase modulation method was developed, and an experimental testing facility was built to test the technique devised for suppressing power oscillation in the test system.

The results from simulations are analyzed and compared to those obtained from the actual experiments in order to identify the feasible power-suppressing technique, and determine the induction machine parameters responsible for causing power unbalance in the test system.

ACKNOWLEDGEMENTS

I would like to express my gratitude to my supervisor, Dr. Barna Szabados for being so kind and patient in his guidance and support throughout my entire thesis work at McMaster University. It has been my honor and privilege to do graduate study under his supervision, and I have learned a lot from him.

To Cheryl Gies, thank you for your help with the administrative aspects of my work. I would also like to thank Adam Marianski for his help with the technical challenges encountered during this thesis and his share of pertinent technical knowledge. To Steve Spencer and Stan Zolinski, thanks for solving all my computer related problems. To Christophe del Perugia, thank you for all the good advices you gave me. I really enjoyed working beside you in the lab.

I would like to thank my parents and sister for their unconditional love and support in keeping me focused at my work. Last but not least, I would like to thank my dear wife Linda for her endless love, patience and understanding during the time I was finishing this thesis work.

TABLE OF CONTENTS

TABLE OF FIGURES

Chapter 1

INTRODUCTION

1.1 Background

Heat run tests performed on electric machines to determine the total loss of energy dissipated as heat are extremely important to both manufacturers and users. It is a well-known fact that the operating temperature of an electric machine has a very strong relationship with the life duration of the insulation. This dependence represents one of the most important aspects in the design process, as well as in the operation of the machine. The insulating materials mostly used for coating the machine's windings are organic in nature, and are adversely affected by thermal aging. This is a chemical process, which strongly depends on time and temperature, ultimately leading to loss of mechanical durability and dielectric strength [1]. A very simple empirical rule [2], which illustrates the dependence of organic insulation materials on temperature, states that for each additional 8° to 10° in temperature, the life of the insulating is reduced by 50%. Such considerations have forced introduction of maximum allowable operating temperatures for electric machine insulation, specified by different regulatory bodies, such as ANSI, IEEE and NEMA [3].

The assessment of temperature rise of an induction machine under full load condition is of major importance for the reliability characteristics of the machine. It also represents valuable information for both the manufacturer and the user [1]. The manufacturer is interested in using the assessment results to verify the predictive performance calculation methods used so that business risks can be minimized during the tendering process, while the user needs the results to be convinced that at full load the machine does not exceed the temperature insulation class limit. This would negatively impact the lifetime of the machine and ultimately cause large, unexpected expenses.

Established business patterns have demonstrated that the number of motors produced decreases as the machine power output increases, and that the provision of motor test plant follows the opposite trend [4]. Direct methods, where the machine is tested under rated load for a period of time until all temperatures are stabilized and then

the winding temperature is measured, suffer from high costs due to complex coupling and loading mechanisms, as well as the sophisticated sensor and measurement instrumentation required. In many cases, a load of sufficient size may be unavailable. Large vertical machines are often quite impossible to test by applying a load to the shaft. Indirect methods suffer from large inaccuracies and mainly cause unacceptable power swings on the power system [5].

For the reasons mentioned above, there is obviously a need for alternative methods to produce full-load heat runs economically and as accurately as possible. A number of proposals have been advanced [6]-[8], [4] for synthetic loading methods which attempt to produce accurate performance verification of induction machines without having to attach mechanical loads to the shaft, and yet the windings have to carry such heavy currents at rated voltage that the normal operating temperature is reached. The two-frequency method [6] is one of the most important among synthetic loading methods for testing three-phase induction machines. It has major advantages over the other methods. It is applicable to both wound rotor and squirrel-cage machines as opposed to Romeira's method [7] which works only with wound rotor machines. Furthermore, it does not require that all six leads of the motor be brought out as in Fong's method [8]. However, further examination of the method in a recent work [1] has established that it did not lead to good results because of the very high fluctuations of stator voltage applied and; therefore, the degree of acceptance of the two-frequency method is questionable. Moreover, a geared generator and a multiphase transformer are usually required, both rated at the test machine rating, and the full rated power oscillates at a low frequency into the power system. The investigation of three synthetic loading methods at full-load temperature evaluation using calorimetric methods has also demonstrated the major drawbacks of the two-frequency method, where results have been compared with the conventional direct loading method [9]. Unfortunately, these results are limited to low capacity induction motors due to the power swing in the power system [5].

Up to this point, the most viable method proposed is the new phase modulation method for full-load testing of large induction machines. The assumption made is that motor manufacturers prefer to build rotating machines used for the test rig rather than buying special purpose large transformers. The method is based on an "inverter-

controlled" phase modulation technique to produce a variable frequency voltage generated by a synchronous generator. The use of two systems in parallel, one system with the test motor and one system with a "recovery" unit, limits the power swing with the power system to the total losses of the five machines used [5].

Simulation results from the new phase modulation method above have shown that if the power exchange between the two systems is in exact opposition of phase, the power flow through the driver motor would be constant. Unfortunately, experimental results have shown otherwise. Although the power generated by one system exactly matches the opposing power absorbed by the other, there are still some degrees of power oscillation in the driver motor. When the power oscillates, there is a power exchange between the utility supply and the test rig. This is not desirable when large induction machines are being tested with the new phase modulation method, as the amount of power swing can become significant and cause considerable disturbance to other loads on the power supply system, and certainly would not be acceptable to the energy provider.

1.2 Objectives

In order to study the problem of power ripple in the driver motor, the first objective of this research is to construct a mathematical model that can closely represent a test system of five interconnected machines as described in [5]. Since each machine can be represented by a set of differential equations, the model is created by integrating five sets of equations and simulated on the computer using Matlab as the main simulation tool. Without a reliable model, it would be very difficult to determine the causes of power oscillation and what machine parameters can be used to help controlling it.

In the latest study on the new phase modulation method proposed [5], two suggestions were made regarding the causes of power oscillation. The first cause comes from the misalignment of the electrical axes between the two generators due to physical constraints on the keyed mechanical coupler which connects the two shafts of the machines together. This constraint prevents a perfect shaft alignment and only allows the shafts to be aligned with each other at no better than about 15°. Thus, the second objective is to find out whether the oscillation can be minimized when mechanical shaft misalignment is electrically corrected by introducing a phase difference between the

controlled excitation voltages of the two generators. Such method is also known as phase-shift correction. The second cause for the power ripple may come from the phase modulation itself. While it is possible to apply the phase opposition voltages to the field windings of the generators, it is difficult to guarantee that both time constants are identical. As a result, although the two excitation currents are in exact opposition of phase, they may not establish their final values symmetrically. Therefore, the third objective is to uncover the culprits behind the asymmetry and unequal time constants between the two excitation currents, and what controlling parameters are suitable for minimizing the power oscillation.

1.3 Thesis Structure

This thesis comprises six chapters. Chapter two explains the general principle of synthetic loading, elaborates on major drawbacks of the two-frequency method, describes how the new phase modulation method can be used, and provides details on how to implement it in practice. Chapter three presents mathematical models of the test system used in the new phase modulation method. Here, the first objective in section 1.2 is met with all the state equations derived for stator and rotor currents so that a computer model of the test system can be developed in order to study the problem of power ripple in the driver motor. Wiring diagram for setting up the machines and equipments, description of electronic control circuits with their schematic drawings, and testing procedures for approximating parameter values in induction machines are all given in chapter four. This chapter also describes all the measurement instruments used to acquire the instantaneous values of voltages and currents in the actual experiments. Chapter five attempts to answer all the questions raised in the last two objectives by presenting the analysis of test and simulation results obtained from the phase shift correction method, and parameter sensitivity case studies. Chapter six presents conclusions, contributions made, and recommendations for future research.

Chapter 2

PRINCIPLES OF SYNTHETIC LOADING AND NEW PHASE MODULATION METHOD

2.1 Principle of Synthetic Loading

Synthetic loading of induction machines is a process in which the induction motor is tested for temperature rise and total losses without the need of attaching any mechanical load to the shaft. The process is based on modulating the frequency and magnitude of the supply voltage, with the main criterion of maintaining the rated RMS values of current and voltage computed over the modulation cycle [10].

Before explaining how the process of synthetic loading works, it is useful to briefly review the operation of an induction motor powered by a fixed-frequency supply voltage. When balanced three phase voltages are applied to the phase windings of the motor's stator, balanced currents flow in these three interconnected windings, producing a magnetic field which rotates within the air gap at the angular frequency of the supply voltage. This is known as the synchronous frequency, and the rotor inside the induction machine has a natural tendency to match its speed with the speed of the rotating magnetic field when power is applied [11]. As a result, when the supply frequency is increased as shown in Figure 2.1, the magnetic field would be rotating much faster than the rotor,

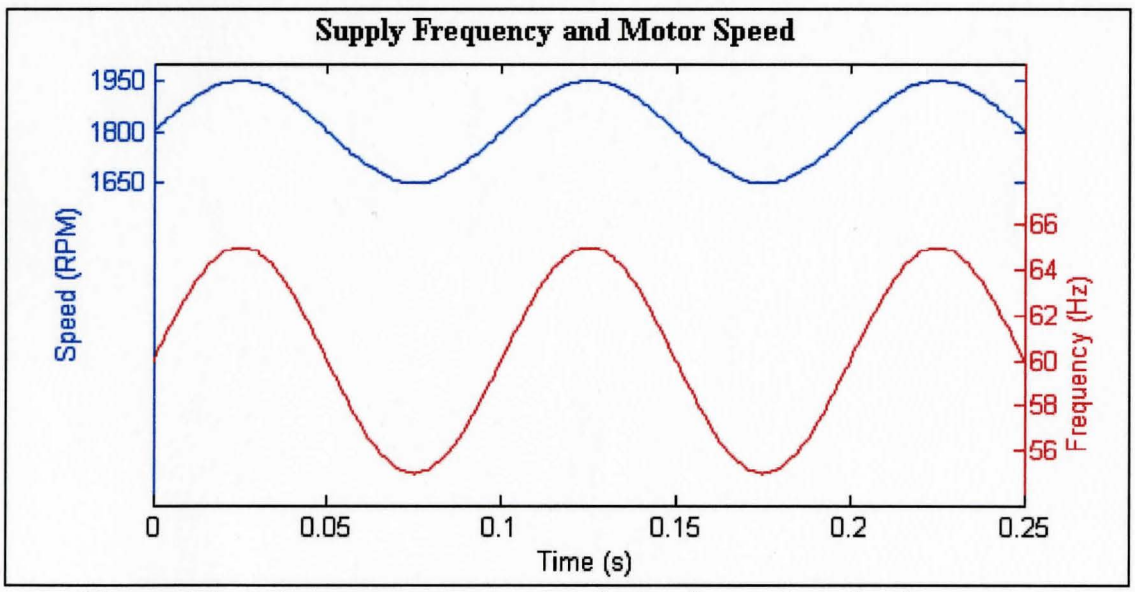

Figure 2.1: *Induction motor operation during the synthetic loading process*

causing the rotor to accelerate in order to catch up with the magnetic field. While the rotor is speeding up, the induction motor absorbs a large amount of power by drawing heavy line currents from the power supply into the stator windings. If the supply frequency is now decreased, the magnetic field would immediately respond to the frequency change by rotating slower than the rotor, forcing the rotor to decelerate to match its speed with the magnetic field. During this time, the excess kinetic energy stored in the rotor is transferred back to the power supply, and the induction motor is in effect acting as generator, with heavy line currents drawn out of the stator windings. Since heat is dissipated in both cases of frequency change, the same amount of temperature rise can be produced as in the direct loading process, provided the criterion for synthetic loading is met.

One of the methods developed for synthetic loading uses two power supplies, with different frequencies and magnitudes, connected in series to produce a supply voltage with variable frequency and magnitude [6]. Such method is widely known as the two-frequency method. On the complex plane representation shown in Figure 2.2(a), the supply voltage V_S is a phasor sum of the two power sources V_1 and V_2. Because these

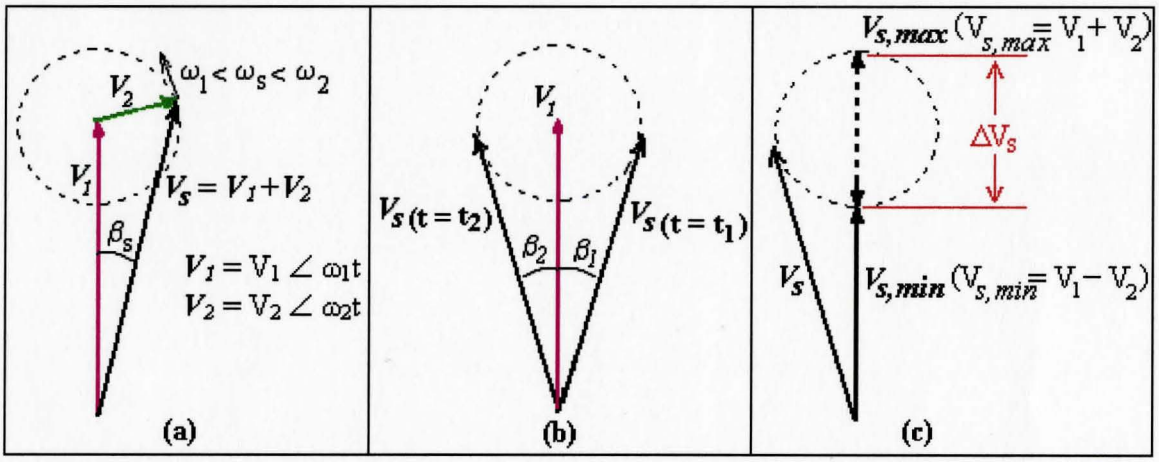

Figure 2.2: *Phasor diagram for the two-frequency method*

two power phasors have different frequencies, the phasor V_2 rotates around the extremity of V_1 at a rate of ω_1 - ω_2, and the magnitude of V_S varies along the dashed circle with an angular speed changing between ω_1 and ω_2. As V_2 rotates around the tip of V_1, the phase angle for V_S varies between β_1 and β_2 as illustrated in Figure 2.2(b), where the phasor diagram shows the superposition of the phasor V_S at different time stamps associated with each phase angle. The drawback of the two-frequency method is pointed out in

Figure 2.2(c) by illustrating another superposition of the phasor V_S with each time stamp corresponding to the phasor's magnitude. In order to have a proper frequency modulation in the two-frequency method, the phasor V_2 should be about 40% of V_1. This means that the supply voltage V_S for the induction motor will fluctuates between 140% and 60% of rated value [5]. Such a large range of voltage fluctuation drives the machine into saturation and undervoltage, introducing major inaccuracies in the measurement of temperature rise and power losses in the induction machine. The supply voltage fluctuation also causes a full rated power swing at the modulation frequency between the power grid and the test machine [5]. This is the reason why manufacturers are reluctant to use the two-frequency method.

2.2 The New Phase Modulation Method

In order to alleviate the apparent problem of large supply voltage fluctuation in the two-frequency method, a new method has been recently proposed, and it is known as the new phase modulation method. The principle of this method and its practical implementation will be explained as follows.

2.2.1 Principle of the New Phase Modulation Method

The principle of this method is to generate the supply voltage V_S using a three-phase synchronous generator, with one rotor field winding arranged in the direct axis, and the other one in the quadrature axis [5]. The spatial phase shift of rotor windings and the phasor diagram of the induced magnetic fluxes are shown in Figure 2.3(a). By

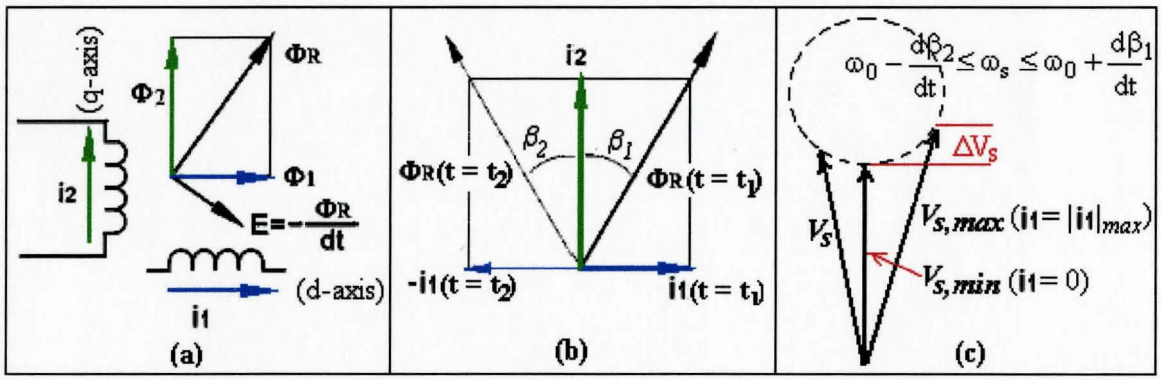

Figure 2.3: *Rotor field winding configuration and phasor diagrams for the new phase modulation method*

appropriately modulating the excitation currents $\mathbf{i_1}$ and $\mathbf{i_2}$ in the rotor windings, the resultant excitation flux $\mathbf{\Phi_R}$ can be modulated with its phase angle varying between β_1 and β_2. The phasor diagram in Figure 2.3(b) shows this phase angle variation with a superposition of $\mathbf{\Phi_R}$ at different time stamps with respect to the direction of the modulated excitation current $\mathbf{i_1}$ along the direct axis. The generator's stator voltage V_S induced by $\mathbf{\Phi_R}$ has a varying frequency and magnitude as expressed in Figure 2.3(c), where the phasor diagram shows a superposition of V_S at different instants with respect to the magnitude of the applied excitation current $\mathbf{i_1}$. This phasor diagram also shows that the magnitude fluctuation in V_S is considerably smaller than that in the two-frequency method. Therefore, the estimate of temperature rise and power losses in induction motor can be achieved with much higher accuracies in the new phase modulation method.

2.2.2 Practical Implementation

The synchronous generator in this method is created using a three-phase wound-rotor induction machine [5] with its rotor windings arrangement reconfigured as shown in Figure 2.4. Since the rotor windings in this machine have been arranged for a three-phase

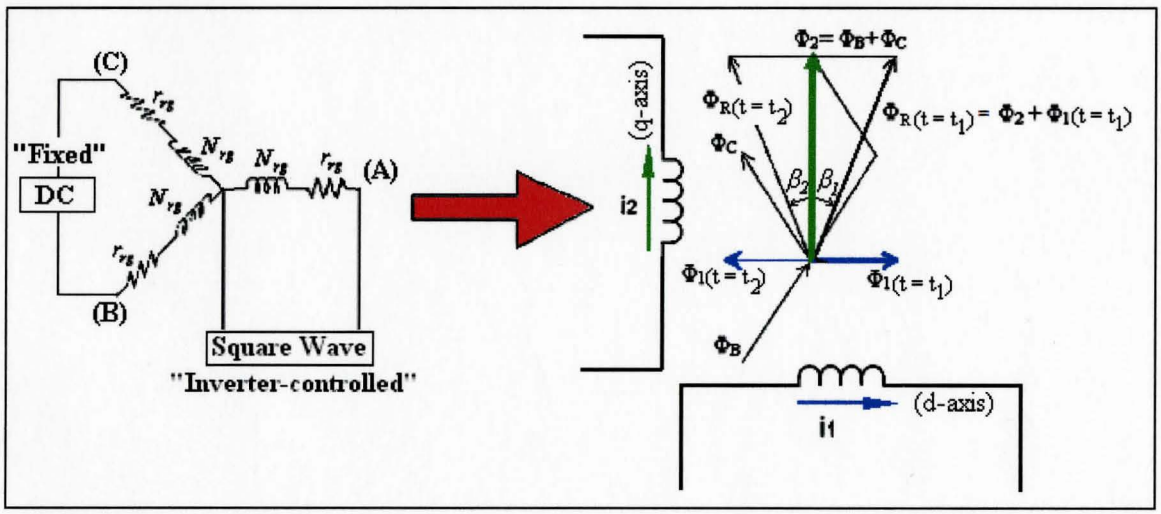

Figure 2.4: *Transforming a wound-rotor induction machine to a synchronous generator*

connection, they must be rearranged with the phase-A winding excited by an "inverter-controlled" square-wave voltage source, while windings for phases B and C are connected together line to line and excited by a fixed DC source. As indicated by the red arrow in Figure 2.4, the three-phase wound-rotor induction machine is now transformed to a synchronous generator with rotor field windings arranged in the same spatial phase

shift as in Figure 2.3(a). By the inverter switching action, the excitation current $\mathbf{i_1}$ in the phase-A winding is modulated between $\mathbf{i_1}$ and $\mathbf{-i_1}$, inducing a flux which varies between $\mathbf{\Phi_1}$ and $\mathbf{-\Phi_1}$ along the direct axis. Since the three rotor windings are identical, sinusoidally distributed windings and displaced by 120°, the flux induced in each winding is also displaced from one another by the same phase angle. Hence, if the windings for phases B and C are connected together in series and powered by a fixed DC source, the magnetic fluxes induced in windings (B) and (C) will be displaced by 120°, and the sum of these two flux components will produce a fixed flux $\mathbf{\Phi_2}$ along the quadrature axis. Because $\mathbf{\Phi_2}$ is always fixed, it is not marked with a time stamp in Figure 2.4. With $\mathbf{\Phi_1}$ induced along the direct axis and $\mathbf{\Phi_2}$ along the quadrature axis, a resultant flux $\mathbf{\Phi_R}$ is produced by adding the two fluxes together on the phasor diagram. Since $\mathbf{\Phi_1}$ is modulated by the inverter switching action, the resultant flux $\mathbf{\Phi_R}$ also changes with respect to time; as a result, both phasors are marked with different time stamps on the phasor diagram in Figure 2.4. Although a square-wave voltage is applied across the rotor winding for phase A, the excitation current $\mathbf{i_1}$ will vary exponentially due to the presence of inductance in each field winding. Thus, the resultant flux $\mathbf{\Phi_R}$ will be produced with a phase angle varying slowly between β_1 and β_2.

2.2.3 Test System Setup

In a single test rig system (Figure 2.5), where a squirrel-cage induction motor D0 is used to "drive" the synchronous generator G implemented in section 2.2.2, the

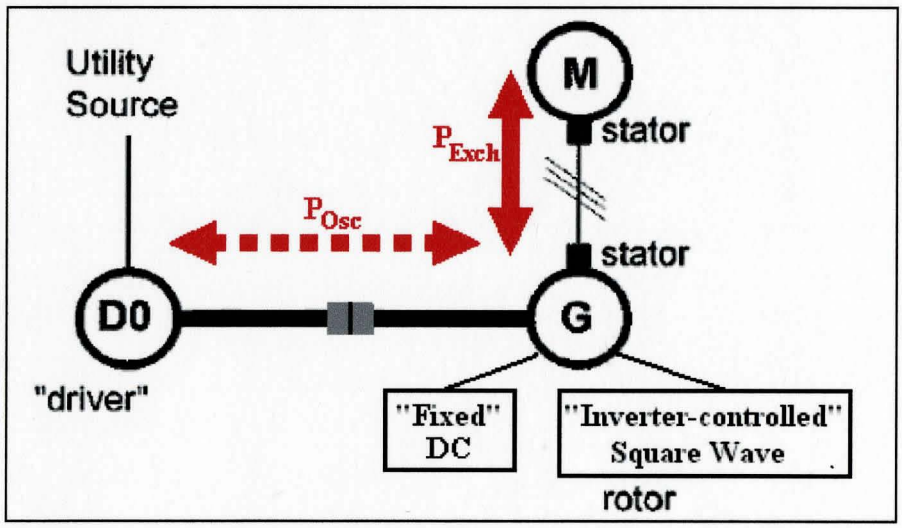

Figure 2.5: *Single test rig system*

generated supply voltage V_S would be used as an input power for the induction motor M under test. When the frequency of V_S is varied by field modulation, the rotor of machine M will accelerate and decelerate continuously, forcing it to alternately absorb power and return it to the generator G. This power exchange between G and M will be transparent to the "driver" motor D0, and will cause a full-rated power swing between the utility source and the single test rig system through D0. If the machine rating for M is large, such power oscillation would be undesirable on the power system.

For the new phase modulation method, which is the most viable method proposed for synthetic loading, two systems similar to the one described above are used. Both systems have their generators G_1 and G_2 driven by the same "driver" motor D0. All three machines are connected together shaft to shaft with mechanical keyed couplers as shown in Figure 2.6 [5]. The generator G_1 of System (1) is rated at the maximum power rating

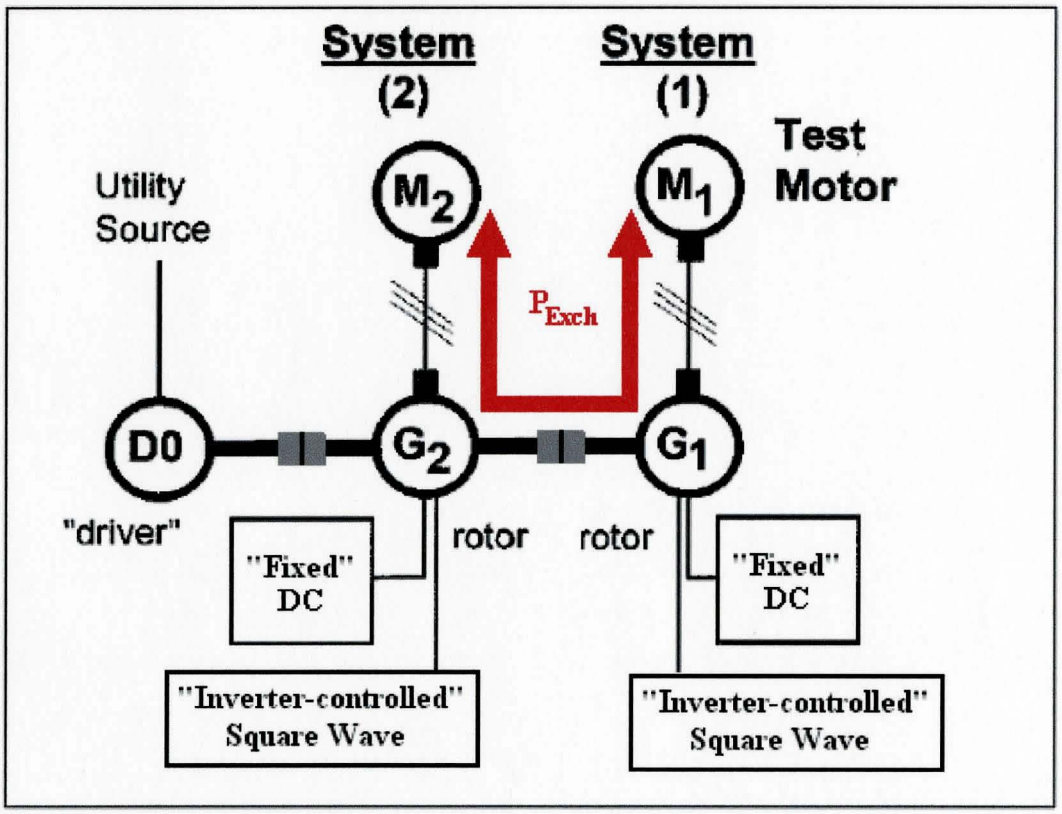

Figure 2.6: *Test setup with two systems in parallel for the new phase modulation method*

P_{max} of the test rig (highest motor rating to be tested), and feeds the motor M_1 under test. The test motor could be either a wound-rotor machine or a squirrel cage machine. Both the generator G_2 and the "recovery" machine M_2 of System (2) are also rated at P_{max}. If

the field modulation of each generator is in opposition of phase, the power generated by each system would be in opposition of phase and, therefore, when one system absorbs power, the other generates it and vice-versa. By adjusting the magnitude of the excitation current in generator G_2, one can adjust the power exchange within System (2) to exactly match the power swing of System (1). When this equilibrium is reached, the driver motor D0 will not see any power oscillation and need to provide only the net losses in all five machines [5].

2.2.4 Selecting Modulation Parameters

The two important modulation parameters to be considered for the new phase modulation method are modulation depth and modulation frequency. Modulation depth is the amount by which the frequency deviates from the rated value (60 Hz), while modulation frequency is the rate at which the frequency deviation occurs [10]. Figure 2.7 below will help clarify the meaning of each parameter.

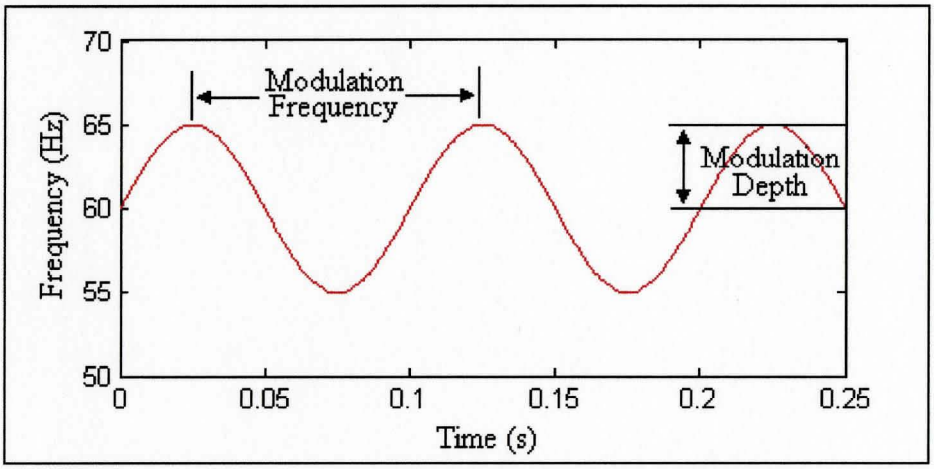

Figure 2.7: *Modulation depth and modulation frequency*

To simulate temperature rise in the machine, the distribution of losses in the motor has to be the same as in the rated-load operation, which requires two conditions [10]:

1. Rated RMS currents through the stator windings
2. Rated voltage and frequency applied to the motor

In order to satisfy the first condition above, the modulation depth and frequency need to be increased, but the range for each of these parameters is restricted by the second

condition, which ensures rated air-gap flux density. The smaller the modulation depth, the better this condition is satisfied. The modulation frequency can not take too low values because it would require a large modulation depth, which would produce large vibrations and unacceptable high stress on the machine. On the other hand, the modulation frequency can not be too high; it should be limited in order to allow the rotor to respond to the excitation in the supply. Although each particular machine has its own best parameter combination, it has been shown [1] that the optimum performance to reach rated load is achieved with a 10-Hz modulation frequency and a 5-Hz modulation depth (55 Hz to 65 Hz).

Chapter 3

MATHEMATICAL MODELING OF THE TEST SYSTEM

3.1 Introduction

As discussed in the previous chapter, the machine setup for this new phase modulation method requires a total of five induction machines, three of which may be squirrel-cage induction motors, while the remaining two are synchronous generators. Such a setup requires a careful study of how all the machines interact with each other as well as how they behave in response to certain values of input parameters so that costly damages to the machines and injuries can be avoided during the experiment. For instance, if the provided excitation voltages are too high in the field windings of a generator, the produced field currents and the induced stator voltages would exceed their rated values specified by the machine's manufacturer, and the result would be severe thermal damage to both the machine's rotor windings and stator windings. This is just one small example of what could happen if the experiment is carried out without knowing in advance the possible responses of the machines.

One way to predict the machines' responses is to simulate the experiment on a computer. This can be done by first representing each machine with a mathematical model, and then combining all these models together into a machine system to represent the actual setup of all five machines.

As described in section 2.2.3, the setup is divided into two identical systems which differ only in the phase of modulation provided to the excitation voltage in each system. Both systems share the same "driver" motor D0, which is chosen as a squirrel-cage induction motor. Each system is created by a combination of a synchronous generator G_i and a squirrel-cage induction motor M_i, with the output stator voltages of the generator feeding directly as inputs into the motor. Note that the subscript 'i' denotes system 1 or 2 in the test system. Here is a diagram showing how the driver motor D0, the generator G_i and the motor M_i are connected together in a system:

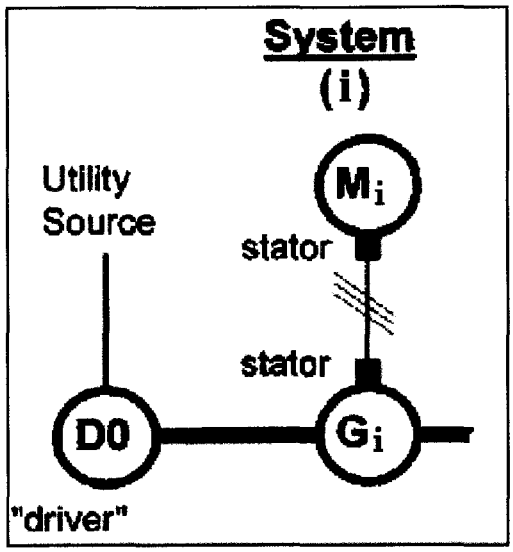

Figure 3.1: Interconnection of machines in a system

From the above figure, the driver motor D0 receives electrical power as input from the utility source and drives the generator G_i of System (i). The three-phase voltages induced in the stator windings of the generator G_i are then used to feed the motor M_i.

Obviously, the three major components required for modeling the machine setup in the new phase modulation method are the driver motor D0, the generator G_i and the motor M_i, and the two mathematical models being used to represent these three machines are the Induction Motor Model and the Synchronous Generator Model. In order to explain these two models clearly, a brief summary on reference-frame transformation needs to be presented first.

3.2 Reference-frame Transformation

The performance of an induction or a synchronous machine can be described by voltage equations in the stator and rotor windings, and the torque equation of the machine. Since some of the machine inductances, used in writing the voltage equations, are time-varying due to their dependencies on the rotor speed, a change of variables must be made in order to eliminate all the time-varying inductances [12]. This can be achieved by transforming the three-phase variables of the stator and the rotor to a frame of reference which may rotate at any angular velocity or remain stationary. All known real transformations may then be obtained by simply assigning the appropriate rotational

speed ω to this so-called *arbitrary reference frame* [12] which in stationary circuits may be expressed as:

$$\mathbf{f}_{qd0s} = \mathbf{K}_s \mathbf{f}_{abcs} \tag{3-1}$$

where $$(\mathbf{f}_{qd0s})^T = \begin{bmatrix} f_{qs} & f_{ds} & f_{0s} \end{bmatrix} \tag{3-2}$$

$$(\mathbf{f}_{abcs})^T = \begin{bmatrix} f_{as} & f_{bs} & f_{cs} \end{bmatrix} \tag{3-3}$$

$$\mathbf{K}_s = \frac{2}{3}\begin{bmatrix} \cos\theta & \cos\left(\theta - \frac{2\pi}{3}\right) & \cos\left(\theta + \frac{2\pi}{3}\right) \\ \sin\theta & \sin\left(\theta - \frac{2\pi}{3}\right) & \sin\left(\theta + \frac{2\pi}{3}\right) \\ \frac{1}{2} & \frac{1}{2} & \frac{1}{2} \end{bmatrix} \tag{3-4}$$

$$(\mathbf{K}_s)^{-1} = \begin{bmatrix} \cos\theta & \sin\theta & 1 \\ \cos\left(\theta - \frac{2\pi}{3}\right) & \sin\left(\theta - \frac{2\pi}{3}\right) & 1 \\ \cos\left(\theta + \frac{2\pi}{3}\right) & \sin\left(\theta + \frac{2\pi}{3}\right) & 1 \end{bmatrix} \tag{3-5}$$

$$\theta = \int_0 \omega(\xi) d\xi + \theta(0) \tag{3-6}$$

where ξ is a dummy variable of integration. In the above equations, f can represent either voltage, current, flux linkage, or electric charge. Note that all the matrices will henceforth be denoted by bold letters. The superscript T denotes the transpose of a matrix. The subscript "s" indicates the variables, parameters, and the transformation associated with stationary circuits, while the subscript "r", which will be seen later, represents quantities associated with rotating parts of the machine. The equations of transformation may be thought of as if the f_{qs} and f_{ds} variables are "directed" along paths orthogonal to each other and rotating at an angular velocity of ω, where upon f_{as}, f_{bs}, and f_{cs} may be considered as variables directed along stationary paths each displaced by 120°. Such trigonometric relationships between variables can be conveniently visualized as shown in Figure 3.2 on the next page. Note that f_{0s} does not appear in this visualization because the 0s variables are not associated with the arbitrary reference frame. Instead, the zero variables are related arithmetically to the *abc* variables, independent of θ and are

stationary quantities, or no torque developing quantities.

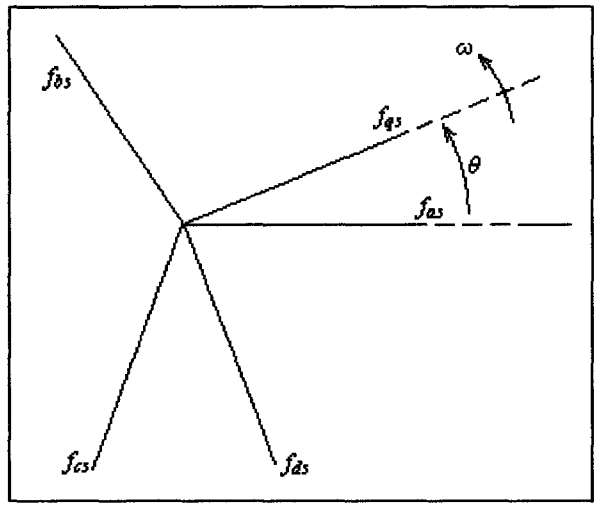

Figure 3.2: *Stationary circuit transformation by trigonometric relationships*

3.3 Mathematical Model of the Squirrel-Cage Induction Motor

The mathematical model of the squirrel-cage induction motor is developed in this section by first undergoing a mathematical derivation to establish the machine voltage and torque equations in the arbitrary reference frame. Then the final model is obtained on the basis of Park's transformation [13] by setting the motor's speed of the arbitrary reference frame equal to the rotor speed of the motor ($\omega_m = \omega_{rm}$) [14].

3.3.1 Voltage Equations in Machine Variables

For a typical 3-phase, wye-connected, symmetrical induction motor, its stator and rotor windings are arranged as shown in the following figure.

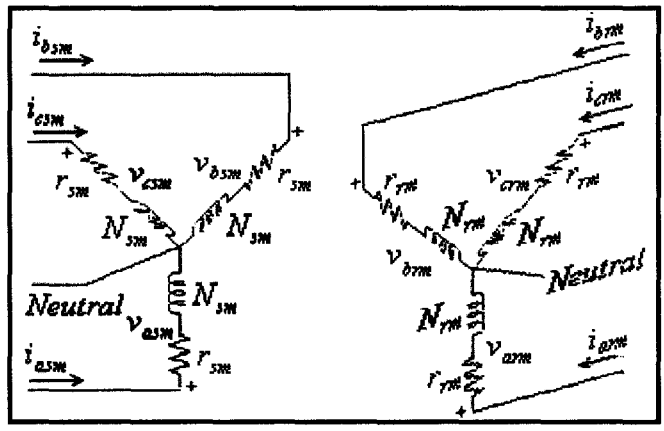

Figure 3.3: *3-phase, wye-connected symmetrical induction motor*

The stator windings in Figure 3.3 are identical, sinusoidally distributed windings, displaced 120°, with N_{sm} equivalent turns and resistance r_{sm}. The rotor windings are also three identical, sinusoidally distributed windings, displaced 120°, with N_{rm} equivalent turns and resistance r_{rm}. Note that the subscript "m" stands for motor. Thus, the voltage equations in machine variables may be expressed as [12]:

$$\mathbf{v}_{abcsm} = \mathbf{r}_{sm}\mathbf{i}_{abcsm} + p\lambda_{abcsm} \tag{3-7}$$

$$\mathbf{v}'_{abcrm} = \mathbf{r}'_{rm}\mathbf{i}'_{abcrm} + p\lambda'_{abcrm} \tag{3-8}$$

where $$(\mathbf{f}_{abcsm})^T = \begin{bmatrix} f_{asm} & f_{bsm} & f_{csm} \end{bmatrix} \tag{3-9}$$

$$(\mathbf{f}'_{abcrm})^T = \begin{bmatrix} f'_{arm} & f'_{brm} & f'_{crm} \end{bmatrix} \tag{3-10}$$

For a magnetically linear system, the flux linkages may be expressed as:

$$\begin{bmatrix} \lambda_{abcsm} \\ \lambda'_{abcrm} \end{bmatrix} = \begin{bmatrix} \mathbf{L}_{sm} & \mathbf{L}'_{srm} \\ (\mathbf{L}'_{srm})^T & \mathbf{L}'_{rm} \end{bmatrix} \begin{bmatrix} \mathbf{i}_{abcsm} \\ \mathbf{i}'_{abcrm} \end{bmatrix} \tag{3-11}$$

where $$\mathbf{L}_{sm} = \begin{bmatrix} L_{lsm} + L_{msm} & -\frac{1}{2}L_{msm} & -\frac{1}{2}L_{msm} \\ -\frac{1}{2}L_{msm} & L_{lsm} + L_{msm} & -\frac{1}{2}L_{msm} \\ -\frac{1}{2}L_{msm} & -\frac{1}{2}L_{msm} & L_{lsm} + L_{msm} \end{bmatrix} \tag{3-12}$$

$$\mathbf{L}'_{rm} = \begin{bmatrix} L'_{lrm} + L_{msm} & -\frac{1}{2}L_{msm} & -\frac{1}{2}L_{msm} \\ -\frac{1}{2}L_{msm} & L'_{lrm} + L_{msm} & -\frac{1}{2}L_{msm} \\ -\frac{1}{2}L_{msm} & -\frac{1}{2}L_{msm} & L'_{lrm} + L_{msm} \end{bmatrix} \tag{3-13}$$

$$\mathbf{L}'_{srm} = L_{msm}\begin{bmatrix} \cos\theta_{rm} & \cos\left(\theta_{rm} + \frac{2\pi}{3}\right) & \cos\left(\theta_{rm} - \frac{2\pi}{3}\right) \\ \cos\left(\theta_{rm} - \frac{2\pi}{3}\right) & \cos\theta_{rm} & \cos\left(\theta_{rm} + \frac{2\pi}{3}\right) \\ \cos\left(\theta_{rm} + \frac{2\pi}{3}\right) & \cos\left(\theta_{rm} - \frac{2\pi}{3}\right) & \cos\theta_{rm} \end{bmatrix} \tag{3-14}$$

In the above voltage and inductance equations, p is the operator d/dt; L_{lsm} and L'_{lrm} are the leakage inductances of the stator and rotor windings, respectively; L_{msm} is the magnetizing inductance of the stator windings. The matrices $\mathbf{L}_{sm}$ and $\mathbf{L}'_{rm}$ describe the

self inductances of the stator and rotor windings, respectively, while $\mathbf{L}'_{srm}$ represents the mutual inductances between windings of the stator and the rotor. The prime symbol indicates that all rotor variables are being conveniently referred to the stator windings by appropriate turn ratios as followed:

$$\mathbf{i}'_{abcrm} = \frac{N_{rm}}{N_{sm}}\mathbf{i}_{abcrm} \tag{3-15}$$

$$\mathbf{v}'_{abcrm} = \frac{N_{sm}}{N_{rm}}\mathbf{v}_{abcrm} \tag{3-16}$$

$$\lambda'_{abcrm} = \frac{N_{sm}}{N_{rm}}\lambda_{abcrm} \tag{3-17}$$

$$\mathbf{r}'_{rm} = \left(\frac{N_{sm}}{N_{rm}}\right)^2 \mathbf{r}_{rm} \tag{3-18}$$

$$L'_{lrm} = \left(\frac{N_{sm}}{N_{rm}}\right)^2 L_{lrm} \tag{3-19}$$

3.3.2 Equations of Transformation for Rotor Circuits

Due to the 3-phase nature of the rotor windings in induction machines, it is desirable to transform the variables associated with the symmetrical rotor windings to the arbitrary reference frame [12]. The transformation can be carried out in a similar fashion as in the case of the stationary circuit variables:

$$\mathbf{f}'_{qd0rm} = \mathbf{K}_{rm}\mathbf{f}'_{abcrm} \tag{3-20}$$

where $$(\mathbf{f}'_{qd0rm})^T = \begin{bmatrix} f'_{qrm} & f'_{drm} & f'_{0rm} \end{bmatrix} \tag{3-21}$$

$$(\mathbf{f}'_{abcrm})^T = \begin{bmatrix} f'_{arm} & f'_{brm} & f'_{crm} \end{bmatrix} \tag{3-22}$$

$$\mathbf{K}_{rm} = \frac{2}{3}\begin{bmatrix} \cos\beta & \cos\left(\beta - \frac{2\pi}{3}\right) & \cos\left(\beta + \frac{2\pi}{3}\right) \\ \sin\beta & \sin\left(\beta - \frac{2\pi}{3}\right) & \sin\left(\beta + \frac{2\pi}{3}\right) \\ \frac{1}{2} & \frac{1}{2} & \frac{1}{2} \end{bmatrix} \tag{3-23}$$

$$(\mathbf{K}_{rm})^{-1} = \begin{bmatrix} \cos\beta & \sin\beta & 1 \\ \cos\left(\beta - \frac{2\pi}{3}\right) & \sin\left(\beta - \frac{2\pi}{3}\right) & 1 \\ \cos\left(\beta + \frac{2\pi}{3}\right) & \sin\left(\beta + \frac{2\pi}{3}\right) & 1 \end{bmatrix} \tag{3-24}$$

$$\beta = \theta_m - \theta_{rm} \tag{3-25}$$

$$\theta_{rm} = \int_0 \omega_{rm}(\xi)d\xi + \theta_{rm}(0) \tag{3-26}$$

It is clear that the above transformation equations for rotor circuits are the transformation equations for stationary circuits with β used as the angular displacement rather than θ_m. As illustrated in the Figure 3.4, β is the angular displacement between the 3-phase variables in the rotor circuits and the transformed variables in the arbitrary reference frame; while θ_{rm} is the motor's angular displacement between the 3-phase variables in the rotor circuits and those in the stationary circuits.

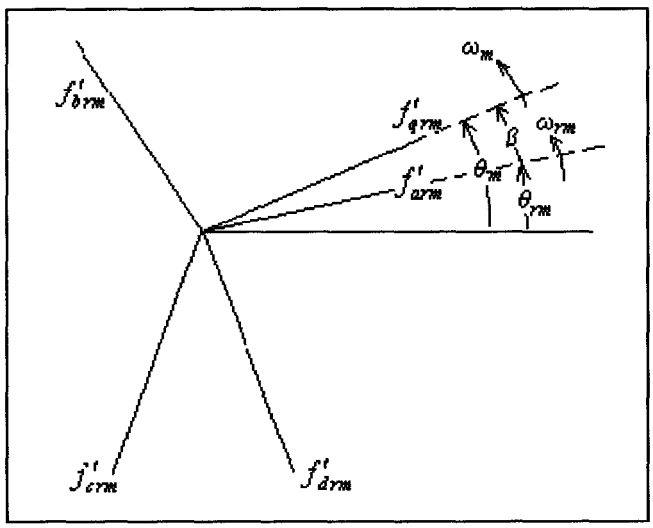

Figure 3.4: *Rotating circuit transformation by trigonometric relationships*

3.3.3 Transforming Circuit Variables to the Arbitrary Reference Frame

Since the voltage equations for induction motors consist of resistances and inductances, it is more convenient to transform these circuit elements separately to the arbitrary reference frame before transforming the voltage equations (3-7) and (3-8) to the arbitrary reference-frame variables [12].

Resistive Elements

For a three-phase resistive circuit:

$$\mathbf{v}_{abcsm} = \mathbf{r}_{sm}\mathbf{i}_{abcsm} \tag{3-27}$$

$$\mathbf{v}'_{abcrm} = \mathbf{r}'_{rm}\mathbf{i}'_{abcrm} \tag{3-28}$$

From (3-1) and (3-20):

$$\mathbf{v}_{qd0sm} = \mathbf{K}_{sm}\mathbf{r}_{sm}(\mathbf{K}_{sm})^{-1}\mathbf{i}_{qd0sm} \tag{3-29}$$

$$\mathbf{v}'_{qd0rm} = \mathbf{K}_{rm}\mathbf{r}'_{rm}(\mathbf{K}_{rm})^{-1}\mathbf{i}'_{qd0rm} \tag{3-30}$$

Since all the stator and rotor phase windings of a symmetrical induction motor are designed to have the same resistance, the matrices $\mathbf{r}_{sm}$ and $\mathbf{r}'_{rm}$ are diagonal matrices with equal nonzero elements. Then,

$$\mathbf{K}_{sm}\mathbf{r}_{sm}(\mathbf{K}_{sm})^{-1} = \mathbf{r}_{sm} \tag{3-31}$$

$$\mathbf{K}_{rm}\mathbf{r}'_{rm}(\mathbf{K}_{rm})^{-1} = \mathbf{r}'_{rm} \tag{3-32}$$

Thus, for both the stator and rotor windings in a symmetrical induction motor, the resistance matrices associated with the arbitrary reference variables are equal to the resistance matrices associated with the actual variables if each phase of the actual circuit has the same resistance [12].

Inductive Elements

For a three-phase inductive circuit:

$$\mathbf{v}_{abcsm} = p\lambda_{abcsm} \tag{3-33}$$

$$\mathbf{v}'_{abcrm} = p\lambda'_{abcrm} \tag{3-34}$$

In terms of the substitute variables, (3-33) and (3-34) become:

$$\mathbf{v}_{qd0sm} = \mathbf{K}_{sm}p\left[(\mathbf{K}_{sm})^{-1}\lambda_{qd0sm}\right] \tag{3-35}$$

$$\mathbf{v}'_{qd0rm} = \mathbf{K}_{rm}p\left[(\mathbf{K}_{rm})^{-1}\lambda'_{qd0rm}\right] \tag{3-36}$$

By the chain rule, (3-35) and (3-36) can be written:

$$\mathbf{v}_{qd0sm} = \mathbf{K}_{sm}p\left[(\mathbf{K}_{sm})^{-1}\right]\lambda_{qd0sm} + \mathbf{K}_{sm}(\mathbf{K}_{sm})^{-1}p\lambda_{qd0sm} \tag{3-37}$$

$$\mathbf{v}'_{qd0rm} = \mathbf{K}_{rm}p\left[(\mathbf{K}_{rm})^{-1}\right]\lambda'_{qd0rm} + \mathbf{K}_{rm}(\mathbf{K}_{rm})^{-1}p\lambda'_{qd0rm} \tag{3-38}$$

Since $\frac{d\theta_m}{dt} = \omega_m$, $\frac{d\theta_{rm}}{dt} = \omega_{rm}$, and $\frac{d\beta}{dt} = \omega_m - \omega_{rm}$, it is easy to show that:

$$p\left[(\mathbf{K}_{sm})^{-1}\right]=\omega_m\begin{bmatrix}-\sin\theta_m & \cos\theta_m & 0\\ -\sin\left(\theta_m-\frac{2\pi}{3}\right) & \cos\left(\theta_m-\frac{2\pi}{3}\right) & 0\\ -\sin\left(\theta_m+\frac{2\pi}{3}\right) & \cos\left(\theta_m+\frac{2\pi}{3}\right) & 0\end{bmatrix} \qquad (3\text{-}39)$$

$$p\left[(\mathbf{K}_{rm})^{-1}\right]=(\omega_m-\omega_{rm})\begin{bmatrix}-\sin\beta & \cos\beta & 0\\ -\sin\left(\beta-\frac{2\pi}{3}\right) & \cos\left(\beta-\frac{2\pi}{3}\right) & 0\\ -\sin\left(\beta+\frac{2\pi}{3}\right) & \cos\left(\beta+\frac{2\pi}{3}\right) & 0\end{bmatrix} \qquad (3\text{-}40)$$

Making use of the following trigonometric identities:

$$\cos^2 x+\cos^2\left(x-\frac{2\pi}{3}\right)+\cos^2\left(x+\frac{2\pi}{3}\right)=\frac{3}{2}$$

$$\sin^2 x+\sin^2\left(x-\frac{2\pi}{3}\right)+\sin^2\left(x+\frac{2\pi}{3}\right)=\frac{3}{2}$$

$$\sin x\cos x+\sin\left(x-\frac{2\pi}{3}\right)\cos\left(x-\frac{2\pi}{3}\right)+\sin\left(x+\frac{2\pi}{3}\right)\cos\left(x+\frac{2\pi}{3}\right)=0$$

$$\cos x+\cos\left(x-\frac{2\pi}{3}\right)+\cos\left(x+\frac{2\pi}{3}\right)=0 \qquad \sin x+\sin\left(x-\frac{2\pi}{3}\right)+\sin\left(x+\frac{2\pi}{3}\right)=0$$

One can show that:

$$\mathbf{K}_{sm}\,p\left[(\mathbf{K}_{sm})^{-1}\right]=\omega_m\begin{bmatrix}0 & 1 & 0\\ -1 & 0 & 0\\ 0 & 0 & 0\end{bmatrix} \qquad (3\text{-}41)$$

$$\mathbf{K}_{rm}\,p\left[(\mathbf{K}_{rm})^{-1}\right]=(\omega_m-\omega_{rm})\begin{bmatrix}0 & 1 & 0\\ -1 & 0 & 0\\ 0 & 0 & 0\end{bmatrix} \qquad (3\text{-}42)$$

Using (3-41) and (3-42), and realizing that $\mathbf{K}_{sm}(\mathbf{K}_{sm})^{-1} = \mathbf{K}_{rm}(\mathbf{K}_{rm})^{-1} = 1$, equations (3-37) and (3-38) can be written as:

$$\mathbf{v}_{qd0sm}=\omega\lambda_{dqsm}+p\lambda_{qd0sm} \qquad (3\text{-}43)$$

$$\mathbf{v}'_{qd0rm}=(\omega_m-\omega_{rm})\lambda'_{dqrm}+p\lambda'_{qd0rm} \qquad (3\text{-}44)$$

where

$$\left(\lambda_{dqsm}\right)^T = \begin{bmatrix} \lambda_{dsm} & -\lambda_{qsm} & 0 \end{bmatrix} \tag{3-45}$$

$$\left(\lambda'_{dqrm}\right)^T = \begin{bmatrix} \lambda'_{drm} & -\lambda'_{qrm} & 0 \end{bmatrix} \tag{3-46}$$

3.3.4 Voltage Equations in Arbitrary Reference-frames Variables

Using the information set forth in the above section, the voltage equations (3-7) and (3-8) can be readily transformed to the arbitrary reference frame as follows:

$$\mathbf{v}_{qd0sm} = \mathbf{r}_{sm}\mathbf{i}_{qd0sm} + \omega_m \lambda_{dqsm} + p\lambda_{qd0sm} \tag{3-47}$$

$$\mathbf{v}'_{qd0rm} = \mathbf{r}'_{rm}\mathbf{i}'_{qd0rm} + (\omega_m - \omega_{rm})\lambda'_{dqrm} + p\lambda'_{qd0rm} \tag{3-48}$$

The set of equations is complete once the expressions for the flux linkages are determined. Transforming the flux linkage equations expressed in *abc* variables (3-11) to the arbitrary reference frame yields:

$$\begin{bmatrix} \lambda_{qd0sm} \\ \lambda'_{qd0rm} \end{bmatrix} = \begin{bmatrix} \mathbf{K}_{sm}\mathbf{L}_{sm}\left(\mathbf{K}_{sm}\right)^{-1} & \mathbf{K}_{sm}\mathbf{L}'_{srm}\left(\mathbf{K}_{rm}\right)^{-1} \\ \mathbf{K}_{rm}\left(\mathbf{L}'_{srm}\right)^T\left(\mathbf{K}_{sm}\right)^{-1} & \mathbf{K}_{rm}\mathbf{L}'_{rm}\left(\mathbf{K}_{rm}\right)^{-1} \end{bmatrix} \begin{bmatrix} \mathbf{i}_{qd0sm} \\ \mathbf{i}'_{qd0rm} \end{bmatrix} \tag{3-49}$$

where the matrices $\mathbf{L}_{sm}$, $\mathbf{L}'_{rm}$ and $\mathbf{L}'_{srm}$ are defined by (3-12), (3-13) and (3-14). Using the double-angle formulas and the trigonometric identities given in section 3.3.3:

$$\mathbf{K}_{sm}\mathbf{L}_{sm}\left(\mathbf{K}_{sm}\right)^{-1} = \begin{bmatrix} L_{lsm}+M & 0 & 0 \\ 0 & L_{lsm}+M & 0 \\ 0 & 0 & L_{lsm} \end{bmatrix} \tag{3-50}$$

$$\mathbf{K}_{rm}\mathbf{L}'_{rm}\left(\mathbf{K}_{rm}\right)^{-1} = \begin{bmatrix} L'_{lrm}+M & 0 & 0 \\ 0 & L'_{lrm}+M & 0 \\ 0 & 0 & L'_{lrm} \end{bmatrix} \tag{3-51}$$

$$M = \frac{3}{2}L_{msm} \tag{3-52}$$

It can also be shown that

$$\mathbf{K}_{sm}\mathbf{L}'_{srm}\left(\mathbf{K}_{rm}\right)^{-1} = \mathbf{K}_{rm}\left(\mathbf{L}'_{srm}\right)^T\left(\mathbf{K}_{sm}\right)^{-1} = \begin{bmatrix} M & 0 & 0 \\ 0 & M & 0 \\ 0 & 0 & 0 \end{bmatrix} \tag{3-53}$$

Making uses of the results in (3-50), (3-51) and (3-53), the flux linkage equations in (3-49) can be expanded in matrix form as:

$$\begin{bmatrix} \lambda_{qsm} \\ \lambda_{dsm} \\ \lambda_{0sm} \\ \lambda'_{qrm} \\ \lambda'_{drm} \\ \lambda'_{0rm} \end{bmatrix} = \begin{bmatrix} L_{lsm}+M & 0 & 0 & M & 0 & 0 \\ 0 & L_{lsm}+M & 0 & 0 & M & 0 \\ 0 & 0 & L_{lsm} & 0 & 0 & 0 \\ M & 0 & 0 & L'_{lrm}+M & 0 & 0 \\ 0 & M & 0 & 0 & L'_{lrm}+M & 0 \\ 0 & 0 & 0 & 0 & 0 & L'_{lrm} \end{bmatrix} \begin{bmatrix} i_{qsm} \\ i_{dsm} \\ i_{0sm} \\ i'_{qrm} \\ i'_{drm} \\ i'_{0rm} \end{bmatrix} \quad (3\text{-}54)$$

With the known values of flux linkages above [12], the voltage equations (3-47) and (3-48) can be written in expanded forms as:

$$v_{qsm} = r_{sm} i_{qsm} + \omega_m \lambda_{dsm} + p\lambda_{qsm} \quad (3\text{-}55)$$

$$v_{dsm} = r_{sm} i_{dsm} - \omega_m \lambda_{qsm} + p\lambda_{dsm} \quad (3\text{-}56)$$

$$v_{0sm} = r_{sm} i_{0sm} + p\lambda_{0sm} \quad (3\text{-}57)$$

$$v'_{qrm} = r'_{rm} i'_{qrm} + (\omega_m - \omega_{rm})\lambda'_{drm} + p\lambda'_{qrm} \quad (3\text{-}58)$$

$$v'_{drm} = r'_{rm} i'_{drm} - (\omega_m - \omega_{rm})\lambda'_{qrm} + p\lambda'_{drm} \quad (3\text{-}59)$$

$$v'_{0rm} = r'_{rm} i'_{0rm} + p\lambda'_{0qrm} \quad (3\text{-}60)$$

The voltage equations (3-55) to (3-60) suggest the following equivalent circuits [12]:

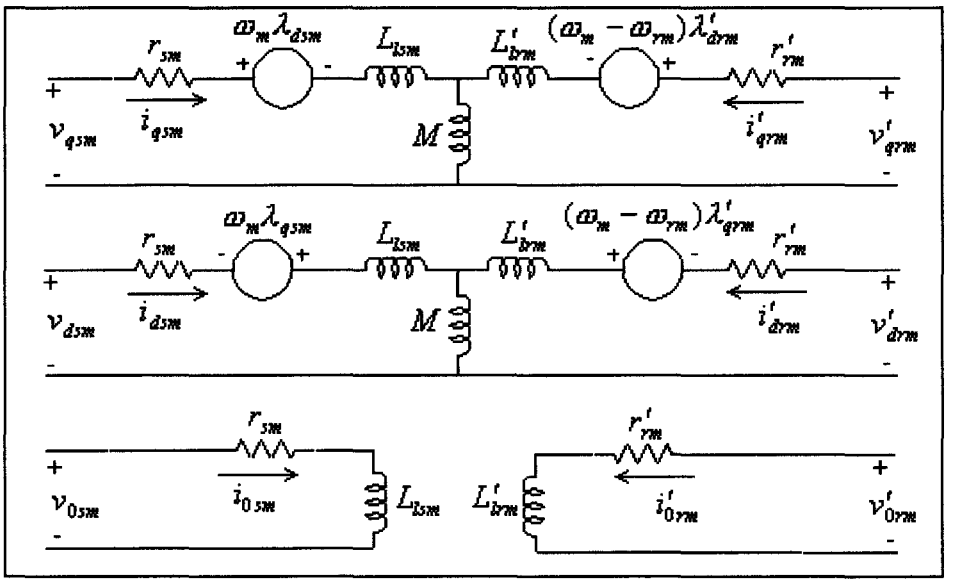

Figure 3.5: *Arbitrary reference-frame equivalent circuits for a 3-phase, symmetrical induction motor*

3.3.5 Arbitrary Reference-frame Equations Expressed in State Variables

From equation (3-54), it is clear that the currents and flux linkages are related and both cannot be independent (or state variables). In computer simulation of induction motors, it is desirable to express the voltage equations in terms of either currents or flux linkages. In this research, the currents are used as state variables. Thus, substituting the currents in (3-54) into equations (3-55)-(3-60) and performing algebraic manipulation to solve for each derivative, we obtain the state variables for currents as followed [12]:

$$\frac{di_{qsm}}{dt} = \frac{1}{D}[-L'_{rr}r_{sm}i_{qsm} - D\omega_m i_{dsm} + Mr'_{rm}i'_{qrm} - (M^2 i_{dsm} + ML'_{rr}i'_{drm})\omega_{rm} + L'_{rr}v_{qsm} - Mv'_{qrm}]$$

$$\frac{di_{dsm}}{dt} = \frac{1}{D}[D\omega_m i_{qsm} - L'_{rr}r_{sm}i_{dsm} + Mr'_{rm}i'_{drm} + (M^2 i_{qsm} + ML'_{rr}i'_{qrm})\omega_{rm} + L'_{rr}v_{dsm} - Mv'_{drm}]$$

$$\frac{di_{0sm}}{dt} = \frac{1}{L_{lsm}}[-r_{sm}i_{0sm} + v_{0sm}] \qquad (3-61)$$

$$\frac{di'_{qrm}}{dt} = \frac{1}{D}[Mr_{sm}i_{qsm} - L_{ss}r'_{rm}i'_{qrm} - D\omega_m i'_{drm} + (ML_{ss}i_{dsm} + L_{ss}L'_{rr}i'_{drm})\omega_{rm} - Mv_{qsm} + L_{ss}v'_{qrm}]$$

$$\frac{di'_{drm}}{dt} = \frac{1}{D}[Mr_{sm}i_{dsm} - L_{ss}r'_{rm}i'_{drm} + D\omega_m i'_{qrm} - (ML_{ss}i_{qsm} + L_{ss}L'_{rr}i'_{qrm})\omega_{rm} - Mv_{dsm} + L_{ss}v'_{drm}]$$

$$\frac{di'_{0rm}}{dt} = \frac{1}{L'_{lrm}}[-r'_{rm}i'_{0rm} + v'_{0rm}]$$

where
$$L_{ss} = L_{lsm} + M$$
$$L'_{rr} = L'_{lrm} + M$$
$$D = L_{ss}L'_{rr} - M^2$$

To complete the mathematical model of an induction machine, the torque equation must be developed in the following section.

3.3.6 Torque Equation for the Induction Motor

For a P-pole, magnetically linear machine, the energy stored in the leakage inductances is not a part of the energy stored in the coupling field W_{fm}; as a result, this field energy is equal to the coenergy W_{cm}. Since $W_{cm} = W_{fm}$ [12], the electromagnetic torque may be evaluated from

$$T_{em}(i_{jm}, \theta_{rm}) = \left(\frac{P}{2}\right)\frac{\partial W_{fm}(i_{jm}, \theta_{rm})}{\partial \theta_{rm}} \qquad (3\text{-}62)$$

where i_{jm} represents any phase current in the stator and the rotor of the motor, and

$W_{fm} = \frac{1}{2}(\mathbf{i}_{abcsm})^T(\mathbf{L}_{sm} - L_{lsm}\mathbf{I})\mathbf{i}_{abcsm} + (\mathbf{i}_{abcsm})^T\mathbf{L}'_{srm}\mathbf{i}'_{abcrm} + \frac{1}{2}(\mathbf{i}'_{abcrm})^T(\mathbf{L}'_{rm} - L'_{lrm}\mathbf{I})\mathbf{i}'_{abcrm}$

Since the matrices $\mathbf{L}_{sm}$ and $\mathbf{L}'_{rm}$ are not functions of θ_{rm}, only $\mathbf{L}'_{srm}$ can survive the differentiation after substituting W_{fm} into equation (3-62), and the electromagnetic torque in Newton meters (N·m) can now be reduced to:

$$T_{em}(i_{jm}, \theta_{rm}) = \left(\frac{P}{2}\right)(\mathbf{i}_{abcsm})^T \frac{\partial}{\partial \theta_{rm}}[\mathbf{L}'_{srm}]\mathbf{i}'_{abcrm} \qquad (3\text{-}63)$$

Substituting the equations of transformation into (3-63) yields the torque expressed in terms of currents as follows:

$$T_{em} = \left(\frac{3}{2}\right)\left(\frac{P}{2}\right)M(i_{qsm}i'_{drm} - i_{dsm}i'_{qrm}) \qquad (3\text{-}64)$$

The torque and rotor speed are related by:

$$T_{em} = J_m\left(\frac{2}{P}\right)p\omega_{rm} + T_L \qquad (3\text{-}65)$$

where J_m is the inertia of the rotor and in some cases the connected load, and T_L is the load torque. Thus, in terms of electromagnetic torque and load torque, the derivative of the rotor speed can be written as

$$\frac{d\omega_{rm}}{dt} = \frac{P}{2J_m}\left[\left(\frac{3}{2}\right)\left(\frac{P}{2}\right)M(i_{qsm}i'_{drm} - i_{dsm}i'_{qrm}) - T_L\right] \qquad (3\text{-}66)$$

Bundling the differential equations listed in equations (3-61) and (3-66) together, we now have a dynamic mathematical model of a three-phase, wye-connected, wound-rotor induction motor in the arbitrary reference frame.

3.3.7 Mathematical Representation of the Squirrel-cage Induction Motor

Since the induction machines being used in the research are squirrel-cage induction motors, the set of equations in (3-61) need to be modified according to the fact that the rotor windings are short-circuited, i.e. $v'_{qrm} = v'_{drm} = 0$. After taking account of the short-circuited factor, the mathematical representation of a squirrel-cage induction **motor** can be obtained by replacing ω_m in (3-61) with ω_{rm} in order to convert it from the arbitrary reference frame to the rotor reference frame. Here is the final set of equations:

$$\frac{di_{qsm}}{dt} = \frac{1}{D}[-L'_{rr}r_{sm}i_{qsm} - L'_{rr}L_{ss}i_{dsm}\omega_{rm} + Mr'_{rm}i'_{qrm} - ML'_{rr}i'_{drm}\omega_{rm} + L'_{rr}v_{qsm}]$$

$$\frac{di_{dsm}}{dt} = \frac{1}{D}[L'_{rr}L_{ss}i_{qsm}\omega_{rm} - L'_{rr}r_{sm}i_{dsm} + ML'_{rr}i'_{qrm}\omega_{rm} + Mr'_{rm}i'_{drm} + L'_{rr}v_{dsm}]$$

$$\frac{di_{0sm}}{dt} = \frac{1}{L_{lsm}}[-r_{sm}i_{0sm} + v_{0sm}]$$

$$\frac{di'_{qrm}}{dt} = \frac{1}{D}[Mr_{sm}i_{qsm} + ML_{ss}i_{dsm}\omega_{rm} - L_{ss}r'_{rm}i'_{qrm} + M^2i'_{drm}\omega_{rm} - Mv_{qsm}] \qquad (3-67)$$

$$\frac{di'_{drm}}{dt} = \frac{1}{D}[-ML_{ss}i_{qsm}\omega_{rm} + Mr_{sm}i_{dsm} - M^2i'_{qrm}\omega_{rm} - L_{ss}r'_{rm}i'_{drm} - Mv_{dsm}]$$

$$\frac{di'_{0rm}}{dt} = \frac{-r'_{rm}i'_{0rm}}{L'_{lrm}}$$

$$\frac{d\omega_{rm}}{dt} = \frac{P}{2J_m}\left[\left(\frac{3}{2}\right)\left(\frac{P}{2}\right)M(i_{qsm}i'_{drm} - i_{dsm}i'_{qrm}) - T_L\right]$$

Note that the reason for writing the above set of state equations in rotor reference frame, which is Park's transformation for induction machine [14], instead of the arbitrary reference frame will become obvious in section 3.5.

3.4 Mathematical Modeling of the Synchronous Generator

As explained in section 2.2.3, the synchronous generator used in the new phase modulation method can modulate the phase with respect to the utility source phasors by having one rotor winding supplied with a square-wave voltage controlled by an inverter, while the other two windings are connected in series and supplied by a fixed DC source. As shown in the phasor diagram of Figure 2.4, such rotor winding configuration causes a DC flux to be induced along the quadrature axis and a modulated flux along the direct axis, leading to an equivalent arrangement of the rotor windings which can be drawn in Figure 3.6 on the next page. Such new configuration greatly simplifies the derivation process of all the mathematical equations that follow later in this section.

Because the synchronous machine here operates as a generator, the directions of positive stator currents in Figure 3.6 are out of the stator terminals. Note that the rotor windings of the equivalent configuration are readily in the rotor reference frame. That is, the winding (A) has now become a direct-axis winding for the rotor with $N_{dr} = N_{rg}$ and $r_{dr} = r_{rg}$, while windings (B) and (C) make up the quadrature-axis winding with $N_{qr} = 2N_{rg}$

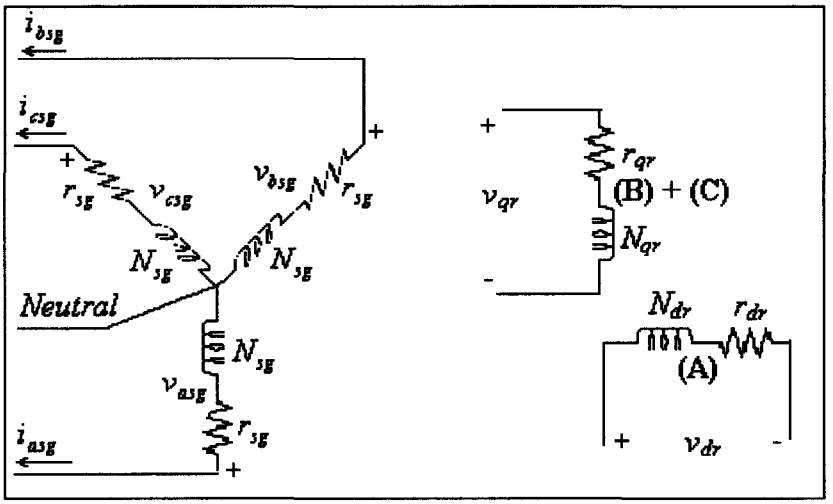

Figure 3.6: *Equivalent configuration of the created synchronous generator*

and $r_{qr} = 2r_{rg}$. With the above assumptions, the voltage equations expressed in terms of machine variables referred to the stator windings are [13]:

$$\mathbf{v}_{abcsg} = -\mathbf{r}_{sg}\mathbf{i}_{abcsg} + \rho\lambda_{abcsg} \tag{3-68}$$

$$\mathbf{v}'_{qdrg} = \mathbf{r}'_{rg}\mathbf{i}'_{qdrg} + \rho\lambda'_{qdrg} \tag{3-69}$$

where $\mathbf{r}'_{rg} = diag\left[r'_{qr} \quad r'_{dr}\right]$, and the flux linkage equations become:

$$\begin{bmatrix} \lambda_{abcsg} \\ \lambda'_{qdrg} \end{bmatrix} = \begin{bmatrix} \mathbf{L}_{sg} & \mathbf{L}'_{srg} \\ \frac{2}{3}\left(\mathbf{L}'_{srg}\right)^T & \mathbf{L}'_{rg} \end{bmatrix} \begin{bmatrix} -\mathbf{i}_{abcsg} \\ \mathbf{i}'_{qdrg} \end{bmatrix} \tag{3-70}$$

Similar to the case of symmetrical induction motors, the matrices $\mathbf{L}_{sg}$ and $\mathbf{L}'_{rg}$ represent the self inductances of the stator and rotor windings, respectively, while $\mathbf{L}'_{srg}$ expresses the mutual inductances between windings of the stator and the rotor. Note the subscript "g" stands for generator. The matrices above are shown as follows:

$$\mathbf{L}_{sg} = \begin{bmatrix} L_{lsg} + L_A - L_B\cos 2\theta_{rg} & -\frac{1}{2}L_A - L_B\cos 2\left(\theta_{rg} - \frac{\pi}{3}\right) & -\frac{1}{2}L_A - L_B\cos 2\left(\theta_{rg} + \frac{\pi}{3}\right) \\ -\frac{1}{2}L_A - L_B\cos 2\left(\theta_{rg} - \frac{\pi}{3}\right) & L_{lsg} + L_A - L_B\cos 2\left(\theta_{rg} - \frac{2\pi}{3}\right) & -\frac{1}{2}L_A - L_B\cos 2\left(\theta_{rg} + \pi\right) \\ -\frac{1}{2}L_A - L_B\cos 2\left(\theta_{rg} + \frac{\pi}{3}\right) & -\frac{1}{2}L_A - L_B\cos 2\left(\theta_{rg} + \pi\right) & L_{lsg} + L_A - L_B\cos 2\left(\theta_{rg} + \frac{2\pi}{3}\right) \end{bmatrix} \tag{3-71}$$

$$\mathbf{L}'_{rg} = \begin{bmatrix} L'_{lqr} + L_{mq} & 0 \\ 0 & L'_{ldr} + L_{md} \end{bmatrix} \tag{3-72}$$

$$\mathbf{L}'_{srg} = \begin{bmatrix} L_{mq}\cos\theta_{rg} & L_{md}\sin\theta_{rg} \\ L_{mq}\cos\left(\theta_{rg}-\frac{2\pi}{3}\right) & L_{md}\sin\left(\theta_{rg}-\frac{2\pi}{3}\right) \\ L_{mq}\cos\left(\theta_{rg}+\frac{2\pi}{3}\right) & L_{md}\sin\left(\theta_{rg}+\frac{2\pi}{3}\right) \end{bmatrix} \tag{3-73}$$

where L_A and L_B are parts of the self inductances in each phase of the stator windings; L'_{lqr} and L'_{ldr} are leakage inductances in the rotor windings; while L_{mq} and L_{md} are the magnetizing inductances expressed in the form of:

$$\begin{aligned} L_{mq} &= \tfrac{3}{2}(L_A - L_B) \\ L_{md} &= \tfrac{3}{2}(L_A + L_B) \end{aligned} \tag{3-74}$$

3.4.1 Voltage Equations in Rotor Reference-frame Variables

In the arbitrary reference frame, the voltage equations for the stator windings in a synchronous generator may be written as [13]:

$$\mathbf{v}_{qd0sg} = -\mathbf{r}_{sg}\mathbf{i}_{qd0sg} + \omega_g \lambda_{dqsg} + \rho\lambda_{qd0sg} \tag{3-75}$$

where $\left(\lambda_{dqsg}\right)^T = \begin{bmatrix} \lambda_{dsg} & -\lambda_{qsg} & 0 \end{bmatrix}$ (3-76)

Since the rotor variables for a synchronous generator are already expressed in the rotor reference frame, the stator variables must also be written in the same reference frame to obtain the Park's equations by setting the speed of the arbitrary reference frame equal to the rotor speed (ω_g=ω_{rg}) [13]. Thus, the voltage equations expressed in the rotor reference frame are:

$$\mathbf{v}_{qd0sg} = -\mathbf{r}_{sg}\mathbf{i}_{qd0sg} + \omega_{rg}\lambda_{dqsg} + \rho\lambda_{qd0sg} \tag{3-77}$$

$$\mathbf{v}'_{qdrg} = \mathbf{r}'_{rg}\mathbf{i}'_{qdrg} + \rho\lambda'_{qdrg} \tag{3-78}$$

For a magnetically linear system, the flux linkages may be written in the rotor reference frame by setting $\theta_g = \theta_{rg}$ in the matrix of $\mathbf{K}_{sg}$, leading to $\mathbf{K}^r_{sg}$ as shown below:

$$\begin{bmatrix} \lambda_{qd0sg} \\ \lambda'_{qdrg} \end{bmatrix} = \begin{bmatrix} \mathbf{K}^r_{sg}\mathbf{L}_{sg}\left(\mathbf{K}^r_{sg}\right)^{-1} & \mathbf{K}^r_{sg}\mathbf{L}'_{srg} \\ \frac{2}{3}\left(\mathbf{L}'_{srg}\right)^T\left(\mathbf{K}^r_{sg}\right)^{-1} & \mathbf{L}'_{rg} \end{bmatrix} \begin{bmatrix} -\mathbf{i}_{qd0sg} \\ \mathbf{i}'_{qdrg} \end{bmatrix} \tag{3-79}$$

where $\mathbf{K}_{sg}^{r}\mathbf{L}_{sg}\left(\mathbf{K}_{sg}^{r}\right)^{-1}=\begin{bmatrix} L_{lsg}+L_{mq} & 0 & 0 \\ 0 & L_{lsg}+L_{mq} & 0 \\ 0 & 0 & L_{lsg} \end{bmatrix}$ (3-80)

$$\mathbf{K}_{sg}^{r}\mathbf{L}'_{srg}=\begin{bmatrix} L_{mq} & 0 \\ 0 & L_{md} \\ 0 & 0 \end{bmatrix} \tag{3-81}$$

$$\tfrac{2}{3}\left(\mathbf{L}'_{srg}\right)^{T}\left(\mathbf{K}_{sg}^{r}\right)^{-1}=\begin{bmatrix} L_{mq} & 0 & 0 \\ 0 & L_{md} & 0 \end{bmatrix} \tag{3-82}$$

Substituting (3-80)-(3-82) into (3-79) gives:

$$\begin{aligned}
\lambda_{qsg} &= -L_{lsg}i_{qsg}+L_{mq}(-i_{qsg}+i'_{qrg})=-L_{q}i_{qsg}+L_{mq}i'_{qrg} \\
\lambda_{dsg} &= -L_{lsg}i_{dsg}+L_{md}(-i_{dsg}+i'_{drg})=-L_{d}i_{dsg}+L_{md}i'_{drg} \\
\lambda_{0sg} &= -L_{lsg}i_{0sg} \\
\lambda'_{qrg} &= L'_{lqr}i'_{qrg}+L_{mq}(-i_{qsg}+i'_{qrg})=L'_{kq}i'_{qrg}-L_{mq}i_{qsg} \\
\lambda'_{drg} &= L'_{ldr}i'_{drg}+L_{md}(-i_{dsg}+i'_{drg})=L'_{kd}i'_{drg}-L_{md}i_{dsg}
\end{aligned} \tag{3-83}$$

With the known values of flux linkages above, the voltage equations (3-77) and (3-78) can be written in expanded forms as [13]:

$$v_{qsg}=-r_{sg}i_{qsg}+\omega_{rg}\lambda_{dsg}+p\lambda_{qsg} \tag{3-84}$$

$$v_{dsg}=-r_{sg}i_{dsg}-\omega_{rg}\lambda_{qsg}+p\lambda_{dsg} \tag{3-85}$$

$$v_{0sg}=-r_{sg}i_{0sg}+p\lambda_{0sg} \tag{3-86}$$

$$v'_{qrg}=r'_{qr}i'_{qrg}+p\lambda'_{qrg} \tag{3-87}$$

$$v'_{drg}=r'_{dr}i'_{drg}+p\lambda'_{drg} \tag{3-88}$$

The voltage equations (3-84) to (3-88) suggest the following equivalent circuits [13]:

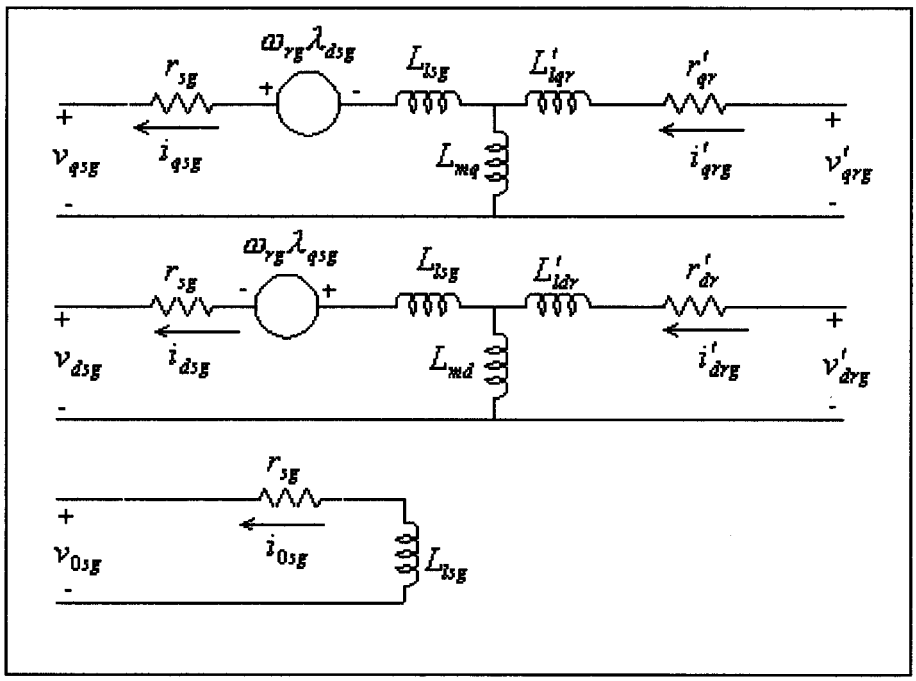

Figure 3.7: *Equivalent circuits of a 3-phase synchronous generator with reference frame fixed in the rotor*

Making use of the values of flux linkages obtained in (3-83), the voltage equations (3-84) to (3-88) can be manipulated and re-expressed in terms of state variables for currents as follows:

$$\frac{di_{qsg}}{dt} = \frac{1}{D_q}\left[-r_{sg}L'_{kq}i_{qsg} - L_d L'_{kq}i_{dsg}\omega_{rg} - L_{mq}r'_{qr}i'_{qrg} + L_{md}L'_{kq}i'_{drg}\omega_{rg} + L_{mq}v'_{qrg} - L'_{kq}v_{qsg}\right]$$

$$\frac{di_{dsg}}{dt} = \frac{1}{D_d}\left[L_q L'_{kd}i_{qsg}\omega_{rg} - r_{sg}L'_{kd}i_{dsg} - L_{mq}L'_{kd}i'_{qrg}\omega_{rg} - L_{md}r'_{dr}i'_{drg} + L_{md}v'_{drg} - L'_{kd}v_{dsg}\right]$$

$$\frac{di_{osg}}{dt} = \frac{1}{L_{lsg}}\left[-r_{sg}i_{osg} - v_{osg}\right] \qquad (3-89)$$

$$\frac{di'_{qrg}}{dt} = \frac{1}{D_q}\left[-r_{sg}L_{mq}i_{qsg} - L_d L_{mq}i_{dsg}\omega_{rg} - L_q r'_{qr}i'_{qrg} + L_{md}L_{mq}i'_{drg}\omega_{rg} + L_q v'_{qrg} - L_{mq}v_{qsg}\right]$$

$$\frac{di'_{drg}}{dt} = \frac{1}{D_d}\left[L_q L_{md}i_{qsg}\omega_{rg} - r_{sg}L_{md}i_{dsg} - L_{mq}L_{md}i'_{qrg}\omega_{rg} - L_d r'_{dr}i'_{drg} + L_d v'_{drg} - L_{md}v_{dsg}\right]$$

where $D_q = L_q L'_{kq} - L^2_{mq}$

$D_d = L_d L'_{kd} - L^2_{md}$

3.4.2 Torque Equation for the Synchronous Generator

The energy stored in the coupling field of a synchronous machine can be expressed as:

$$W_{fg} = \tfrac{1}{2}(i_{abcsg})^T(L_{sg} - L_{lsg}I)i_{abcsg} - (i_{abcsg})^T L'_{srg} i'_{qdrg} + \tfrac{1}{2}\left(\tfrac{3}{2}\right)(i'_{qdrg})^T(L'_{rg} - L'_{lrg}I)i'_{qdrg} \qquad (3-90)$$

Since the magnetic system is assumed to be linear, $W_{fg} = W_{cg}$ [12], and the torque for a P-pole machine can be expressed by equation (3-62), the electromagnetic torque equation can be obtained as:

$$T_{eg}(i_{jg}, \theta_{rg}) = \left(\frac{P}{2}\right)\left\{\frac{-1}{2}(i_{abcsg})^T \frac{\partial}{\partial\theta_{rg}}[L_{sg} - L_{lsg}I]i_{abcsg} + (i_{abcsg})^T \frac{\partial}{\partial\theta_{rg}}[L'_{srg}]i'_{dqrg}\right\} \qquad (3-91)$$

Note that the third term in equation (3-90) did not survive the differentiation with respect to θ_{rg} because all elements in $\mathbf{L}'_{rg}$ and $\mathbf{L}'_{lrg}$ are independent of θ_{rg}, and a negative sign is added in front of (3-62) to make T_{eg} positive for generator action. After considerable amount of work, the above equation reduces to:

$$T_{eg} = \left(\frac{3}{2}\right)\left(\frac{P}{2}\right)\left[L_{md}(-i_{dsg} + i'_{drg})i_{qsg} - L_{mq}(-i_{qsg} + i'_{qrg})i_{dsg}\right] \qquad (3\text{-}92)$$

The torque and rotor speed are related by

$$T_{eg} = -J_g\left(\frac{2}{P}\right)p\omega_{rg} + T_L \qquad (3\text{-}93)$$

where J_g is often the combined inertia of the rotor and prime mover, and T_L is the load torque. Thus, in terms of electromagnetic torque and load torque, the derivative of the rotor speed can be obtained as:

$$\frac{d\omega_{rg}}{dt} = \frac{-P}{2J_g}\left[\left(\frac{3}{2}\right)\left(\frac{P}{2}\right)\left[L_{md}(-i_{dsg} + i'_{drg})i_{qsg} - L_{mq}(-i_{qsg} + i'_{qrg})i_{dsg}\right] - T_L\right] \qquad (3\text{-}94)$$

Bundling the differential equations listed in (3-89) and (3-94) together, we now have a dynamic mathematical model of a three-phase, wye-connected, synchronous generator created from a wound-rotor induction machine.

3.5 Mathematical Representation of the Test System

With all the equations being readily available for the squirrel-cage induction motor and the synchronous generator, they can now be used to derive the state equations

for currents in individual parallel systems as previously shown in Figure 2.6. For ease of explaining, the diagram of machine setup in Figure 3.1 for a single system is slightly modified as follows:

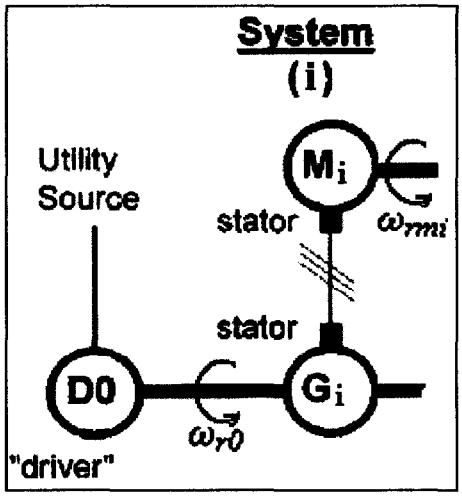

Figure 3.8: *Modified diagram of the machine setup in a single system*

In the above figure, the shaft of the driver motor D0 is coupled to generator G_i. Since the voltage equations of the generator must be expressed in the rotor reference frame [13], those of the induction motor D0 must also be written in the same frame of reference [14]. As a result, when the rotor of D0 rotates and reaches synchronous speed ω_{r0}, the output voltages in G_i would be induced with an angular frequency of ω_{r0}. These output voltages feed directly as input into the test motor M_i whose rotor would be spinning at its own angular frequency of ω_{rmi}. Because the test motor does not have its rotor connected to that of the generator, its voltage equations cannot be written in the same rotor reference frame as those of the generator and driver motor; however, the equations can be expressed in the synchronously rotating reference frame by setting $\omega_{mi}=\omega_{r0}$ [15].

Since the output voltage in the generator is an input to the motor in Figure 3.8, the stator circuits between the two machines are connected in parallel as shown in Figure 3.9 on the next page; as a result, both machines share the same stator voltages. From this reasoning, one can derive the equations for all state currents in this system by setting the generator voltage equations equal to those of the motor stator voltages. Note that the red dashed line was traced on the circuit of Figure 3.9 to indicate which part of the circuit

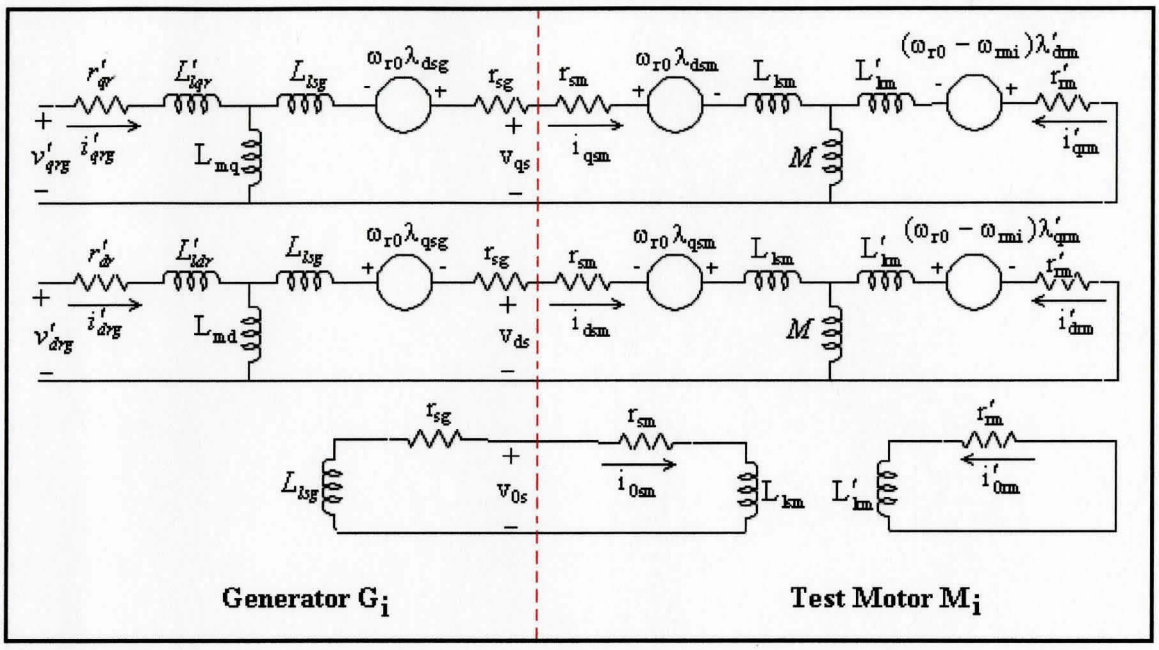

Figure 3.9: *Equivalent circuit of the machine setup in a single system*

belongs to the generator G_i and which part is for the test motor M_i. Using equations (3-55)-(3-60), and (3-84)-(3-88), the derivation starts as follows:

$$v_{qs} = r_{sm} i_{qs} + \omega_{r0}\lambda_{dsm} + p\lambda_{qsm} = -r_{sg} i_{qs} + \omega_{r0}\lambda_{dsg} + p\lambda_{qsg} \qquad (3\text{-}95)$$

$$v_{ds} = r_{sm} i_{ds} + \omega_{r0}\lambda_{qsm} + p\lambda_{dsm} = -r_{sg} i_{ds} + \omega_{r0}\lambda_{qsg} + p\lambda_{dsg} \qquad (3\text{-}96)$$

$$v_{0s} = r_{sm} i_{0s} + p\lambda_{0s} = -r_{sg} i_{0s} + p\lambda_{0s} \qquad (3\text{-}97)$$

$$v'_{qrm} = 0 = r'_{rm} i'_{qrm} + (\omega_{r0} - \omega_{rmi})\lambda'_{drm} + p\lambda'_{qrm} \qquad (3\text{-}98)$$

$$v'_{drm} = 0 = r'_{rm} i'_{drm} - (\omega_{r0} - \omega_{rmi})\lambda'_{qrm} + p\lambda'_{drm} \qquad (3\text{-}99)$$

$$v'_{qrg} = r'_{qr} i'_{qrg} + p\lambda'_{qrg} \qquad (3\text{-}100)$$

$$v'_{drg} = r'_{dr} i'_{drg} + p\lambda'_{drg} \qquad (3\text{-}101)$$

Using equations in (3-54) and (3-83) for the motor and generator flux linkages, respectively, to expand the voltage equations above, and isolating the term for each stator current derivative from each equation yields:

$$\frac{di_{qs}}{dt}=\frac{1}{L_{sq}}[-R_s i_{qs}-\omega_{r0}L_{sd}i_{ds}+L_{mq}\frac{di'_{qrg}}{dt}+\omega_{r0}L_{md}i'_{drg}-M\frac{di_{qrm}}{dt}-\omega_{r0}Mi_{drm}]$$

$$\frac{di_{ds}}{dt}=\frac{1}{L_{sd}}[\omega_{r0}L_{sd}i_{qs}-R_s i_{ds}-\omega_{r0}L_{mq}i'_{qrg}+L_{md}\frac{di'_{drg}}{dt}+\omega_{r0}Mi_{qrm}-M\frac{di_{drm}}{dt}]$$

$$\frac{di_{0s}}{dt}=\frac{-1}{L_{lsm}+L_{lsm}}[r_{sg}+r_{sm}]i_{0s}$$

$$\frac{di'_{qrg}}{dt}=\frac{1}{L'_{kq}}[v'_{qrg}+L_{mq}\frac{di_{qs}}{dt}-r'_{qr}i'_{qrg}] \qquad (3-102)$$

$$\frac{di'_{drg}}{dt}=\frac{1}{L'_{kd}}[v'_{drg}+L_{md}\frac{di_{ds}}{dt}-r'_{dr}i'_{drg}]$$

$$\frac{di'_{qrm}}{dt}=\frac{1}{L'_{rr}}[-M\frac{di_{qs}}{dt}-(\omega_{r0}-\omega_{rmi})Mi_{ds}-r'_{rm}i'_{qrm}-(\omega_{r0}-\omega_{rmi})L'_{rr}i_{drm}]$$

$$\frac{di'_{drm}}{dt}=\frac{1}{L'_{rr}}[(\omega_{r0}-\omega_{rmi})Mi_{qs}-M\frac{di_{ds}}{dt}+(\omega_{r0}-\omega_{rmi})L'_{rr}i'_{qrm}-r'_{rm}i_{drm}]$$

where $R_s=r_{sg}+r_{sm}, L_{sd}=L_{ss}+L_d, L_{sq}=L_{ss}+L_q$.

By direct substitution between the equations above, each state variable for the current can be solved with considerable amount of work, and the final equations for state variables in the system are in the form of:

$$\frac{di_{qs}}{dt}=D_{qs}[-R_s i_{qs}+(\omega_{r0}Z_{xd}-\omega_{rmi}Z_{xm})i_{ds}-Z_{1q}i'_{qrg}+\omega_{r0}L_{md}i'_{drg}+Z_2 i'_{qrm}-\omega_{rmi}Mi'_{drm}+Z_{3q}v'_{qrg}]$$

$$\frac{di_{ds}}{dt}=D_{ds}[(\omega_{r0}Z_{xq}+\omega_{rmi}Z_{xm})i_{qs}-R_s i_{ds}-\omega_{r0}L_{mq}i'_{qrg}-Z_{1d}i'_{drg}-\omega_{rmi}Mi'_{qrm}+Z_2 i'_{drm}+Z_{3d}v'_{drg}]$$

$$\frac{di_{os}}{dt}=\frac{-1}{L_{lsm}+L_{lsg}}[R_{sg}+R_{sm}]$$

$$\frac{di'_{qrg}}{dt}=D_{qrg}[-R_s i_{qs}+(\omega_{r0}Z_{xd}-\omega_{rmi}Z_{xm})i_{ds}-Z_{4q}i'_{qrg}+\omega_{r0}L_{md}i'_{drg}+Z_2 i'_{qrm}-\omega_{rmi}Mi'_{drm}+Z_{5q}v'_{qrg}] \qquad (3-103)$$

$$\frac{di'_{drg}}{dt}=D_{drg}[(\omega_{r0}Z_{xq}+\omega_{rmi}Z_{xm})i_{qs}-R_s i_{ds}-\omega_{r0}L_{mq}i'_{qrg}-Z_{4d}i'_{drg}-\omega_{rmi}Mi'_{qrm}+Z_2 i'_{drm}+Z_{5d}v'_{drg}]$$

$$\frac{di'_{qrm}}{dt}=D_{qrm}[-R_s i_{qs}+(\omega_{r0}Z_{xdq}-\omega_{rmi}Z_{m1q})i_{ds}-Z_{1q}i'_{qrg}+\omega_{r0}L_{md}i'_{drg}+Z_{6q}i'_{qrm}+(\omega_{r0}Z_{7q}-\omega_{rmi}Z_{m2q})i'_{drm}+Z_{3q}v'_{qrg}]$$

$$\frac{di'_{drm}}{dt}=D_{drm}[(\omega_{r0}Z_{xqd}+\omega_{rmi}Z_{m1d})i_{qs}-R_s i_{ds}-\omega_{r0}L_{mq}i'_{qrg}-Z_{1d}i'_{drg}-(\omega_{r0}Z_{7d}+\omega_{rmi}Z_{m2d})i'_{qrm}+Z_{6d}i'_{drm}+Z_{3d}v'_{qrg}]$$

where the following terms represent impedances in equation (3-103):

$$D_{qs} = \frac{1}{L_{sq}}\left(1-\left(\frac{L_{mq}^2}{L'_{kq}}+\frac{M^2}{L'_{rr}}\right)\Big/L_{sq}\right)^{-1}, \quad D_{ds} = \frac{1}{L_{sd}}\left(1-\left(\frac{L_{md}^2}{L'_{kd}}+\frac{M^2}{L'_{rr}}\right)\Big/L_{sd}\right)^{-1}$$

$$D_{qrg} = \frac{L_{mq}}{L'_{kq}}D_{qs}, \quad D_{drg} = \frac{L_{md}}{L'_{kd}}D_{ds}$$

$$D_{qrm} = \frac{-M}{L'_{rr}}D_{qs}, \quad D_{drg} = \frac{-M}{L'_{rr}}D_{ds}$$

$$Z_{xm} = \frac{M^2}{L'_{rr}}, \quad Z_{xq} = L_{sq} - Z_{xm}, \quad Z_{xd} = Z_{xm} - L_{sd}$$

$$Z_{xdq} = Z_{xd} + \frac{1}{D_{qs}}, \quad Z_{xqd} = Z_{xq} - \frac{1}{D_{ds}}$$

$$Z_{m1q} = Z_{xm} + \frac{1}{D_{qs}}, \quad Z_{m1d} = Z_{xm} + \frac{1}{D_{ds}}$$

$$Z_{1q} = \frac{L_{mq}r'_{qr}}{L'_{kq}}, \quad Z_{1d} = \frac{L_{md}r'_{dr}}{L'_{kd}}$$

$$Z_2 = \frac{Mr'_{rm}}{L'_{rr}}$$

$$Z_{3q} = \frac{L_{mq}}{L'_{kq}}, \quad Z_{3d} = \frac{L_{md}}{L'_{kd}}$$

$$Z_{4q} = Z_{1q} + \frac{r'_{qr}}{L_{mq}D_{qs}}, \quad Z_{4d} = Z_{1d} + \frac{r'_{dr}}{L_{md}D_{ds}}$$

$$Z_{5q} = Z_{3q} + \frac{1}{L_{mq}D_{qs}}, \quad Z_{5d} = Z_{3d} + \frac{1}{L_{md}D_{ds}}$$

$$Z_{6q} = Z_2 + \frac{r'_{rm}}{MD_{qs}}, \quad Z_{6d} = Z_2 + \frac{r'_{rm}}{MD_{ds}}$$

$$Z_{7q} = \frac{L'_{rr}}{MD_{qs}}, \quad Z_{7d} = \frac{L'_{rr}}{MD_{ds}}$$

$$Z_{m2q} = Z_{7q} + M, \quad Z_{m2d} = M - Z_{7d}$$

3.5.1 Load Torque Equation for the Driver Motor

Since the driver motor D0 drives the two generators G_1 and G_2 with their shafts coupled to one another, all three machines are rotating at the same speed of ω_{r0}, and its load torque equation can be derived as follows.

For the driver motor D0, its speed equation is:

$$\frac{d\omega_{r0}}{dt} = \omega_0\left(\frac{T_{e0} - T_L}{2H_0}\right) \tag{3-104}$$

Similarly, the speed equations for generators G_1 and G_2, respectively, are:

$$\frac{d\omega_{r0}}{dt} = \omega_0\left(\frac{T_{I1} - T_{eg1}}{2H_{g1}}\right) \tag{3-105}$$

$$\frac{d\omega_{r0}}{dt} = \omega_0\left(\frac{T_{I2} - T_{eg2}}{2H_{g2}}\right) \tag{3-106}$$

where T_L, T_{eg1} and T_{eg2} are the load torques for D0, G_1 and G_2, respectively. In the no-load case, T_L would have been zero for D0. However, when the shaft of D0 is coupled with G_1 and G_2, the load torque in the driver motor is:

$$T_L = T_{I1} + T_{I2} \tag{3-107}$$

Setting (3-104) equal to (3-105), T_{I1} can be solved as:

$$T_{I1} = \frac{T_{e0} - T_L}{H_0} H_{g1} + T_{eg1} \tag{3-108}$$

Similarly, setting (3-104) equal to (3-106), T_{I2} can be solved as:

$$T_{I2} = \frac{T_{e0} - T_L}{H_0} H_{g2} + T_{eg2} \tag{3-109}$$

Substituting (3-108) and (3-109) into (3-107) gives the load torque equation for D0 as follows:

$$\begin{aligned} T_L &= T_{I1} + T_{I2} \\ &= \frac{T_{em0} - T_L}{H_{m0}} H_{g1} + T_{eg1} + \frac{T_{em0} - T_L}{H_{m0}} H_{g2} + T_{eg2} \\ &= \frac{T_{e0} - T_L}{H_0}\left(H_{g1} + H_{g2}\right) + T_{eg1} + T_{eg2} \\ \therefore T_L &= \frac{1}{H_0 + H_{g1} + H_{g2}}\left[T_{e0}\left(H_{g1} + H_{g2}\right) + H_{m0}\left(T_{eg1} + T_{eg2}\right)\right] \end{aligned} \tag{3-110}$$

3.5.2 Final Mathematical Model for the Entire Test System

The final mathematical model for the entire system of five interconnected machines can now be obtained by making use of equations derived in previous sections.

This model is composed of three sets of state equations. They are for the "driver" motor D0, the System (1) or the G_1/M_1 parallel system, and the System (2) or the G_2/M_2 parallel system. Here is the set of state equations for D0:

$$\frac{di_{qs0}}{dt} = \frac{1}{D}[-L'_{rr}r_{s0}i_{qs0} - L'_{rr}L_{ss}i_{ds0}\omega_{r0} + Mr'_{r0}i'_{qr0} - ML'_{rr}i'_{dr0}\omega_{r0} + L'_{rr}v_{qs0}]$$

$$\frac{di_{ds0}}{dt} = \frac{1}{D}[L'_{rr}L_{ss}i_{qs0}\omega_{r0} - L'_{rr}r_{s0}i_{ds0} + ML'_{rr}i'_{qr0}\omega_{r0} + Mr'_{r0}i'_{dr0} + L'_{rr}v_{ds0}]$$

$$\frac{di_{0s0}}{dt} = \frac{1}{L_{ls0}}[-r_{sm}i_{0s0} + v_{0s0}]$$

$$\frac{di'_{qr0}}{dt} = \frac{1}{D}[Mr_{s0}i_{qs0} + ML_{ss}i_{ds0}\omega_{r0} - L_{ss}r'_{r0}i'_{qr0} + M^2i'_{dr0}\omega_{r0} - Mv_{qs0}]$$

$$\frac{di'_{dr0}}{dt} = \frac{1}{D}[-ML_{ss}i_{qs0}\omega_{r0} + Mr_{sm}i_{ds0} - M^2i'_{qr0}\omega_{r0} - L_{ss}r'_{r0}i'_{dr0} - Mv_{ds0}]$$

$$\frac{di'_{0r0}}{dt} = \frac{-r'_{r0}i'_{0r0}}{L'_{lrm}}$$

$$\frac{d\omega_{r0}}{dt} = \frac{P}{2J_m}[T_{e0} - T_L]$$

$$T_{e0} = \left(\frac{3}{2}\right)\left(\frac{P}{2}\right)M(i_{qs0}i'_{dr0} - i_{ds0}i'_{qr0})$$

$$T_L = \frac{1}{H_0 + H_{g1} + H_{g2}}[T_{e0}(H_{g1} + H_{g2}) + H_0(T_{eg1} + T_{eg2})]$$

} Driver D0

The next set of state equations is for System (1):

$$
\left.
\begin{aligned}
\frac{di_{qs1}}{dt} &= D_{qs1}\left[-R_{s1}i_{qs1} + (\omega_{r0}Z_{xd1} - \omega_{rm1}Z_{xm1})i_{ds1} - Z_{1q1}i'_{qrg1} + \omega_{r0}L_{md1}i'_{drg1} + Z_{21}i'_{qrm1} - \omega_{rm1}M_1 i'_{drm1} + Z_{3q1}v'_{qrg1}\right] \\
\frac{di_{ds1}}{dt} &= D_{ds1}\left[(\omega_{r0}Z_{xq1} + \omega_{rm1}Z_{xm1})i_{qs1} - R_{s1}i_{ds1} - \omega_{r0}L_{mq1}i'_{qrg1} - Z_{1d1}i'_{drg1} - \omega_{rm1}M_1 i'_{qrm1} + Z_{21}i'_{drm1} + Z_{3d1}v'_{drg1}\right] \\
\frac{di_{os1}}{dt} &= \frac{-1}{L_{lsm1} + L_{lsg1}}\left[R_{sg1} + R_{sm1}\right] \\
\frac{di'_{qrg1}}{dt} &= D_{qrg1}\left[-R_{s1}i_{qs1} + (\omega_{r0}Z_{xd1} - \omega_{rm1}Z_{xm1})i_{ds1} - Z_{4q1}i'_{qrg1} + \omega_{r0}L_{md1}i'_{drg1} + Z_{21}i'_{qrm1} - \omega_{rm1}M_1 i'_{drm1} + Z_{5q1}v'_{qrg1}\right] \\
\frac{di'_{drg1}}{dt} &= D_{drg1}\left[(\omega_{r0}Z_{xq1} + \omega_{rm1}Z_{xm1})i_{qs1} - R_{s1}i_{ds1} - \omega_{r0}L_{mq1}i'_{qrg1} - Z_{4d1}i'_{drg1} - \omega_{rm1}M_1 i'_{qrm1} + Z_2 i'_{drm1} + Z_{5d1}v'_{drg1}\right] \\
\frac{di'_{qrm1}}{dt} &= D_{qrm1}\left[-R_{s1}i_{qs1} + (\omega_{r0}Z_{xdq1} - \omega_{rm1}Z_{m1q1})i_{ds1} - Z_{1q1}i'_{qrg1} + \omega_{r0}L_{md1}i'_{drg1} + Z_{6q1}i'_{qrm1} + (\omega_{r0}Z_{7q1} - \omega_{rm1}Z_{m2q1})i'_{drm1} + Z_{3q1}v'_{qrg1}\right] \\
\frac{di'_{drm1}}{dt} &= D_{drm1}\left[(\omega_{r0}Z_{xqd1} + \omega_{rm1}Z_{m1d1})i_{qs1} - R_{s1}i_{ds1} - \omega_{r0}L_{mq1}i'_{qrg1} - Z_{1d1}i'_{drg1} - (\omega_{r0}Z_{7d1} + \omega_{rm1}Z_{m2d1})i'_{qrm1} + Z_{6d1}i'_{drm1} + Z_{3d1}v'_{qrg1}\right] \\
T_{eg1} &= \left(\frac{3}{2}\right)\left(\frac{P}{2}\right)\left[L_{md1}(-i_{ds1} + i'_{drg1})i_{qs1} - L_{mq1}(-i_{qs1} + i'_{qrg1})i_{ds1}\right]
\end{aligned}
\right\} \text{System(1)}
$$

With a change of index from '1' to '2' in System (1), the set of state equations for System (2) can be obtained as follows:

$$
\left.
\begin{aligned}
\frac{di_{qs2}}{dt} &= D_{qs2}\left[-R_{s2}i_{qs2} + (\omega_{r0}Z_{xd2} - \omega_{rm2}Z_{xm2})i_{ds2} - Z_{1q2}i'_{qrg2} + \omega_{r0}L_{md2}i'_{drg2} + Z_{22}i'_{qrm2} - \omega_{rm2}M_2 i'_{drm2} + Z_{3q2}v'_{qrg2}\right] \\
\frac{di_{ds2}}{dt} &= D_{ds2}\left[(\omega_{r0}Z_{xq2} + \omega_{rm2}Z_{xm2})i_{qs2} - R_{s2}i_{ds2} - \omega_{r0}L_{mq2}i'_{qrg2} - Z_{1d2}i'_{drg2} - \omega_{rm2}M_2 i'_{qrm2} + Z_{22}i'_{drm2} + Z_{3d2}v'_{drg2}\right] \\
\frac{di_{os2}}{dt} &= \frac{-1}{L_{lsm2} + L_{lsg2}}\left[R_{sg2} + R_{sm2}\right] \\
\frac{di'_{qrg2}}{dt} &= D_{qrg2}\left[-R_{s2}i_{qs2} + (\omega_{r0}Z_{xd2} - \omega_{rm2}Z_{xm2})i_{ds2} - Z_{4q2}i'_{qrg2} + \omega_{r0}L_{md2}i'_{drg2} + Z_{22}i'_{qrm2} - \omega_{rm2}M_2 i'_{drm2} + Z_{5q2}v'_{qrg2}\right] \\
\frac{di'_{drg2}}{dt} &= D_{drg2}\left[(\omega_{r0}Z_{xq2} + \omega_{rm2}Z_{xm2})i_{qs2} - R_{s2}i_{ds2} - \omega_{r0}L_{mq2}i'_{qrg2} - Z_{4d2}i'_{drg2} - \omega_{rm2}M_2 i'_{qrm2} + Z_2 i'_{drm2} + Z_{5d2}v'_{drg2}\right] \\
\frac{di'_{qrm2}}{dt} &= D_{qrm2}\left[-R_{s2}i_{qs2} + (\omega_{r0}Z_{xdq2} - \omega_{rm2}Z_{m1q2})i_{ds2} - Z_{1q2}i'_{qrg2} + \omega_{r0}L_{md2}i'_{drg2} + Z_{6q2}i'_{qrm2} + (\omega_{r0}Z_{7q2} - \omega_{rm2}Z_{m2q2})i'_{drm2} + Z_{3q2}v'_{qrg2}\right] \\
\frac{di'_{drm2}}{dt} &= D_{drm2}\left[(\omega_{r0}Z_{xqd2} + \omega_{rm2}Z_{m1d2})i_{qs2} - R_{s2}i_{ds2} - \omega_{r0}L_{mq2}i'_{qrg2} - Z_{1d2}i'_{drg2} - (\omega_{r0}Z_{7d2} + \omega_{rm2}Z_{m2d2})i'_{qrm2} + Z_{6d2}i'_{drm2} + Z_{3d2}v'_{qrg2}\right] \\
T_{eg2} &= \left(\frac{3}{2}\right)\left(\frac{P}{2}\right)\left[L_{md2}(-i_{ds2} + i'_{drg2})i_{qs2} - L_{mq2}(-i_{qs2} + i'_{qrg2})i_{ds2}\right]
\end{aligned}
\right\} \text{System(2)}
$$

where the circuit impedances in Systems (1) and (2) are presented in the groups Impedance (1) and (2), respectively, on the following two pages:

$$D_{qs1}=\frac{1}{L_{sq1}}\left(1-\left(\frac{L_{mq1}^2}{L'_{kq1}}+\frac{M_1^{\,2}}{L'_{rr1}}\right)\Big/L_{sq1}\right)^{-1},\qquad D_{ds1}=\frac{1}{L_{sd1}}\left(1-\left(\frac{L_{md1}^2}{L'_{kd1}}+\frac{M_1^{\,2}}{L'_{rr1}}\right)\Big/L_{sd1}\right)^{-1}$$

$$D_{qrg1}=\frac{L_{mq1}}{L'_{kq1}}D_{qs1},\qquad D_{drg1}=\frac{L_{md1}}{L'_{kd1}}D_{ds1}$$

$$D_{qrm1}=\frac{-M_1}{L'_{rr1}}D_{qs1},\qquad D_{drg1}=\frac{-M_1}{L'_{rr1}}D_{ds1}$$

$$Z_{xm1}=\frac{M_1^{\,2}}{L'_{rr1}},\qquad Z_{xq1}=L_{sq1}-Z_{xm1},\qquad Z_{xd1}=Z_{xm1}-L_{sd1}$$

$$Z_{xdq1}=Z_{xd1}+\frac{1}{D_{qs1}},\qquad Z_{xqd1}=Z_{xq1}-\frac{1}{D_{ds1}}$$

$$Z_{m1q1}=Z_{xm1}+\frac{1}{D_{qs1}},\qquad Z_{m1d1}=Z_{xm1}+\frac{1}{D_{ds1}}$$

$$Z_{1q1}=\frac{L_{mq1}r'_{qr1}}{L'_{kq1}},\qquad Z_{1d1}=\frac{L_{md1}r'_{dr1}}{L'_{kd1}}$$

$$Z_{21}=\frac{M_1r'_{rm1}}{L'_{rr1}}$$

$$Z_{3q1}=\frac{L_{mq1}}{L'_{kq1}},\qquad Z_{3d1}=\frac{L_{md1}}{L'_{kd1}}$$

$$Z_{4q1}=Z_{1q1}+\frac{r'_{qr1}}{L_{mq1}D_{qs1}},\qquad Z_{4d1}=Z_{1d1}+\frac{r'_{dr1}}{L_{md1}D_{ds1}}$$

$$Z_{5q1}=Z_{3q1}+\frac{1}{L_{mq1}D_{qs1}},\qquad Z_{5d1}=Z_{3d1}+\frac{1}{L_{md1}D_{ds1}}$$

$$Z_{6q1}=Z_{21}+\frac{r'_{rm1}}{M_1D_{qs1}},\qquad Z_{6d1}=Z_{21}+\frac{r'_{rm1}}{M_1D_{ds1}}$$

$$Z_{7q1}=\frac{L'_{rr1}}{M_1D_{qs1}},\qquad Z_{7d1}=\frac{L'_{rr1}}{M_1D_{ds1}}$$

$$Z_{m2q1}=Z_{7q1}+M_1,\qquad Z_{m2d1}=M_1-Z_{7d1}$$

} Impedance(1)

$$D_{qs2}=\frac{1}{L_{sq1}}\left(1-\left(\frac{L_{mq2}^2}{L'_{kq2}}+\frac{M_2^{\,2}}{L'_{rr2}}\right)\Big/L_{sq2}\right)^{-1},\qquad D_{ds2}=\frac{1}{L_{sd2}}\left(1-\left(\frac{L_{md2}^2}{L'_{kd2}}+\frac{M_2^{\,2}}{L'_{rr2}}\right)\Big/L_{sd2}\right)^{-1}$$

$$D_{qrg2}=\frac{L_{mq2}}{L'_{kq2}}D_{qs2},\qquad D_{drg2}=\frac{L_{md2}}{L'_{kd2}}D_{ds2}$$

$$D_{qrm2}=\frac{-M_2}{L'_{rr2}}D_{qs2},\qquad D_{drg2}=\frac{-M_2}{L'_{rr2}}D_{ds2}$$

$$Z_{xm2}=\frac{M_2^{\,2}}{L'_{rr2}},\qquad Z_{xq2}=L_{sq2}-Z_{xm2},\qquad Z_{xd2}=Z_{xm2}-L_{sd2}$$

$$Z_{xdq2}=Z_{xd2}+\frac{1}{D_{qs2}},\qquad Z_{xqd2}=Z_{xq2}-\frac{1}{D_{ds2}}$$

$$Z_{m1q2}=Z_{xm2}+\frac{1}{D_{qs2}},\qquad Z_{m1d2}=Z_{xm2}+\frac{1}{D_{ds2}}$$

$$Z_{1q2}=\frac{L_{mq2}r'_{qr2}}{L'_{kq2}},\qquad Z_{1d2}=\frac{L_{md2}r'_{dr2}}{L'_{kd2}}$$

$$Z_{22}=\frac{M_2r'_{rm2}}{L'_{rr2}}$$

$$Z_{3q2}=\frac{L_{mq2}}{L'_{kq2}},\qquad Z_{3d2}=\frac{L_{md2}}{L'_{kd2}}$$

$$Z_{4q2}=Z_{1q2}+\frac{r'_{qr2}}{L_{mq2}D_{qs2}},\qquad Z_{4d2}=Z_{1d2}+\frac{r'_{dr2}}{L_{md2}D_{ds2}}$$

$$Z_{5q2}=Z_{3q2}+\frac{1}{L_{mq2}D_{qs2}},\qquad Z_{5d2}=Z_{3d2}+\frac{1}{L_{md2}D_{ds2}}$$

$$Z_{6q2}=Z_{22}+\frac{r'_{rm2}}{M_2D_{qs2}},\qquad Z_{6d2}=Z_{22}+\frac{r'_{rm2}}{M_2D_{ds2}}$$

$$Z_{7q2}=\frac{L'_{rr2}}{M_2D_{qs2}},\qquad Z_{7d2}=\frac{L'_{rr2}}{M_2D_{ds2}}$$

$$Z_{m2q2}=Z_{7q2}+M_2,\qquad Z_{m2d2}=M_2-Z_{7d2}$$

} Impedance(2)

3.6 Computer Simulation of the Test System

In order to illustrate the computer simulation of the test system, a block diagram in Figure 3.10 is created to show the interactions among the five machines involved. The first group of computational blocks at the top half of this diagram compute the set of state current equations, the electric torque T_{e0} and the rotor speed ω_{r0} for the "driver" motor

D0. The transformations here are defined by the matrix K_s^r because the machine equations are written in rotor reference frame.

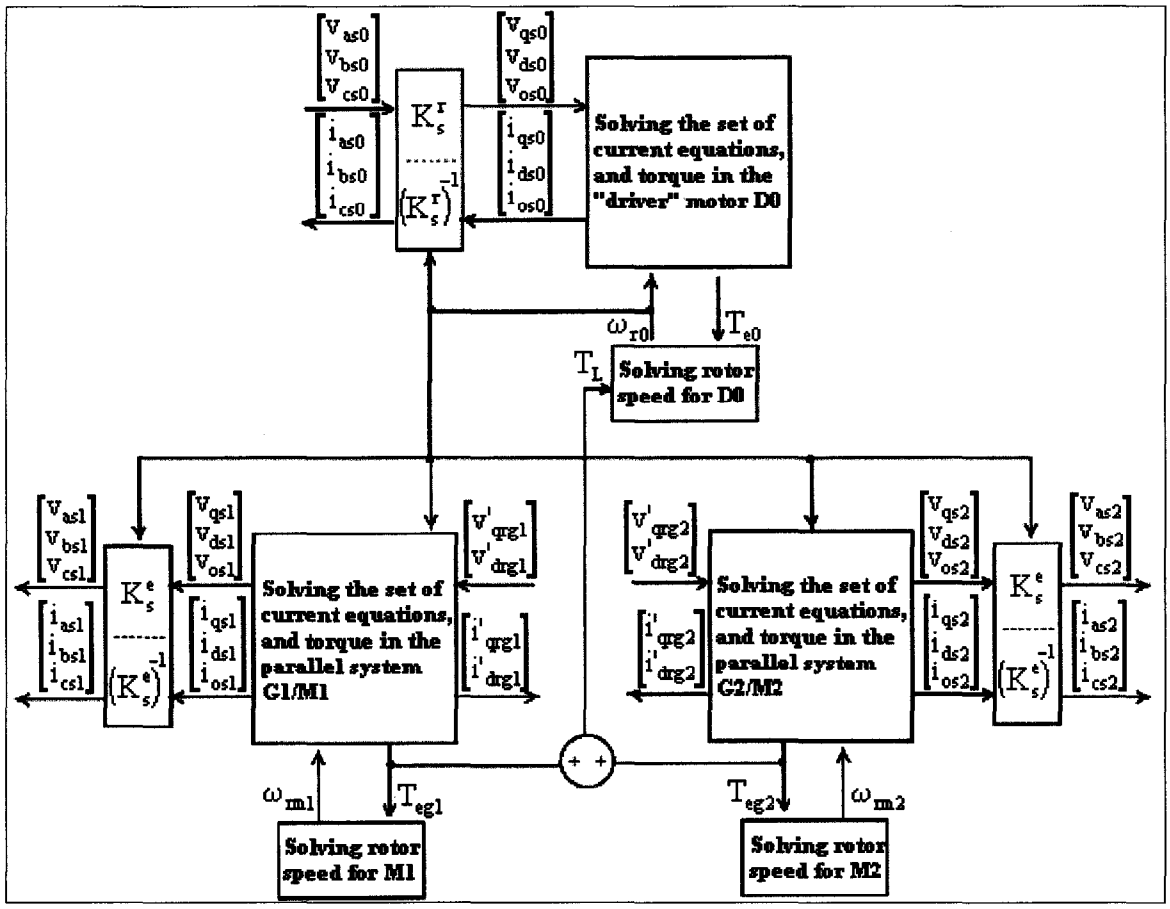

Figure 3.10: *Simulation of the test system shown in block diagram form*

Since the motor D0 is the prime mover for the entire test system, the most important output variable from the first group of functional blocks is the rotor speed ω_{r0} because not only is it used as feedback input to the transformation matrix K_s^r for the motor D0, but it is also used as the synchronously rotating speed for input to the matrix K_s^e and the computational blocks for the parallel systems G_1/M_1 and G_2/M_2 at the bottom half of the block diagram. Each group of these computational blocks accept the excitation voltages v'_{qri} and v'_{dri} as input variables, and solve the set of stator currents, the torque T_{egi} and the rotor speed ω_{rmi} for the test motor M_i, where the subscript index "i" denotes either System (1) or (2). Since the motor D0 has its rotor shaft coupled with those of the

generator G_1 and G_2, the combination of electric torques T_{egl} and T_{eg2} produced in both parallel systems serves as a load torque T_L to the driver motor D0. As a result, the rotor speed ω_{r0} is not only affected by its own electric torque T_{e0}, but it is also affected by the combined electric torques T_{egl} and T_{eg2}, and that is how the five machines are interrelated.

In each computational block, the set of current equations are solved using the Runge-Kutta fourth-order method. Such high order formula takes far fewer arithmetic operations as compared with the lower order methods; as a result, it is less badly affected by rounding errors. The Runge-Kutta method is more convenient to use than the Taylor series because no differentiation is needed in the computation [16].

3.7 Conclusion

In this chapter, the first objective of the thesis research has been met by deriving a complete mathematical model for the test system of five interconnected machines. Then the model representing the machine system can be simulated on the computer by solving the sets of current equations using the Runge-Kutta fourth-order numerical method. All the results obtained from simulating this test system will be presented in chapter five, and will be compared with the actual experimental data to determine the viability of different techniques used in suppressing the power oscillation through the "driver" motor D0.

Chapter 4

MACHINE AND EQUIPMENT SETUP

4.1 Introduction

This chapter will give a full description of each machine, equipment, module, metering instruments, and power electronic components used in the test setup for the thesis experiment. As shown in Figure 2.6 of section 2.2.3, five machines were required in order to carry out the new phase modulation method for performing heat run test on an induction motor. Two of these machines were identical 2-kW wound-rotor induction machines, used for implementing the synchronous generators G_1 and G_2, while the other three were identical 2-kW squirrel-cage induction motors used for the "driver" motor D0, test motor M_1 and the "recovery" motor M_2. All five machines were readily available as part of the *Lab-Volt 2-kW Electromechanical Training System*, as used by the Power Research Laboratory at McMaster University to educate engineering students on theories and techniques associated with the generation and use of electrical energy. The following table shows a list of machines, equipments, modules, metering instruments, and power electronic components necessary for setting up the test system in Figure 2.6.

Table 4.1: List of equipments used in the test setup

Description	**Quantity**
Four-pole squirrel-cage induction machine	3
Wiring module for squirrel-cage induction machine	3
Wound-rotor induction machine	2
Wiring module for wound-rotor induction machine	2
Power supply module	3
AC Ammeter	3
AC Voltmeter	3
DC Volt/Ammeter	4
Current transformer	5
Oscilloscope	4
Voltage probe	8
Function generator	1
Three-phase variac	2
Three-phase transformer	2
Inverter	2

In order to deal with such a large variety of equipments used in the test setup, all items have been sorted out into different groups according to the power level with which they were involved, and each group will be explained in a separate section in the chapter to reflect clearly the role of each piece of equipment used in the test setup. Thus, section 4.2 will give a general description of the *Lab-Volt 2-kW Electromechanical Training System*, and detailed explanations on the design and construction of individual *Lab-Volt* machines and modules used. Section 4.3 illustrates the test setup by showing how each machine was connected to the power source, and how each power source was available and configured in order to meet the power requirement in the experiment. The design and implementation, and usage of electronic control circuits will be discussed in section 4.4. Section 4.5 will show how experimental data were acquired, and how electrical quantities were obtained. The last section 4.6 deals with estimating parameter values of an induction machine by applying the *DC resistance* test, the *blocked-rotor* test, and the *minimum-slip* test to each phase of the machine windings. The parameter values will be approximated based on the model of equivalent circuit of an induction machine. The reason for conducting the three tests above will also be discussed in this section.

4.2 The *Lab-Volt* 2-kW Electromechanical Training System

The *Lab-Volt 2-kW Electromechanical Training System*, Model 8013, is a modular system in electric power technology. The system consists of several modules, each of which can be inserted into a mobile workstation, Model 8110. The modules were constructed from heavy-gauge steel, finished in baked enamel. Symbols and diagrams specific to each module were clearly silk-screened on the faceplates. Standard color-coded safety 4-mm jacks were used on these faceplates to interconnect all system components.

Each Lab-Volt 2-kW machine was permanently mounted on a mobile cart, and included a double-extension shaft terminated with geared-type flanges. Different machines may be joined with a hard rubber coupling device and a locking fastener designed to eliminate vibrations [17]. Any combination of machines may be studied simultaneously.

The machines have a relatively high inertia, with a continuous service factor. The insulation class of the machines is B (80° temperature rise), and the construction of the open type. In addition, all machines are equipped with search coils through which the magnetic flux distribution at various locations in the machine can be observed on an oscilloscope. All machine windings are brought out to the faceplate of a connection module through a 3-m (10-ft) long, heavy-duty, interconnecting cable fitted with a keyed connector; therefore, a particular machine can only be connected to its associated connection module. That is, all windings in a machine are individually accessible on the faceplate of the connection module associated with that machine [17].

Power windings are terminated on 4-mm color-coded safety jacks and search coils on 2-mm banana jacks. The different size jacks prevent accidental connections between the power windings and the search coils. The connection modules are fitted into half-size modules, and they must be placed at the bottom of a full height section in a workstation to allow connection. The following subsections will give brief description of individual *Lab-Volt* module used in the test setup.

4.2.1 Four-pole Squirrel-cage Induction Machine – Model 8503

The four-pole squirrel-cage induction motor (Figure 4.1) consists of a 3-phase

Figure 4.1: *Four-pole squirrel-cage induction machine – Model 8503*

machine rated at 2 kW. Each phase of the stator winding is accessible via the connection module to allow wye or delta connections. The machine is equipped with a standard cast-aluminum squirrel-cage rotor. The winding dimensions permit the study of machine operation as a squirrel-cage induction motor or as an asynchronous generator when driven by a prime mover. The machine has a 5-turn, full-pitch stator search coil to allow the observation of the instantaneous flux distribution [17].

4.2.2 Wiring Module For Squirrel-cage Induction Machine – Model 8504

The wiring module for squirrel-cage induction motor (SCIM) consists of a connection module. It provides connection access to the four-pole squirrel-cage induction motor from the mobile workstation through a flexible connecting cable. The module has six 4-mm color-coded safety jacks numbered from 1 to 6 for the power windings and two 2-mm jacks for the stator search coil. Jacks of different sizes prevent accidental connections between the power windings and the search coil [17]. As mentioned earlier, the schematic diagram for making electrical power connection to the squirrel-cage induction motor was readily silk-screened on the faceplate of the module. The drawings of three-phase stator windings are shown on the left, and the squirrel-cage rotor is shown on the right. Figure 4.2 shows a picture of the module with wiring diagram on the faceplate, and a socket at the back of the module for connection access to the flexible, heavy-duty cable from the squirrel-cage induction machine.

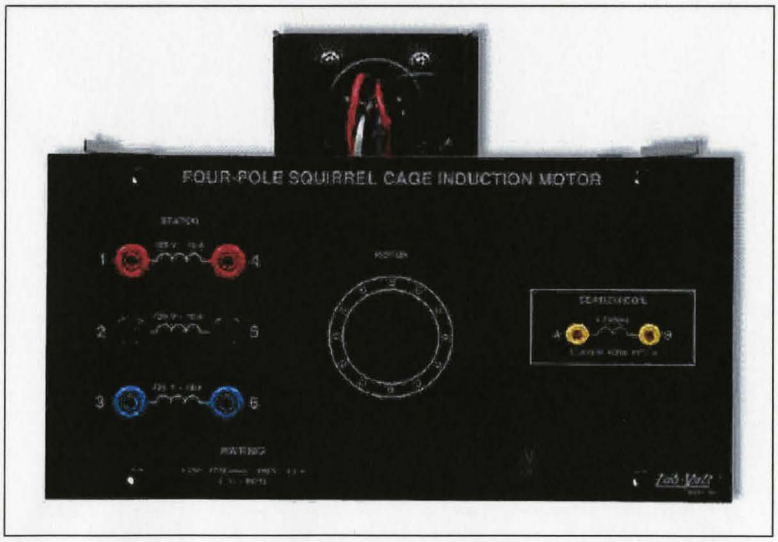

Figure 4.2: *Wiring module for squirrel-cage induction machine – Model 8504*

4.2.3 Three-phase Wound-rotor Induction Machine – Model 8505

The three-phase wound-rotor induction motor consists of a 4-pole machine rated at 2 kW. Each phase of the stator winding is accessible via the connection module to allow wye or delta connections. The rotor is wye connected to four slip rings to give access to all windings, including neutral. The winding dimensions permit the study of machine operation as a wound-rotor induction motor, a frequency converter, a phase-shifter, a position controller, a variable-coupling single-phase transformer, a three-phase transformer, and an asynchronous induction generator. The machine also has three search coils permitting observation of the flux distribution at one pole of the stator, at one tooth, and at the full-pitch of the rotor. Below is a picture of the wound-rotor induction machine (Figure 4.3). From the exterior, it looks identical to the squirrel-cage induction machine with the 3-m long, heavy-duty cable readily mounted on the on a mobile cart. The frames of the machines are equipped with transparent shatter-proof shields for inspection of the interior [17].

Figure 4.3: *Three-phase wound-rotor induction machine - Model 8505*

4.2.4 Wiring Module For Wound-rotor Induction Machine – Model 8606

The wiring module for wound-rotor induction motor (WRIM) consists of a connection module. It provides connection access to the three-phase wound-rotor induction motor from the mobile workstation through a flexible connecting cable. The module has ten 4-mm color-coded safety jacks numbered from 1 to 10 for the power windings and six 2-mm jacks for the search coils. Jacks of different sizes prevent accidental connections between the power windings and the search coils [17]. Figure 4.4 shows the wiring module with schematic diagram silk-screened on the faceplate.

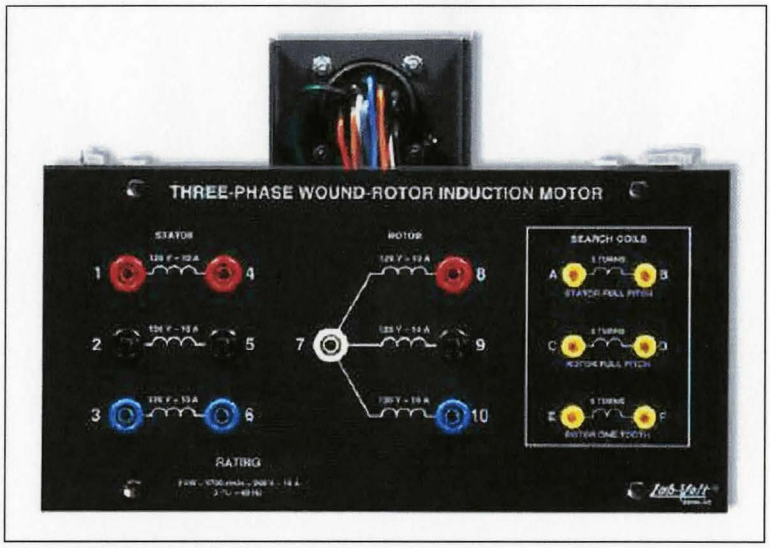

Figure 4.4: *Wiring module for wound-rotor induction machine - Model 8506*

Analogous to the wiring module for squirrel-cage induction machine, the drawings for three-phase stator windings are shown on the left, and those for the wye-connected rotor windings are depicted on the right. The back of the module also has a socket for connection access to the wound-rotor induction machine through the flexible, heavy-duty cable.

4.2.5 Power Supply Module – Model 8525

The power supply (PS) module is the primary component of the *Lab-Volt Electromechanical Training system*. All associated equipments are powered by this power supply. A flexible, 5-wire power cord, terminated with a 5-prong, twist-lock plug and line cap, feeds the module. A mechanical interlock on the line cap was designed to prevent the removal of an energized power supply from its locked position in the

workstation. The power supply requires a 3-phase, wye-connected, 5-wire service installation. An appropriate wall outlet was shipped with each power supply so that site power can be properly terminated to receive the power cord. In addition to the 3-phase legs and the neutral, a separate copper ground provides proper grounding for the power supply chassis and workstation cabinets, thus ensuring added safety when the equipment is used. The power supply provides fixed and variable AC and DC voltage sources all terminated with 4-mm safety jacks. They can be used simultaneously, up to a total load current equal to the rating of the fixed 3-phase output. The voltage level of both variable AC and DC voltage sources can be controlled by adjusting the power knob from 0 to 100. Figure 4.5 below shows clearly that the three-phase variable AC supply can be accessed

Figure 4.5: *The power supply module - Model 8525*

at jacks 4, 5, and 6, and the variable DC supply at jack 7. However, the fixed AC supply can be obtained at jacks 1, 2, and 3, and the fixed DC supply at jack 8. Independent circuit breakers and the reset button at the front panel protect the power supply inputs and outputs. Indicator lamps monitor the presence of input voltage in each phase. When a

phase leg of the site power service is out, the lamp goes off to reflect this condition. A voltmeter, connected through a selector switch, monitors the outputs [17].

4.2.6 AC Ammeter Module – Model 8514

The AC Ammeter module consists of three separate multi-range AC Ammeters for simultaneous measurement of three-phase currents. Two of the three meters have identical ranges while the third instrument has one additional higher range for measurement of the starting current of single-phase motors. Figure 4.6 shows that connections are also made through 4-mm color-coded jacks [17].

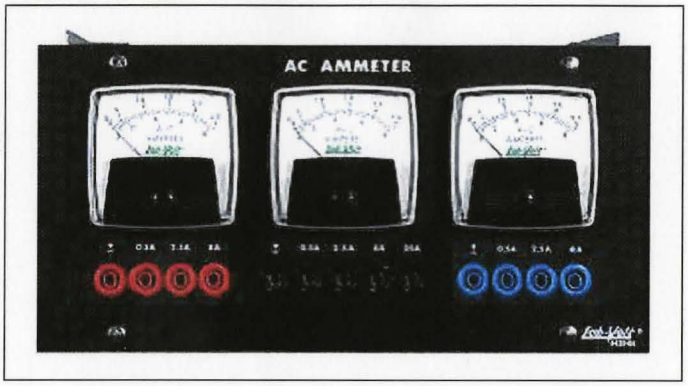

Figure 4.6: *AC Ammeter - Model 8514*

4.2.7 AC Voltmeter Module – Model 8426

The AC Voltmeter module is fitted with three separate multi-range AC voltmeters for simultaneous measurement of three-phase voltages (Figure 4.7) [17].

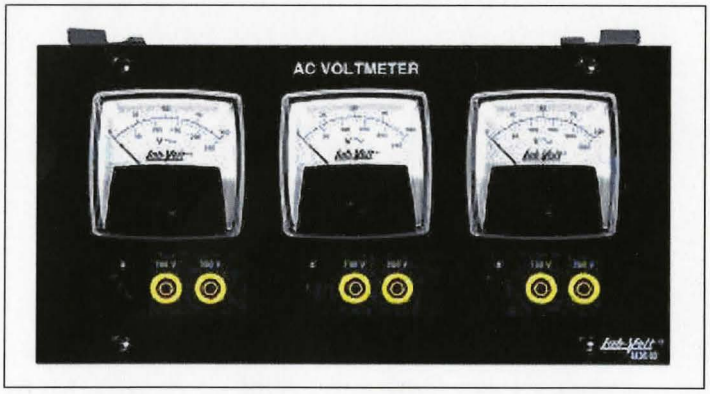

Figure 4.7: *AC Voltmeter - Model 8426*

4.2.8 DC Volt/Ammeter Module – Model 8513

The DC Voltmeter/Ammeter consists of one voltmeter, one milli-ammeter, and one ammeter. Ranges have been selected to facilitate the simultaneous measurement of the voltage, the shunt field current, and the armature current of the DC Motor/Generator. Connections are made through 4-mm color-coded jacks (Figure 4.8) [17].

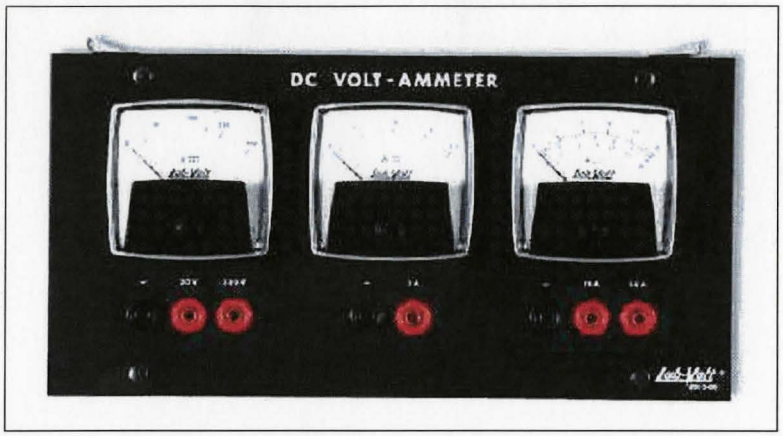

Figure 4.8: *DC Volt/Ammeter - Model 8513*

4.3 Machine Setup

In order to provide a clear explanation of how the five machines were set up for the thesis experiment, this section is divided into two separate parts, each of which consists of schematic diagrams of electrical connection and arrangement of power electronic components required for the test setup. The first part will show wiring connection made between the "driver" motor D0 and the power supply module, and how synchronous generator G_i was connected to motor M_i in each of the two parallel systems. The last part will explain how different DC power supplies were obtained, and specify their arrangement with the corresponding rotor windings in each synchronous generator such that correct phase modulation can be achieved.

4.3.1 Electrical Wiring Connecting Modules

Before making any wiring connection, all the *Lab-Volt* modules were inserted into the mobile workstations and organized to form three separate groups. The first group is for connecting power to the "driver" motor D0. The second and third groups are identical to one another, and they are used for wiring up the parallel Systems (1) and (2) as

previously shown in Figure 2.6. In order to accommodate all the modules and arrange them in an orderly fashion, two mobile workstations were employed, and they were placed side by side as shown in Figure 4.9. The areas shaded in grey on the drawings of each mobile workstation indicate empty areas of no *Lab-Volt* modules.

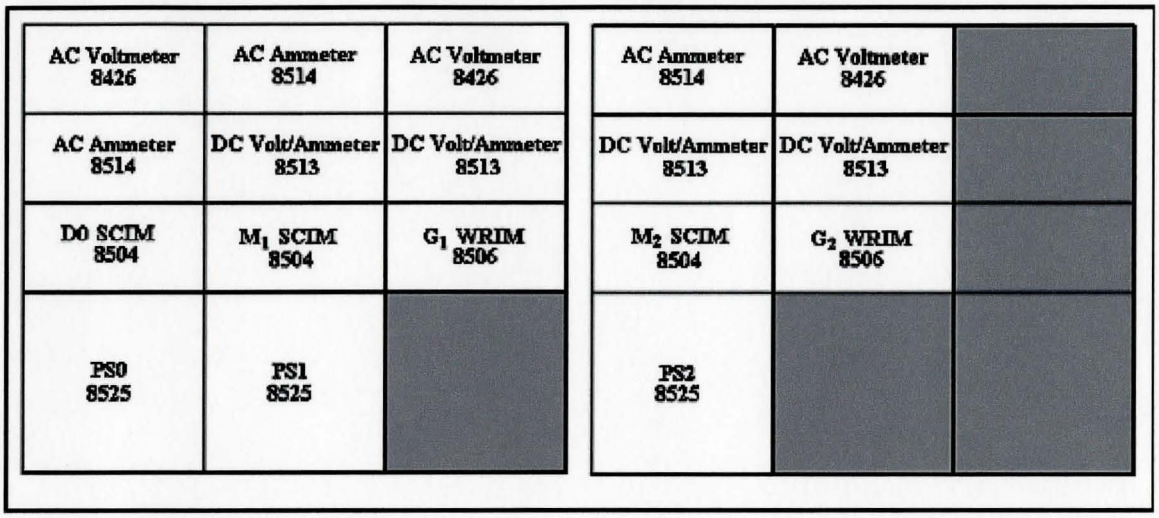

Figure 4.9: *Arrangement of the Lab-Volt modules on two mobile workstations*

Once the *Lab-Volt* modules have been correctly arranged, wiring connection can start with the first group of four modules located in the first column on the first mobile workstation on the left. This group of modules was used to connect the power supply to the "driver" motor D0, and monitor the line currents and voltages feeding into the motor's stator windings. As shown in Figure 4.10, the motor was wye-connected with

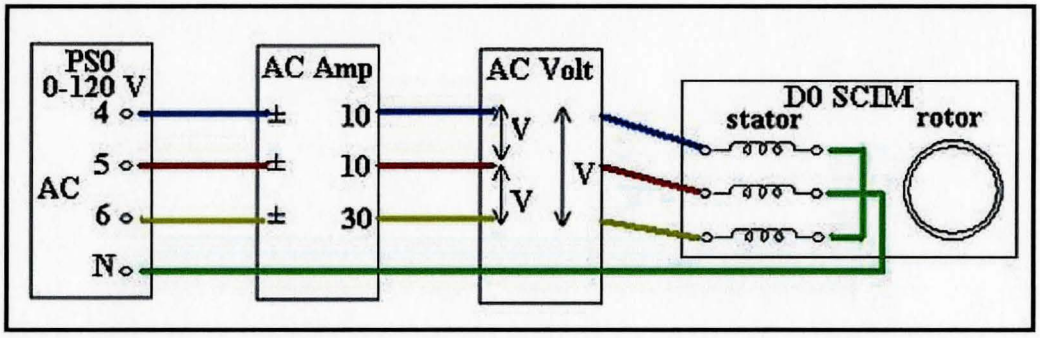

Figure 4.10: *D0 connection to the power supply*

each of its stator windings connected to the phase power on the variable AC power supply. Each line current was monitored with the Ammeter in series with the stator winding, while the line voltage was measured between the phase windings. The Ammeter was very useful in ensuring that the stator currents did not exceed 15 A at the start-up of

motor D0. Before starting the motor, the power supply must be set to zero by turning its control knob to the counter-clockwise direction. Once the motor attained its synchronous speed, the supply voltage was applied to the stator windings until the AC Voltmeter indicated that the rated line voltages of 208 V have been reached.

The second group consisted of the remaining modules on the first mobile workstation minus the power supply PS1, while the third one contained all the modules on the second workstation except the power supply PS2. The two power supplies were not need here; however, they were reserved for providing excitation voltages to the rotor windings in the generators. Since the two groups were identical (Figure 4.9), only one schematic diagram will be shown on the next page to illustrate electrical connection among the modules. As described in section 3.1, the "driver" motor D0, the synchronous generators G_1 and G_2 were coupled together shaft to shaft. Thus, each generator was driven by the "driver" motor D0 and electrical power was produced at the stator winding terminals of the generator. Since the output power from generator G_i was used as input power to motor M_i in System (i), both machines shared the same stator voltages and currents. Due to the phase modulating action imposed on rotor windings in each generator, the voltages and currents produced in System (i) were modulated according to the frequency applied. Figure 4.11 below shows the wiring connection between G_i and M_i,

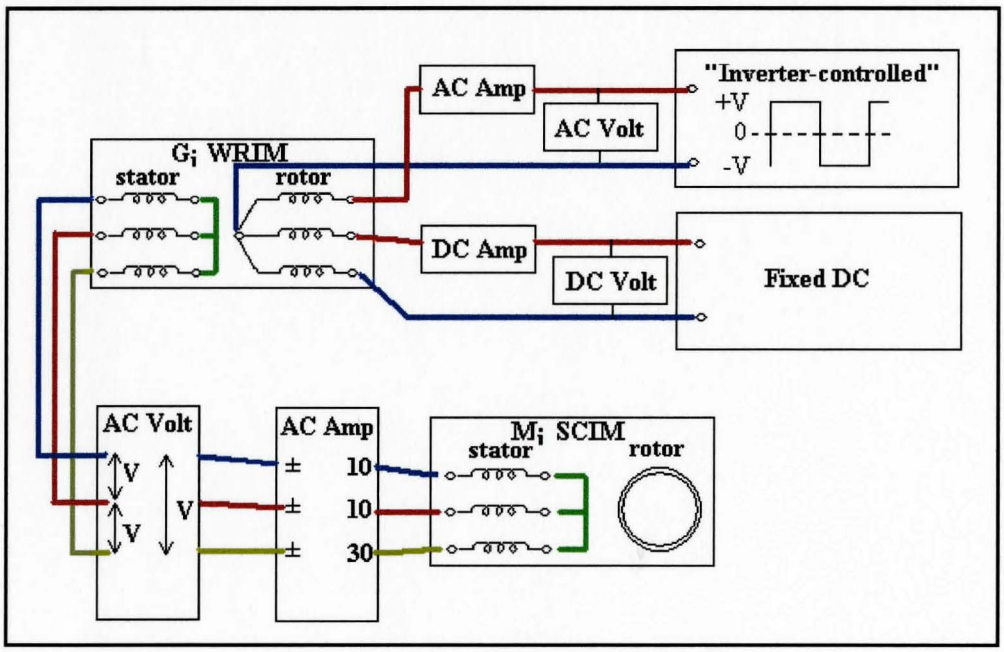

Figure 4.11: *Wiring connection between generator G_i and motor M_i*

and how the electrical quantities were monitored with the *Lab-Volt* metering modules. The line currents and voltages in the stator windings of both generator G_i and motor M_i here were measured the same way as those monitored between D0 and the power supply module (Figure 4.10). Instead of getting power from the power supply module, each motor M_i in this part received power by having its stator windings connected to those of the generator G_i. As illustrated in Figure 4.11, the phase modulation in output power of each generator was obtained by a combined action of the square-wave "inverter-controlled" source voltage and the fixed DC source applied to the rotor's direct-axis winding and the quadrature-axis windings, respectively. Details on how to implement the inverter-controlled source voltage will be given later in section 4.4. Since the inverter's switching action forced the direct-axis winding voltage to take a square wave, which is an AC waveform, the voltage and current induced in this winding were monitored with the AC Voltmeter and AC Ammeter, respectively, while the DC Volt/Ammeter was used to measure the voltage and current in the quadrature-axis winding.

4.3.2 DC Power Supplies For Rotor Windings

In order to provide a matching power exchange between Systems (1) and (2), the magnitude of excitation voltage for the generator in one system must be equal to the excitation voltage in the other system. This means that the excitation voltage applied to individual rotor windings in one generator must be equal to the excitation voltage applied to the corresponding rotor windings in the other generator. Therefore, the square-wave source voltage in generator G_1 must have the same magnitude as the square-wave source voltage in generator G_2, and the magnitude of the fixed DC voltage in generator G_1 must also be equal to its counterpart in generator G_2.

Between the two source voltages above, the fixed DC source was readily available on the *Lab-Volt* power supply module, and its arrangement with the rotor windings was fairly straight forward. Intuitively, two power supply modules would have been required, one for each fixed DC source in individual generator. As discussed in the above paragraph, however, both generators required the same magnitude of DC voltage to excite each of their quadrature-axis rotor windings. This means that the two generators can share the same DC voltage for their quadrature-axis rotor windings by connecting

one winding in parallel to the other, and then connecting them in parallel to the variable DC supply on the power supply module PS2.

Figure 4.12 below shows the wiring configuration between the fixed DC source voltage and the two quadrature-axis rotor windings in both generators. Since the current rating on each winding was 10 A, connecting both in parallel would result with a total current drawn of 20 A from the variable DC supply. This current was well under the rated current of 25 A on the power supply module; therefore, the operating condition specified by *Lab-Volt* on the module was satisfied here.

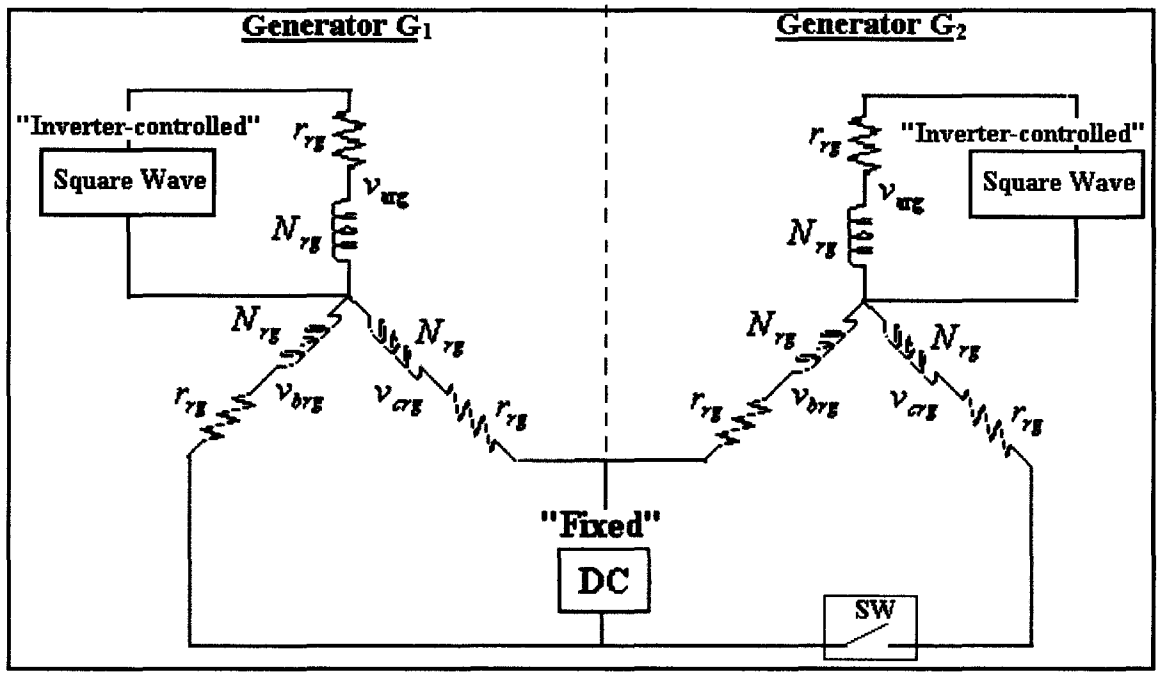

Figure 4.12: *Wiring configuration for the source voltages and the windings*

In addition to showing the wiring configuration, the above figure also shows the switch SW on the rotor winding of generator G_2. The purpose of this switch was to start each parallel system sequentially. Due to the unbalance of machine properties between the two systems, applying excitation voltage to the rotor windings in both generators to start the motors M_1 and M_2 simultaneously can result in over-rated current in the rotor winding in one of the generators. This is because one of the motor may require higher starting current than the other, and, in turn, demand larger input stator voltage from its generator. Consequently, more voltage is required to excite the generator's rotor winding. Because of the parallel connection to the fixed DC supply, the excitation voltage of rotor winding in the other generator is also increased. If the rotor winding in one generator experiences

an over-rated current, the other one parallel to it also experiences the same thing. Since starting an induction motor might require a fairly long time, sustaining an over-rated current for a prolonged period can result in extensive thermal damage to the rotor windings in both generators. This was the reason why the switch SW was used to allow one parallel system to begin after the other was properly started. Figure 4.13 shows a more detailed wiring connection between the modules and how winding currents and voltages were monitored with DC Volt/Ammeters. That is, when the fixed DC source

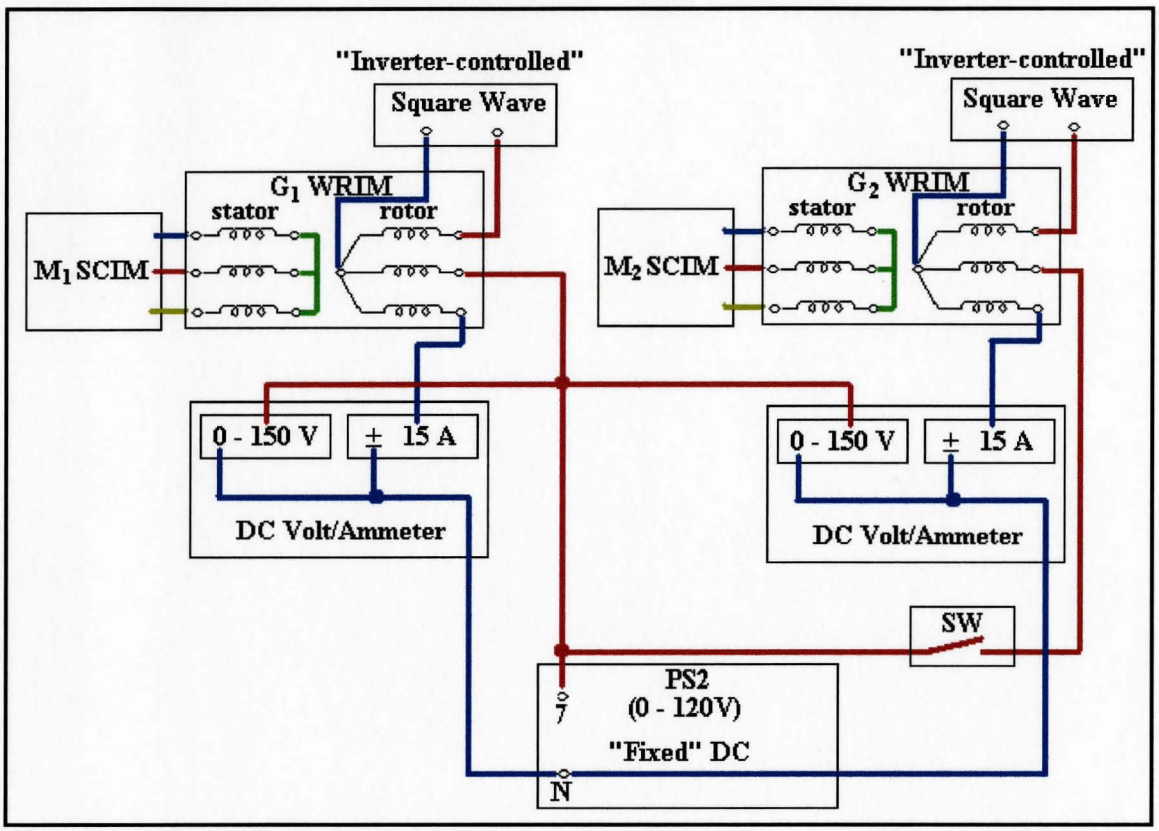

Figure 4.13: *Detailed wiring of how DC2 was shared*

voltage was applied to the quadratuer-axis rotor winding of generator G_1 the switch was left open. Once the motor M_1 in System (1) reached synchronous speed, the switch was closed to start up the motor M_2 in System (2), resulting in an immediate drop in the level of excitation voltage applied to both rotor field windings. Turning the control knob clock-wise on the power supply module increased the excitation voltage back to the level where System (1) was before closing the switch. Since the motor M_2 could not attain synchronous speed at this level, the DC source voltage must be increased further to allow M_2 to reach its synchronous speed. During the process, the rotor windings in both

generators experienced over-rated current; however, the duration of time the rotor winding in generator G_2 being exposed to this current was significantly shortened with such switching sequence.

The next part will describe how the DC voltage source was set up to supply the inverter for producing a square-wave source voltage to modulate the excitation voltage applied to the direct-axis rotor winding in each generator. Although the magnitude of excitation voltage was the same in each generator, the phase of modulation, however, must be opposite between the two inverter-controlled sources. This required the DC voltage source of the inverter used for one generator to be completely isolated from the corresponding power supply for the other generator, and both must have floating grounds so they could be isolated from the fixed DC source voltage. The purpose of isolation between the three source voltages was to prevent the ground loop problem which usually occurs when two or more devices are connected to a common ground through different paths. Without proper isolation, currents flow through these multiple paths and develop voltages which can cause serious damage to all the machines and equipments used. Thus, isolation is crucially important in preventing damage and ensuring correct operation of the equipments. Below is a schematic drawing showing how isolation was done, and the setup of the DC power supply for the inverter. Since both parallel systems required the same setup, only one diagram is shown here.

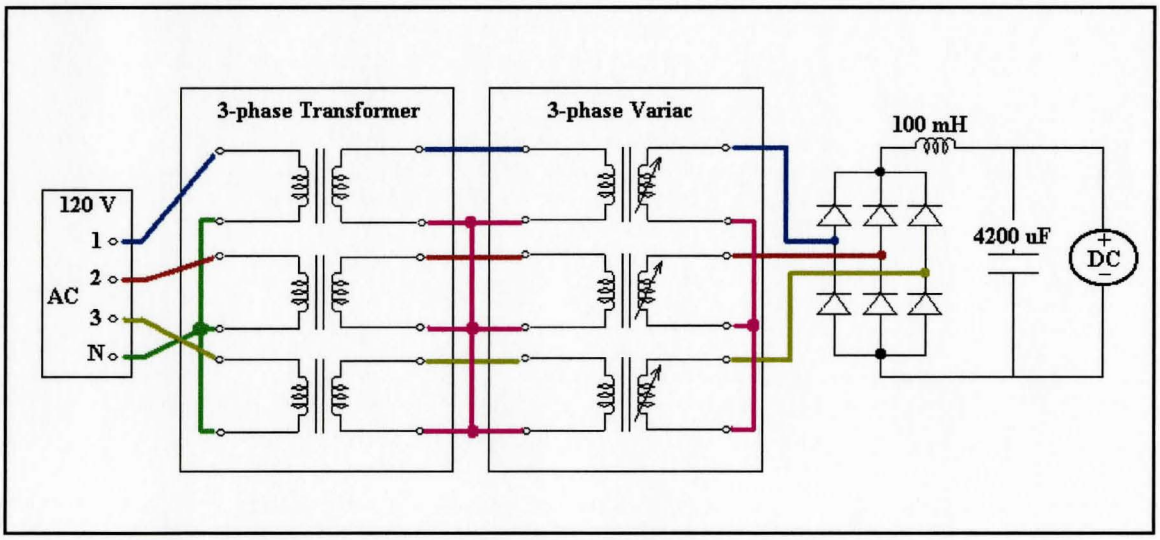

Figure 4.14: *Setup of the DC voltage source for the inverter*

In order to isolate the power supply of the inverter from the ground of the fixed DC source, a three-phase isolation transformer with winding ratio of 1:1 was used. The fixed AC input voltage of 120 V was obtained by connecting the wye-connected primary windings of the transformer to terminals 1, 2, and 3 on the power supply module. Through the transformer's wye-connected secondary windings, the induced output voltage on the secondary side acquired an automatically floating ground. Since the secondary voltage was fixed at 120 V AC, a three-phase variable transformer or variac must be used in order to obtain the ability to vary the level of the DC supply voltage. Hence, the secondary output voltage was directly fed into the three input terminals of the variac, whose output voltage was then used as input for the three-phase bridge rectifier. The purpose of using this three-phase bridge rectifier was to obtain a DC voltage from the AC output voltage of the variac. Due to the rectifier's action, the DC voltage was produced with a ripple which must be filtered out by connecting an LC filter to the output terminals of the rectifier. The result was a smooth DC voltage, which can be used as the DC supply for the H-bridge inverter. Details of how this inverter was designed will be explained next.

4.4 Design and Implementation of the H-Bridge Inverter

In previous studies [5], modulation of the excitation currents i_1 and i_2 in the rotor windings of each generator was performed by switching the DC voltage source in a bang-bang mode with a DC chopper, while keeping the DC voltage source at a fixed value. Due to the reactance of the rotor windings, the chopper's "on/off" action caused the excitation current i_1 to vary exponentially between zero and a maximum value. The current waveform was repeated periodically according to the chopper's frequency. As shown in section 2.2.1, the phase angle of the supply voltage β_s can be computed with the excitation currents as follows:

$$\beta_s = \left(\frac{180°}{\pi}\right) \cdot \tan^{-1}\left(\frac{i_1}{i_2}\right) \qquad (4\text{-}1)$$

Since the DC voltage source for the chopper was kept constant, the excitation current i_2 in equation (4-1) above would never go to zero. On the other hand, each time the DC chopper switched off its voltage source, the excitation current i_1 would decay to zero,

causing the argument in the inverse tangent function in equation (4-1) to go to zero, which in turn forced the phase angle β_s to become zero. Clearly, the "on/off" action of the DC chopper could only get β_s to vary exponentially between 0 and β. Unfortunately, such phase angle variation satisfied only half the condition required in the synthetic loading method, where the induction machine under test needs to operate as both the motor and the generator.

In order to fully satisfy the synthetic loading condition, the β_s must be able to vary exponentially between $-\beta$ and $+\beta$. Since equation (4-1) already showed that a positive phase angle was obtained with a positive excitation current i_1, a negative phase angle could also be acquired if the excitation current i_1 became negative. To turn i_1 negative, the source voltage for i_1 must change its polarity from positive to negative, and this can only be done through the switching operation of an H-bridge inverter. Therefore, this section will mainly focus on the inverter design and the construction of electronic control circuits required for the inverter operations.

4.4.1 Inverter Specification

There are numerous inverter designs available for use in order to meet the requirements of various applications, and one design can be more complex than another depending on how many features are specified on the inverter. In this thesis research, the requirement was a very simple one. As described above, the inverter's primary function was to provide a 10-Hz modulation to the excitation current i_1 in the direct-axis rotor winding by converting the DC voltage into an alternating voltage so that the β_s could vary between $-\beta$ and $+\beta$. Since most applications require an inverter to convert a DC voltage into an AC voltage with sinusoidal waveform, a pulse-width modulator (PWM) would be needed in order to perform the task. However, the PWM was not used here because the inverter was only required to output voltage with a simple waveform of square wave with frequency of 10 Hz in this initial investigation. Full modulation strategies could be used later to improve the performance. Since each rotor winding in the generator was rated for 10 A, all the components used in the inverter must be able to handle a load current of 10 A or more in order to keep the phase modulation process safe and free from any thermal damages.

4.4.2 Inverter Operations

A basic circuit is illustrated in Figure 4.15 below in order to explain the operations of the H-bridge inverter, which operates by switching only one pair of

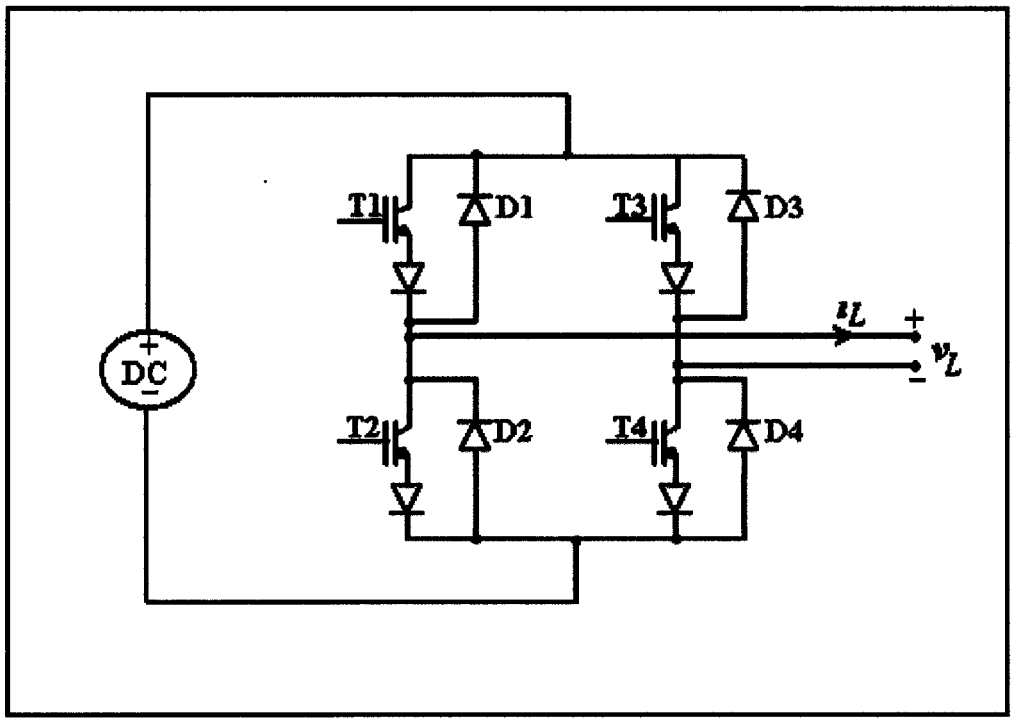

Figure 4.15: *Circuit topology of the H-bridge inverter*

switches on or off at any one time. With four switches, there are six combinations to be examined in the inverter operations [18]:

1. ***T1-T2 "ON" or T3-T4 "ON":*** Both pairs create short circuits across the DC source voltage and are invalid
2. ***T1-T4 "ON":*** Connects the DC source to the load. If the load current i_L is in a positive direction, it will pass through the switches T1-T4; otherwise, for i_L negative, the load current flows through the diodes D1-D4 and returns energy to the DC source.
3. ***T2-T3 "ON":*** Connects the DC source to the load. With i_L positive, the current flows through D2-D3 and returns energy to the DC source. If i_L is negative, the current flows through T2-T3 and draws energy from the supply.
4. ***T1-T3 "ON":*** Applies zero volts across the load. For i_L positive, the path for the load current is through T1-T3. For i_L negative, the path is via D1-T3.

5. ***T2-T4 "ON":*** Applies zero volts across the load. For i_L positive, the path is through T2-T4. For i_L negative, the path is T2-D4.

In most practical cases, the inverter only operates with combinations 2 and 3 above. If the load of Figure 4.15 were pure resistance, then the alternate "turning ON" of switches T1-T4 and T2-T3 will place the DC source in alternate senses across the load, giving it a square wave. However, with an inductive load, the load current can not reverse its direction immediately after the polarity of load voltage is switched from positive to negative or vice versa. Thus, an anti-parallel diode is always connected across each switch to provide an alternative path for the peak inductive load current to return energy back to the source when the switch is turned off. Note that an extra diode is also placed in series with each switch to provide it with an extra protection from the reversed load current whenever the anti-parallel diode malfunctions.

4.4.3 Power Switch Selection

Current and voltage ratings of T1, T2, T3, and T4 were the first factors to be determined. Since the maximum output current requirement for the inverter was 10 A, considering some safety margin, switching devices rated at 15~25 A would be proper selections for current rating. In order to modulate the excitation current i_f in the rotor winding, the DC bus voltage required from DC1 was 20 V with some safety margin. Due to the switching operation, the single switching device should be able to block voltage as high as the DC bus voltage at OFF state. Therefore, ideal selections would be switching devices with voltage rating of 20 V and current rating of 15~25 A.

Generally, the candidates available for switching devices in an inverter would be the bipolar power transistor, the insulated gate bipolar transistor (IGBT), the metal oxide semiconductor field-effect transistor (MOSFET), or the thyristor family. However, the IGBT was selected here due to its fast turn-on and turn-off time, and less demanding firing requirements as compared to other switching devices. Thus, the IGBT IRG4BC30S was chosen in this experiment in order to satisfy the required modulation frequency of 10 Hz. This IGBT was optimized for a minimum saturation voltage and low operating frequencies less than 1 kHz, with a maximum collector-emitter voltage at OFF state of 600 V. Its collector current was 18 and 34 A at case temperatures of 100°C and 25° C,

respectively. In order to build two H-bridge inverters, each of which was used for modulating the excitation current i_1 in each generator, a total of eight IGBTs were required. Since each IGBT required two diodes of similar ratings – one for an extra protection and the other for freewheeling (see Figure 4.15), sixteen 30CPF06 diodes were purchased for the eight IGBTs. These were soft recovery rectifier diodes, and they have been optimized for combined short reverse recovery time and low forward voltage drop, with 30 A of average forward current and 600 V of maximum peak reverse voltage.

4.4.4 Heat Sink Selection

All semiconductor devices, including the selected IGBTs and diodes above, have some electrical resistance, just like resistors and coils, etc. This means that when the devices are switching or otherwise controlling reasonable currents, they dissipate power as heat energy. If the device is not to be damaged by this, the heat must be removed from inside the device at a fast enough rate to prevent excessive temperature rise. The most common way to do this is by using a heat sink. The first step is to select a heat sink by determining the heat sink thermal resistance, also known as the sink-to-ambient resistance (R_{sa}), of the device as follows [19]:

$$R_{sa} = \frac{(T_j - T_a)}{P_d} - R_{jc} - R_{cs} = R_{ja} - R_{jc} - R_{cs} \qquad (4\text{-}2)$$

where P_d = Maximum operating power dissipation of the device.

T_j = Maximum junction temperature of the device in °C.

T_a = Ambient air temperature in °C.

R_{jc} = Thermal resistance between the junction and the case of a device.

R_{cs} = Thermal resistance between the case of a device to the heat sink.

R_{ja} = Thermal resistance from junction to ambient.

In equation (4-2) above, T_j, P_d, R_{cs}, R_{ja} and R_{jc} are usually provided by the device manufacturer, and T_a is the user defined parameter, which depends on the operating environment in which the component is expected to be used. With all the parameters on the right side of the R_{sa} expression identified, it becomes the required maximum thermal resistance of a heat sink for the application. In other words, the thermal resistance value

of a chosen heat sink for the application has to be equal to or less than R_{sa} value for the junction temperature to be maintained at or below the specified T_j [19].

From datasheets of the IGBT and the diode above, the values of R_{cs}, R_{ja} **and** R_{jc} were almost the same between the two devices. Since calculation showed that 38 **C°/W** was the lowest thermal resistance value, twenty four heat sinks with such thermal resistivity were purchased in order to accommodate eight IGBTs and sixteen diodes for the two H-bridge inverters.

Before screwing each semiconductor device onto the heat sink, thermal joint compound must be carefully applied between the mating surfaces to improve energy transfer from the device to the heat sink. Once the devices have been mounted onto the heat sinks, they were positioned with their pins through holes drilled in the insulation board, and the pins were soldered together underneath the board according to the circuit layout in Figure 4.15. Below are pictures of the two H-bridge inverters roughly assembled with heat sinks, IGBTs and diodes.

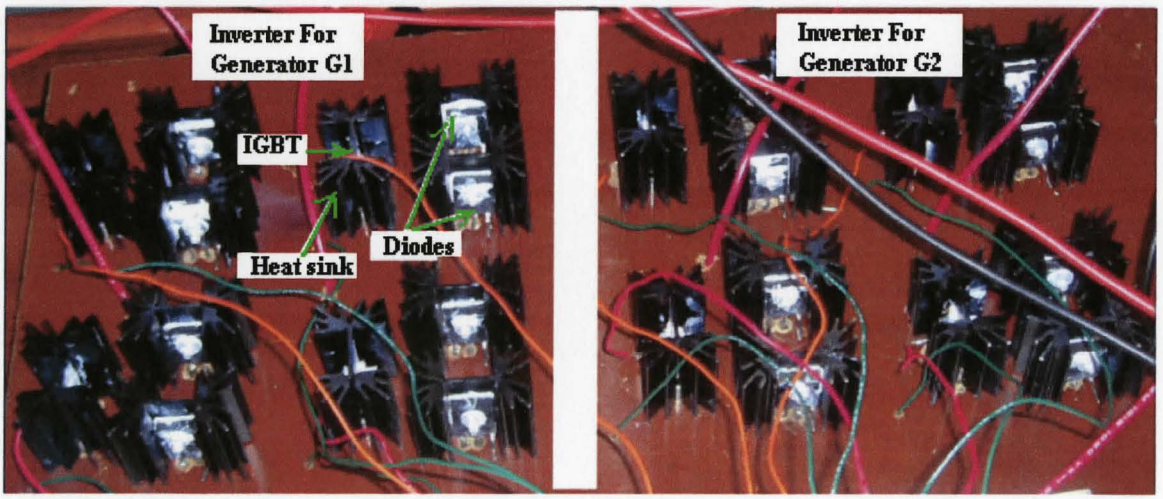

Figure 4.16: *Pictures of the two H-bridge inverters*

4.4.5 IGBT Gate Driver

In order to control the switching sequences of the four power switches T1, T2, T3 and T4, two IR21814 gate drivers from International Rectifier were used. The IR21814s were high voltage, high speed power MOSFET and IGBT drivers with independent high and low side referenced output channels. These gate drivers featured a high pulse current buffer stage designed for minimum driver cross-conduction, with floating channels

capable of driving an IGBT in the high side configuration which operated up to 600 V. For each gate driver, two input signals HIN and LIN were needed to control the switching operations of the "high" and "low" IGBTs, respectively, on each leg of the H-bridge inverter. Since the driver's output signals HO and LO could not be used directly to drive the gates of the IGBTs due to the limited voltage/current capability of the driver's output pins and safety concerns, the low power circuit must be electrically isolated from the high power circuit with HCPL-3150 optocouplers. Figure 4.17 illustrates the control circuit for

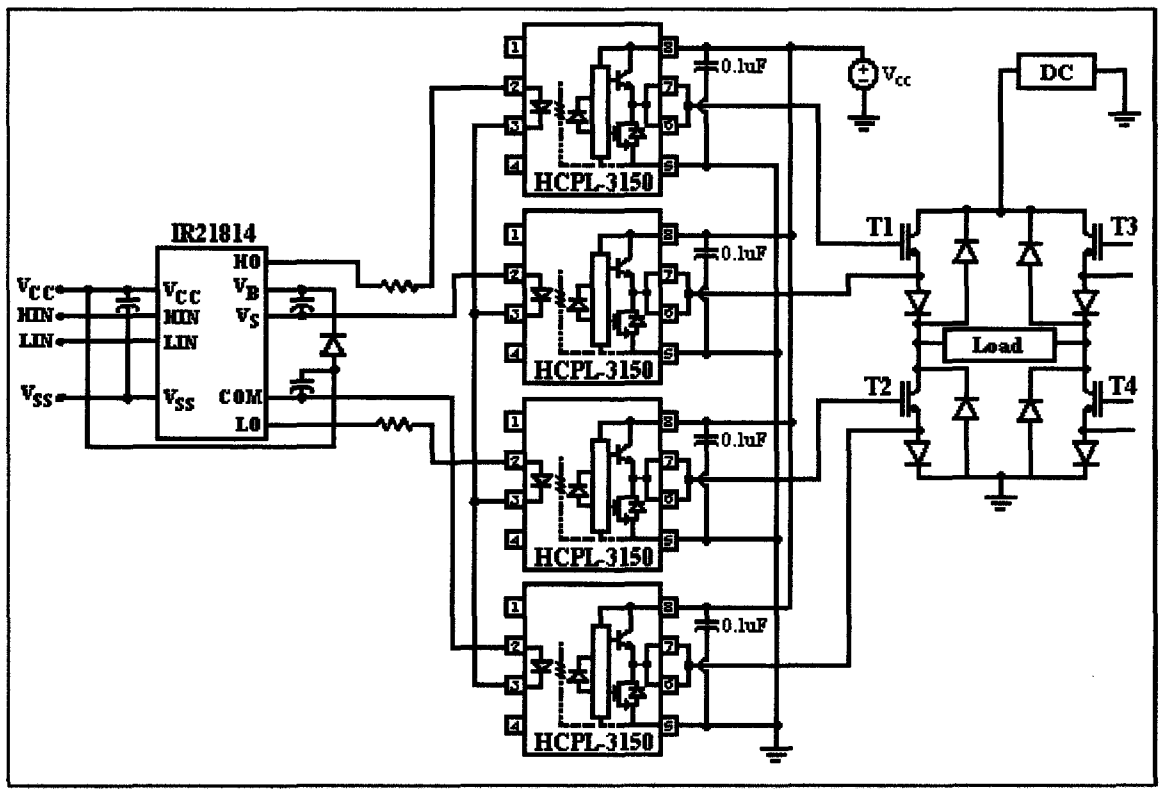

Figure 4.17: *Control circuit for the first half of the H-bridge inverter*

one side of the H-bridge inverter. The other side was controlled by an identical circuit; however, its diagram was not shown here due to space constraints in the drawing. Clearly, one inverter would require two IGBT gate drivers, with one on each leg, and a total of eight HCPL-3150 optocouplers in order to isolate the low power gate driver circuits from the high power switching devices in the inverter. Of course, the number of components doubled when two H-bridge inverters were built for the experiment. Below is an overall schematic diagram showing how the low power circuits were isolated from the high power ones with optocouplers. This diagram was greatly simplified with functional

blocks of other electronic circuits necessary for the inverter operations. The purpose for these electronic circuits in the overall phase modulation circuit will be discussed next.

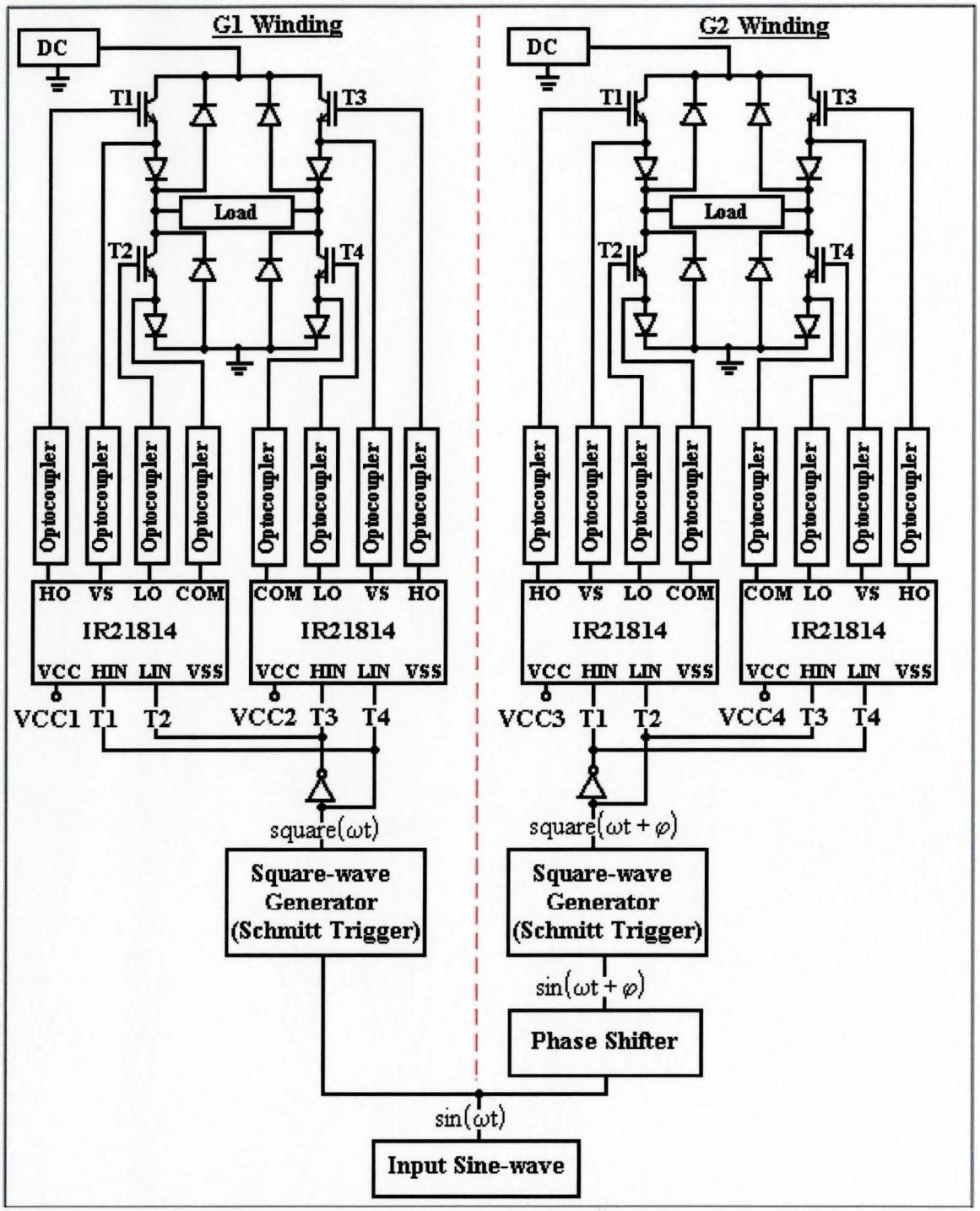

***Figure 4.18**: Phase modulation circuits for generators G_1 and G_2*

Since investigating the viability of the phase-shift correction method was an important part of the study, the input signals feeding into the gate drivers of one parallel

system must be phase shifted from those input signals of another parallel system with an electronic phase shifter. This means that a variable time delay was introduced into the control input signals in one of the parallel systems to determine whether suppression of power oscillation in the "driver" motor could be improved. Through numerous experiments, it was discovered that phase shifting a square wave signal was much more difficult than phase shifting a sinusoidal signal because the square wave was badly distorted after being phase shifted. This was the reason why the original input signal in Figure 4.18 was a sine wave, which was then phase shifted in the modulation circuit of generator G_2 to produce another sine wave of the same magnitude and different phase. Consequently, this phase-shifted sine wave signal was converted into a square wave signal of the same frequency and phase by the use of a square-wave generator. Details of how the electronic phase shifter and the square-wave generator circuits were built will be presented later in sections 4.4.6 and 4.4.7, respectively. A picture taken for the actual modulation circuits is shown in Figure 4.18 with all the components labeled.

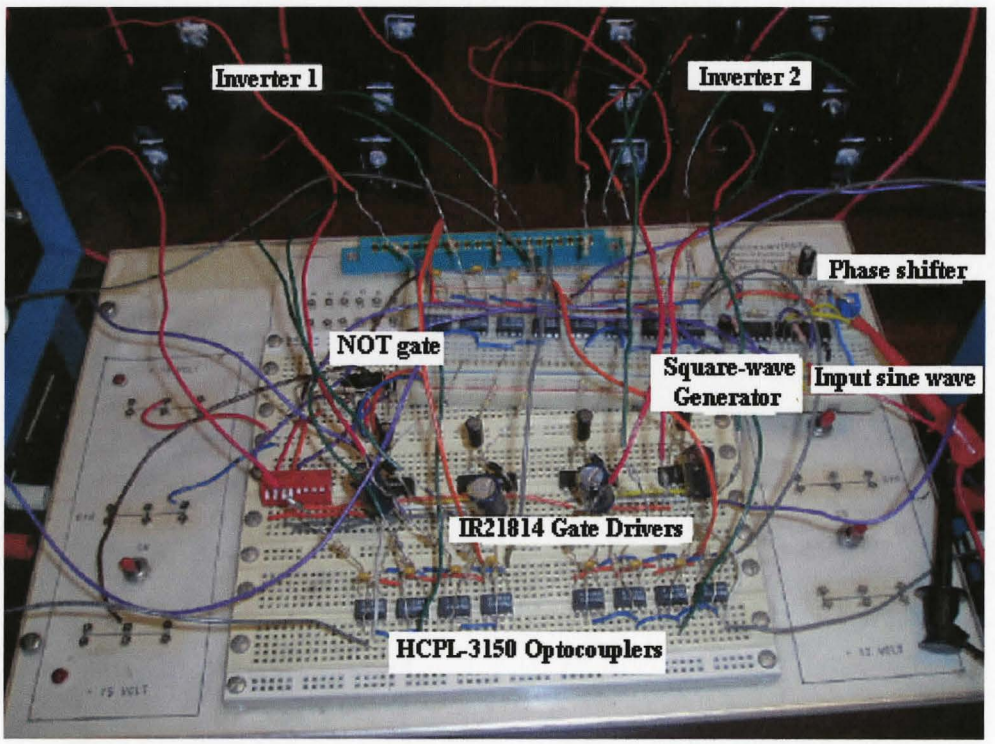

Figure 4.19: *Picture of the modulation circuits*

As mentioned in inverter operations, in order to generate an alternating voltage at the load, the switches must be turned on and off in pairs. This means that if the gate

signal applied to IGBTs T1 and T4 was "High", the gate signal to T2 and T3 must be "Low", and vice versa. As shown in Figure 4.18, in order to make sure each IGBT received the correct gate signal, some input pins to the gate drivers must be wired directly to the Schmitt trigger (square wave generator); that is, before the NOT gate, while the others were connected after the NOT gate. Here, the NOT gate did not only help negating the input signal to the drivers' input pins so that each pair of IGBTs turned on and off correctly, it also enabled the field modulation in one generator to be in opposite phase to the field modulation in the other generator. This opposition of phase in field modulation between the two generators is shown in Figure 4.19 through the voltage waveforms applied to the gates of each IGBT pair, the voltage waveform v_1 across the quadrature-axis rotor winding, and the corresponding excitation current i_1.

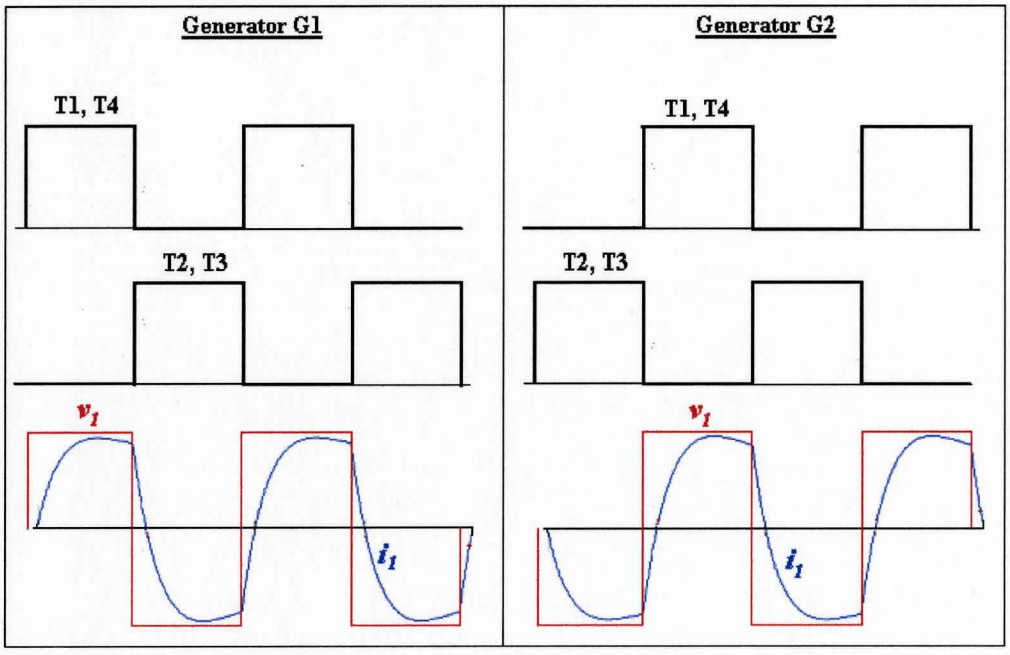

Figure 4.20: *Modulated waveforms in the two generators*

4.4.6 Electronic Phase Shifter

This phase-shifting circuit was designed by taking advantage of the two inputs of modern op-amps. As shown in Figure 4.21, the original signal was fed to both the inverting- and none inverting-input terminals, with the RC split into a C and variable R at the noninverting input of the op-amp. Varying the R at the positive input caused the phase to change from 0 to 180 degrees [20]. In order to change the resistance at the non-

inverting input, a potentiometer was used so that phase-shifting could be performed manually. Since the op-amp in this circuit was configured with negative feedback,

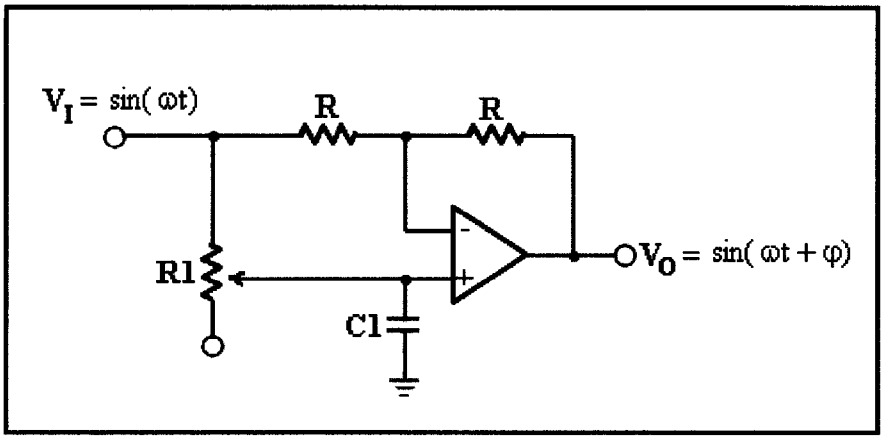

Figure 4.21: *An electronic phase shifter circuit*

deriving the response of the phase shifter can be done by applying the golden rules [21] for ideal op-amps as follows:

1. The voltage difference between the input, $V_- - V_+$, is zero. (Negative feedback will ensure that this is the case.)
2. Both inverting and non-inverting inputs draw no current; that is, $i_- = i_+ = 0$. (This is true in the approximation that the input impedance of the op-amp is much larger than any other current path available to the inputs.)

Therefore, the response of the above circuit can be derived to be:

$$\frac{V_O}{V_I} = -\frac{\left(s - \frac{1}{R_1 C_1}\right)}{\left(s + \frac{1}{R_1 C_1}\right)} \qquad (4\text{-}3)$$

The phase shift this circuit realized at any given frequency can be found by:

$$\varphi = \tan^{-1}\left(\frac{\frac{2\omega}{R_1 C_1}}{\omega^2 - \left(\frac{1}{R_1 C_1}\right)^2}\right) \qquad (4\text{-}4)$$

4.4.7 Square-wave Generator

Whether or not the input sinusoidal voltage V_I was phase shifted, it must be eventually converted into a square wave with the same frequency as the input sine wave by using a square-wave generator in Figure 4.22 below. This circuit was implemented by a Schmitt trigger, a voltage follower, and an inverting amplifier.

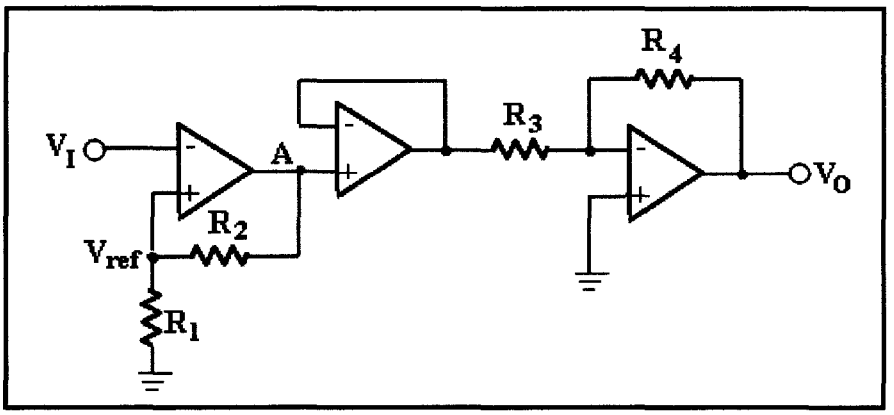

Figure 4.22: *Schmitt trigger circuit*

The Schmitt trigger was designed with a comparator whose reference voltage V_{ref} was derived from a voltage divider across the output. The input signal was applied to the inverting-input terminal, and the reference voltage was applied to the noninverting input (positive feedback). For positive output voltages at point A, $V_{ref} = \beta V_{CC}$, but for negative output voltages, $V_{ref} = -\beta V_{EE}$, where $\beta = R1/(R1 + R2)$. Thus, the reference voltage changed when the output switched state [21]. That is, when an input voltage was increasing from below V_{ref}, the output was at V_{CC} and $V_{ref} = \beta V_{CC}$. As the input voltage crossed through V_{ref}, the output voltage switched state to $-V_{EE}$, and V_{ref} simultaneously dropped, reinforcing the voltage across the comparator input. In order to cause the comparator to switch states a second time, the input must now drop below $V_{ref} = -\beta V_{EE}$. On the other hand, if the input was decreasing from a high level, the output was at $-V_{EE}$ and $V_{ref} = -\beta V_{EE}$. As the input voltage crossed through V_{ref}, the output switched state to V_{CC}, and V_{ref} simultaneously increased, again reinforcing the voltage across the comparator input [21]. Therefore, the Schmitt trigger was said to exhibit hysteresis in its voltage transfer characteristics, and would not respond to input noise that has a magnitude V_N smaller than the difference between the two threshold voltages [21]:

$$V_N < \beta[V_{CC} - (-V_{EE})] = \beta(V_{CC} + V_{EE}) \qquad (4\text{-}5)$$

Since the output square wave at point A of Figure 4.22 was inverted with respect to the input sine wave, and saturated at V_{CC} and $-V_{EE}$, its magnitude must be scaled down by a factor of K, where K = -R4/R3, with an inverting amplifier to obtain the desired amplitude of the square-wave voltage for feeding into the gate drivers. Because the reference voltage can never be zero in this circuit design, there will always be a phase shift between the square wave generated and the input sine wave. However, this phase shift can be minimized with a smaller V_{ref} by selecting proper values for the R1 and R2.

Finally, the voltage follower was placed at point A in order to isolate the output impedance of the Schmitt trigger from the inverting amplifier, while maintaining the output voltage of the Schmitt trigger at point A.

4.5 Data Acquisition

The fundamental quantities necessary in order to describe an electric circuit are the voltage and the current. Once these values are known, other variables such as active and reactive power can be calculated. If the voltage and current were sinusoidal in their waveforms, the power meter would be able to determine the active and reactive power without any difficulty. However, the waveforms in this experiment were non-sinusoidal due to the phase modulation being performed in each generator. As a result, the power meter would perform poorly and the validity of measurements is questionable under such conditions. Instantaneous values of voltage and current must be used when the waveforms are not sinusoidal, or when electrical transients are present.

This section describes the measurement setup and the equipment used to continuously monitor and store the instantaneous values of line voltage and current at each machine in the test setup.

4.5.1 Measurement Setup

Since the three-phase power source and load used in the experiment were balanced, only one line voltage and current per machine were required to calculate the active power drawn by the load; the power source being the variable AC power supply or the generators, and the load being each motor. In order to measure the necessary electrical quantities in all five machines, eight measurement channels were needed – six for the stator line voltages and currents in D0, M_1/G_1 and M_2/G_2; and two for the

modulated excitation currents in generators G_1 and G_2. Figure 4.23 depicts the general layout of the measurement setup used for capturing the instantaneous values of voltage

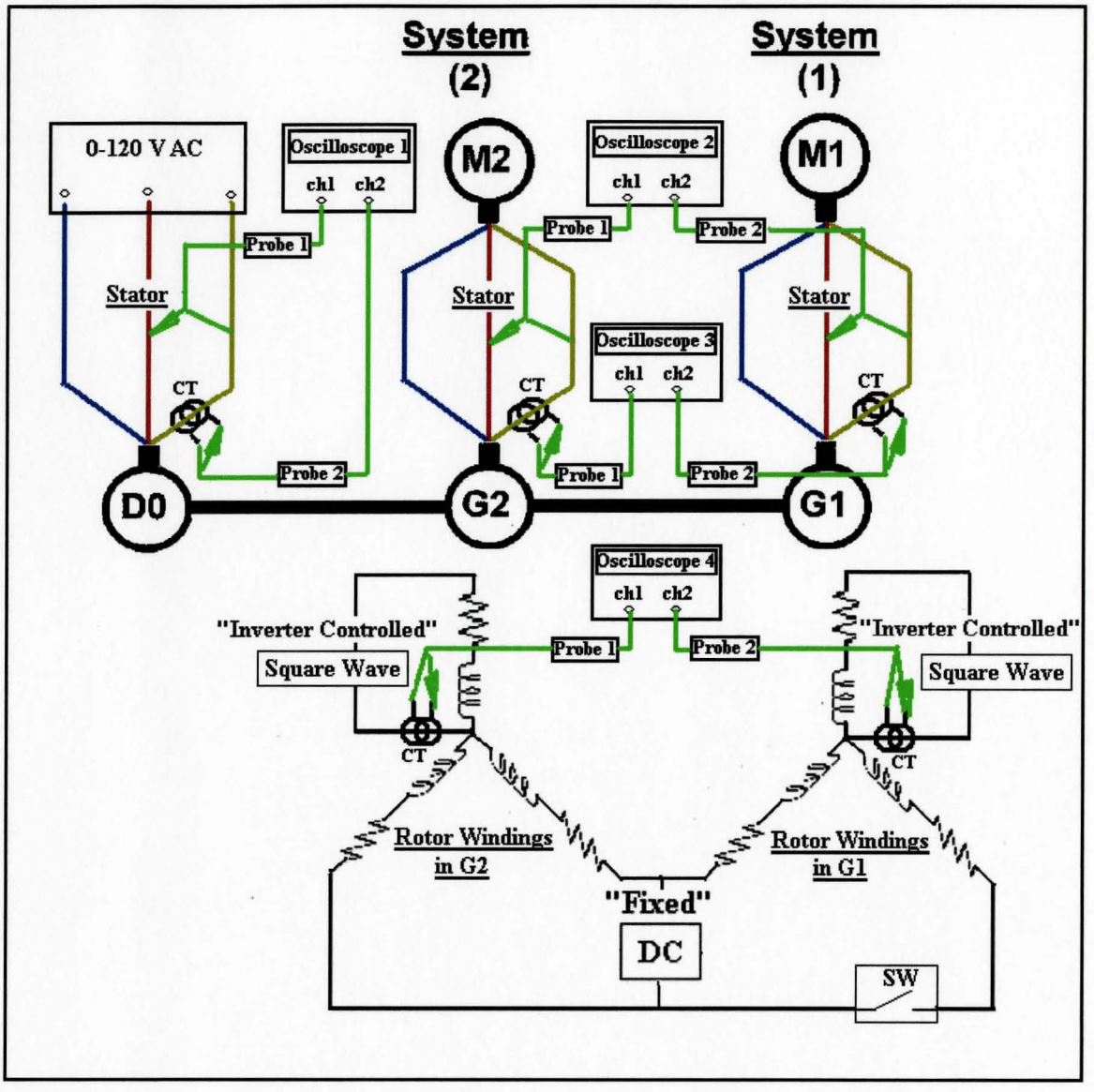

Figure 4.23: *General layout of the measurement setup*

and current. As illustrated in the above figure, each pair of measurement channel was provided by the Agilent 54621D oscilloscope, and the line voltages and currents were measured with the Agilent N2772A differential probes. Therefore, a total of four oscilloscopes and eight voltage probes were used for measuring all the required electrical quantities. This measurement equipment will be briefly described in the following sections.

4.5.2 The Agilent 54621D Oscilloscope

The Agilent 54621D oscilloscope shown in Figure 4.24 is a two-channel mixed signal oscilloscope that gives the ability to display and monitor the analog signals on the two channels simultaneously. This oscilloscope can acquire and display up to 16 channels of digital data, allowing measurement of AC signals with DC components, analysis of magnitude, frequency and phase relationships between two signals. Its built-in 1.44 MB floppy drive makes it easy to store waveform data, screen images, and scope setups. The waveform images can be saved as TIF or BMP files and the waveform data as ASCII files for easy import into other PC applications, specifically Microsoft Excel [22].

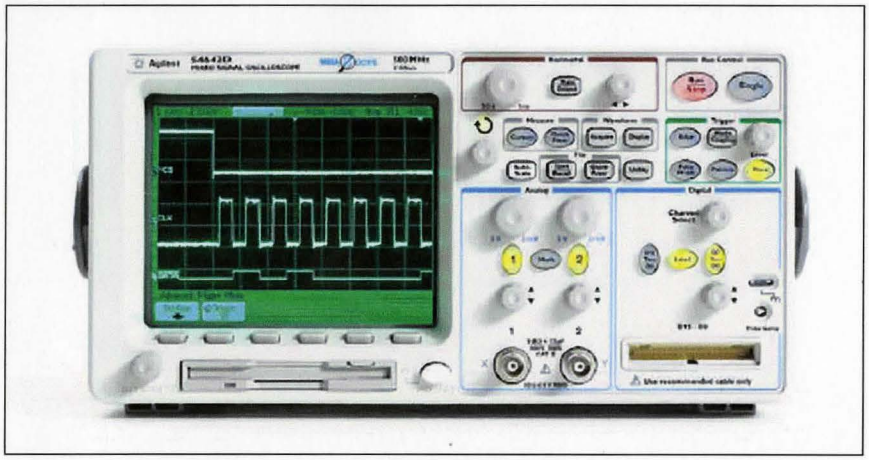

Figure 4.24: *The Agilent 54621D oscilloscope*

4.5.3 The Agilent N2772A Differential Probe

The Agilent N2772A differential probe, shown in Figure 4.25 below, can be used with any of the 54600-Series oscilloscopes to safely measure floating circuits with the

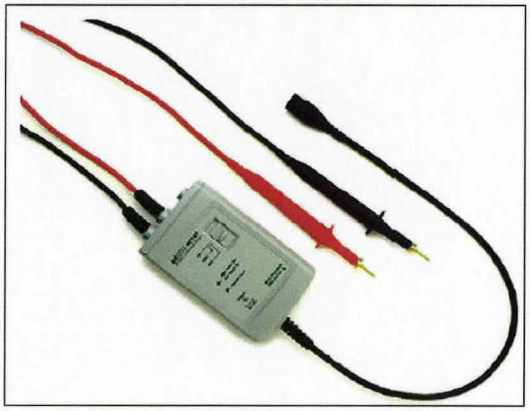

Figure 4.25: *Agilent N2772A differential probe*

oscilloscope grounded. With 20 MHz bandwidth and switchable attenuation of 20:1 and 200:1, it provides the versatility for a broad range of applications including high-voltage circuits, motor speed controls, power supply design, and electronic high-power converters. Each probe comes with two sharp probe tips for use on small components and in tight places, two retractable probe hooks for connecting to smaller wires and through-hole components, and two alligator clips for use with larger cables. This probe requires a 9 V battery or Agilent N2773A power supply [23].

4.5.4 Line Voltage and Current Measurements

As shown in Figure 4.23, line voltage measurement was made with the Agilent N2772A differential probe connected across the two stator windings of phase B and C, and the line current was measured on phase C in all three machines to ensure consistency in active power comparison between the machines, which will be discussed later in Chapter 5.

In order to measure the line currents and the modulated excitation currents, each winding cable being monitored was threaded through a 50/60 Hz current transformer (CT) shown in Figure 4.26(a). This CT was rated for 15 A of primary current, with Volt per Amp ratio of 0.1V/A for a 100-ohm load. As shown in Figure 4.26(b), the load was a terminating resistor connected across the secondary winding of the CT. The voltage drop across this resistor was measured with the Agilent N2772A differential probe, and then multiplied with an appropriate form factor in order to obtain the correct value for the current being measured.

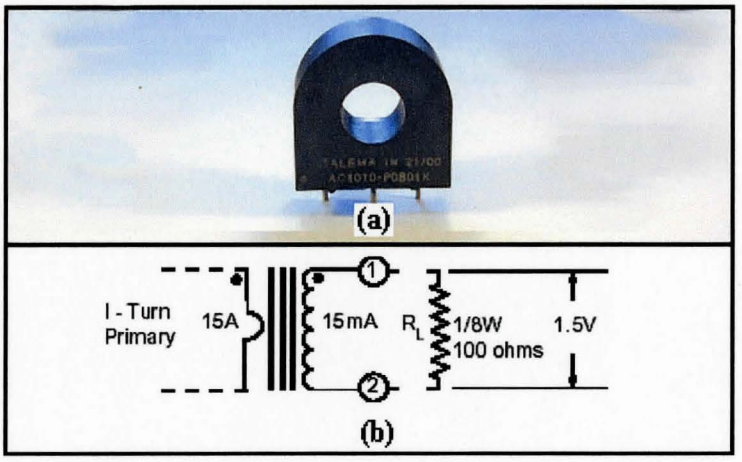

Figure 4.26: *Current transformer for measuring current*

Figure 4.27 shows the overall setup for the 2-kW machines and measurement equipments for the thesis experiment:

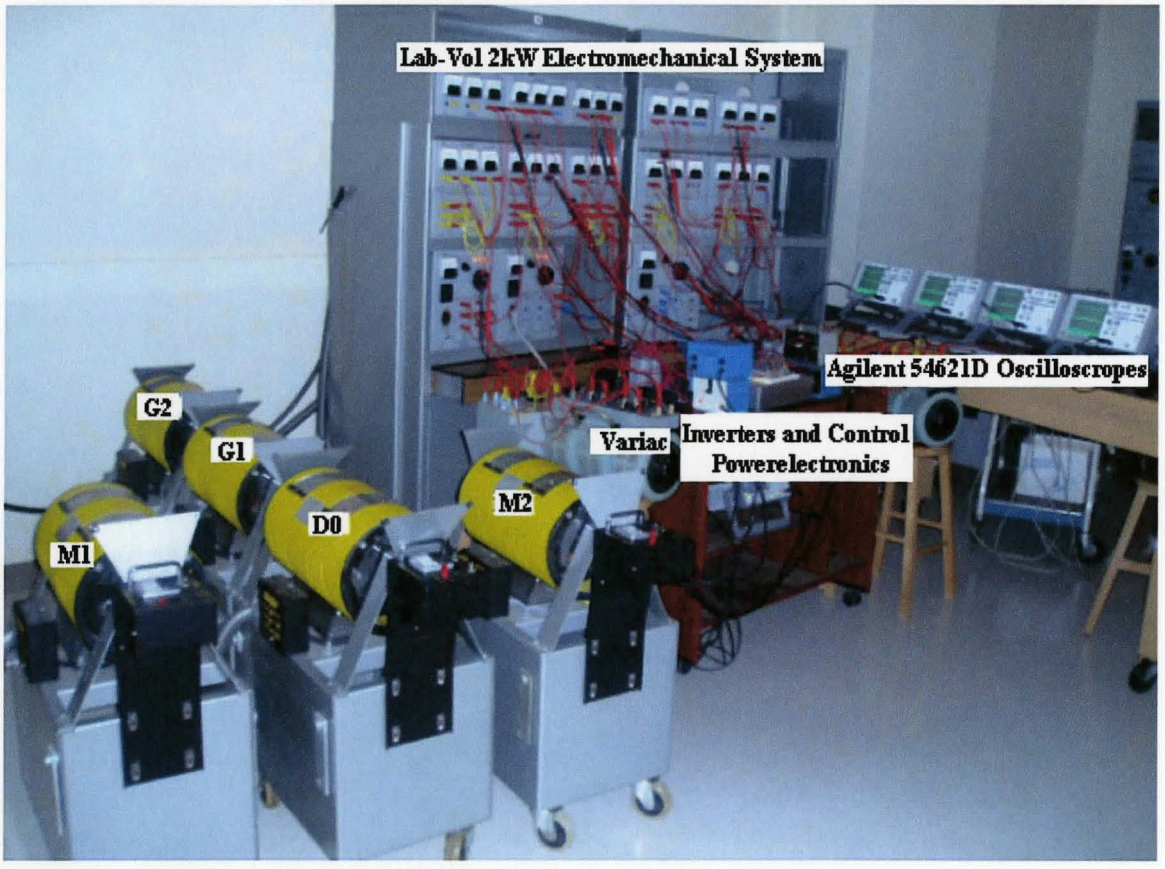

Figure 4.27: *Overall setup of the 2-kW machines and measurement equipments*

4.6 Determination of Induction Machine Parameters

All the 2-kW machines available in the machine lab at McMaster University were fairly old, and they have been used and misused numerous times due to errors made by students during the power experiments. As a result, the parameter values of these machines have changed over the years when compared to their original values available from the manufacturer; hence, they had to be measured again so that their actual values can be entered into the computer simulation of the experiment.

This section will show how the parameters can be approximated from a DC resistance test, a blocked-rotor test and a no-load test. The approximation of these parameters was entirely based on a per-phase equivalent circuit of an induction machine with all parameters referred to the stator [24]. Although such method of estimating

machine parameters does not give the best accuracy, the results obtained from this method are sufficiently accurate for the purpose of comparing the properties between two induction machines of the same rating. The per-phase circuit is illustrated in Figure 4.28 as follows [24]:

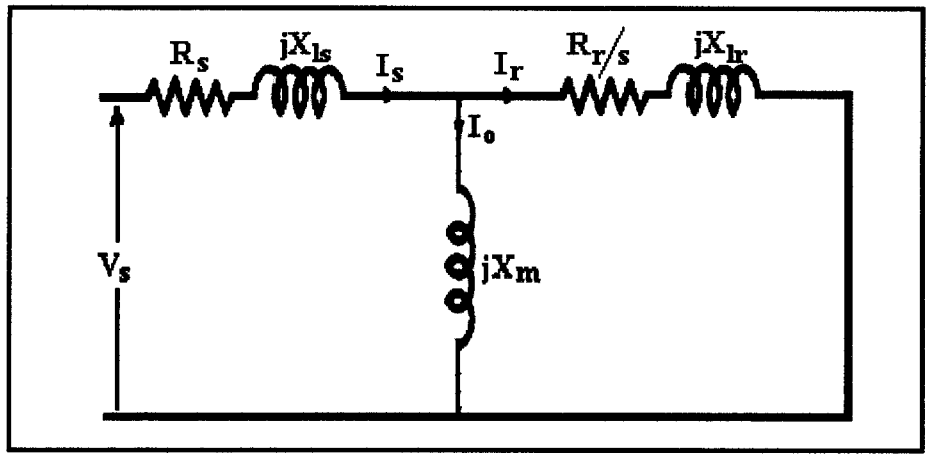

Figure 4.28: *Equivalent circuit of an induction machine with all parameters referred to the stator*

Where R_s = stator resistance per phase

X_{ls} = stator leakage reactance per phase

R_r = rotor resistance per phase referred to the stator

X_{ls} = rotor leakage reactance per phase referred to the stator

X_m = equivalent reactance accounting for the magnetizing current per phase

I_s = actual stator current per phase

I_r = rotor current per phase referred to the stator

I_o = exciting current (no-load) current per phase

$$s = \frac{n_s - n_r}{n_s} = \text{slip}$$

n_s = synchronous speed or speed of the rotating flux (r/min)

n_r = rotor speed (r/min)

V_s = stator voltage per phase

4.6.1 DC Resistance Test

This test was used to determine the per-phase stator resistance R_s in the equivalent circuit above. The DC resistance of each stator winding on the SCIM was measured using

the SCIM wiring module and the voltmeter-ammeter method detailed in Figure 4.29 [25]. Here, the DC source was adjusted to provide approximately rated stator current, and the resultant values of voltage and current in each winding were recorded. Finally, R_s can be obtained by averaging resistance values of the three stator windings of the induction machine [25]. Since the machine operates at 60 Hz, the obtained DC resistance should be converted to an equivalent AC resistance value by taking account of the skin effect at frequency of 60 Hz [26]. However, the copper conductors in this 2-kW induction machine are much small than size 4 AWG [27]. As a result, the skin effect can be ignored and the measured DC value for R_S in this particular machine is equal to its AC value at 60 Hz.

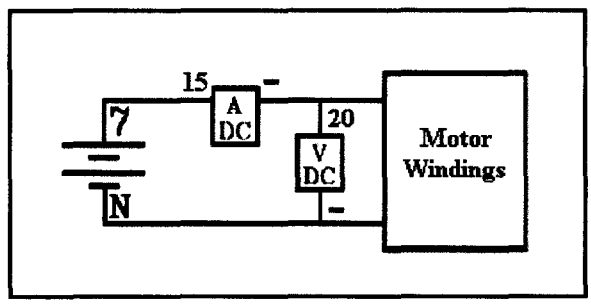

Figure 4.29: *DC resistance test*

4.6.2 Blocked-Rotor Test

The blocked-rotor test was used to determine X_{ls} and X_{lr}. When combined with data from the DC resistance test, the value of R_r can also be determined. This test was performed by blocking the rotor so that it could not turn, and carefully applying the balanced three-phase stator voltages until rated stator currents were obtained [28]. The frequency of the applied voltages was less than rated in order to obtain a representative value of R_r since, during normal operation, the frequency of the rotor currents is low and the rotor resistances of some induction machines vary considerably with frequency [29]. The readings of stator voltages, stator currents and three-phase power input to the stator were recorded as quickly as possible to avoid thermal damage, since there was no rotation aiding cooling. Wiring connections for this test are shown in Figure 4.30 [25].

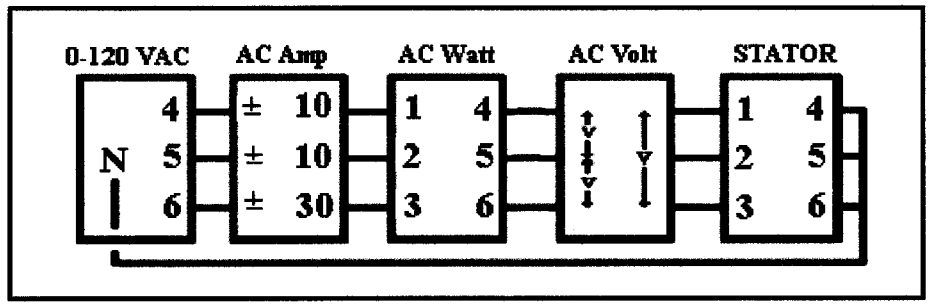

Figure 4.30: *Motor connection*

During stall, the slip is s = 1 and the exciting current I_o is considerably less than the rotor current I_r because the impedance $R_r + jX_{lr}$ is much smaller in magnitude than X_m. Hence, the current I_o may be neglected by omitting the branch with X_m from the per-phase equivalent circuit in Figure 4.28, resulting with a simplified circuit as shown below.

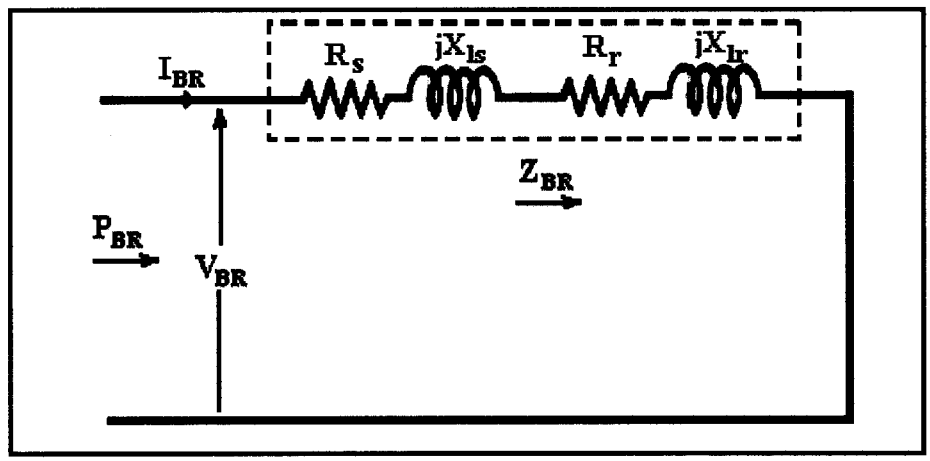

Figure 4.31: *Equivalent circuit per phase for blocked-rotor test*

Referring to Figure 4.31, the per-phase values of machine parameters in this test are:

$$Z_{BR} = R_{BR} + jX_{BR} = \frac{V_{BR}}{\sqrt{3}I_{BR}} \qquad (4\text{-}6)$$

$$R_{BR} = R_s + R_r = \frac{P_{BR}}{I_{BR}^2} \qquad (4\text{-}7)$$

$$X_{BR} = X_{ls} + X_{lr} = \sqrt{Z_{BR}^2 - R_{BR}^2} \qquad (4\text{-}8)$$

Thus, the rotor resistance R_r can be determined using the value of R_s obtained from the DC test as follows:

$$R_r = R_{BR} - R_s \qquad (4\text{-}9)$$

Generally, X_{ls} and X_{ls} are assumed equal; however, if the NEMA design letter of the induction machine is known, a different ratio is suggested [30].

4.6.3 No-Load Test

The no-load test was used to determine the magnetizing reactance X_m in the equivalent circuit. The connections for this test remain the same as those shown in Figure 4.30 for the blocked-rotor test. The only difference is that the rotor is now unblocked and allowed to run unloaded at rated voltage and rated frequency [28]. At no load, the operating speed is very close to synchronous speed, and the resulting slip is $s \approx 0$, causing the current in the R_r/s branch to be very small, which in effect is an open circuit. Thus, this branch can be omitted from the per-phase equivalent circuit in Figure 4.28. The resulted equivalent circuit for no-load test is simplified as shown in Figure 4.32.

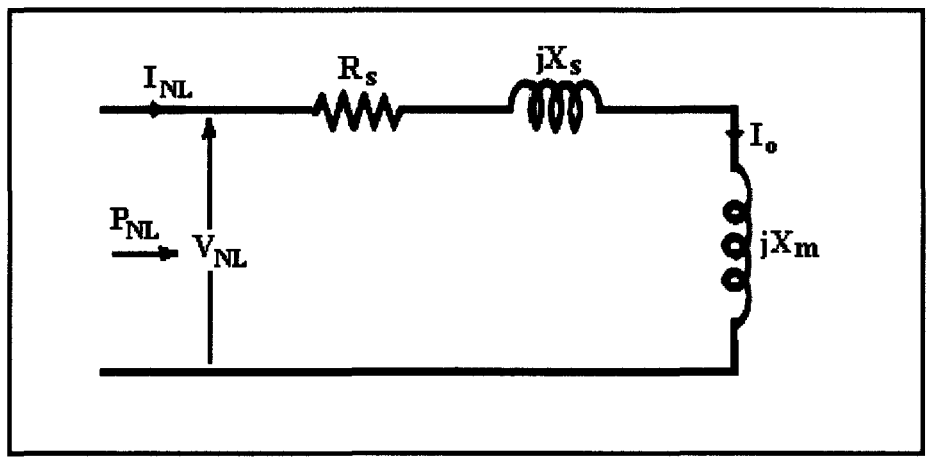

Figure 4.32: *Equivalent circuit per phase for no-load test*

Referring to the approximate equivalent circuit in the above figure, the last parameter X_m can be determined as follows:

$$S_{NL} = \sqrt{3} V_{NL} I_{NL} \qquad (4.10)$$

$$Q_{NL} = \sqrt{S_{NL}^2 - P_{NL}^2} = I_{NL}^2 X_{NL} \qquad (4.11)$$

$$X_{NL} = X_s + X_m = \frac{Q_{NL}}{I_{NL}^2} \qquad (4.12)$$

$$X_m = X_{NL} - X_s \qquad (4.13)$$

Chapter 5

ANALYSIS OF TESTS AND SIMULATION RESULTS

5.1 Waveforms of Computer Simulation and the Experiment

Based on the assumption that generators G_1 and G_2 are custom built in such a way that the equivalent circuit parameters in G_1 are equal to those in G_2, they can be left out of consideration in this research. The only machines that need to be carefully taken account of are test motors M_1 and M_2. Since both test motors were constructed with the same power rating by the same manufacturer at the same time, their nameplate values and parameter values are considered to be equal, and tabulated in Tables 1 and 2 as followed:

Table 5.1: *Nameplate Values*

	Test Motors (Squirrel Cage)	
	M1	*M2*
kW	2	2
RPM	1770	1770
Volt	120/208	120/208
F. L. Amps	15.2/8.8	15.2/8.8
Phase	3	3
Hz	60	60
Power Factor	0.77	0.77
Ins. Class	B	B

Table 5.2: *Parameter Values in Equivalent Circuit Model*

	Test Motors (Squirrel Cage)	
	M1	*M2*
R_s	0.6 Ω	0.6 Ω
R_r	0.4 Ω	0.4 Ω
X_{ls}	0.7 Ω	0.7 Ω
X_{lr}	0.7 Ω	0.7 Ω
X_m	23 Ω	23 Ω
J	0.0189 kg-m^2	0.0189 kg-m^2

Since the above values are equal between M_1 and M_2, the magnitudes of excitation voltages being applied to G_1 and G_2 must also be equal, and the expected result would be a perfectly balanced system as shown in the Figure 5.1, where the simulation shows a perfect symmetry in the established excitation currents of the two generators, and the

power waveforms in test motors M_1 and M_2 (Figures 5.1(c), (d) and (e)). Figure 5.1(b) shows that both motors M_1 and M_2 reach synchronous speeds at the same time, and their speed waveforms are symmetrical to each other about the driver motor's speed. Figure 5.1(f) shows that there is no power oscillation in the driver motor D0 because its speed at

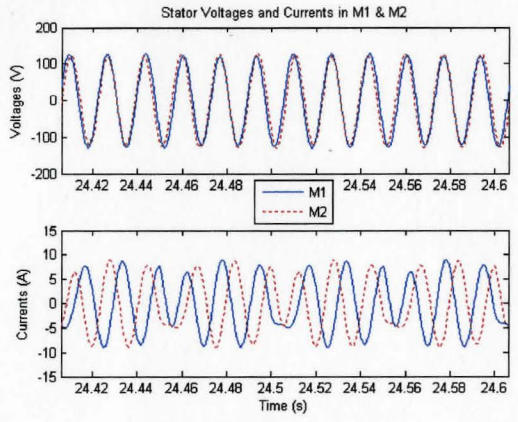

5.1(a)

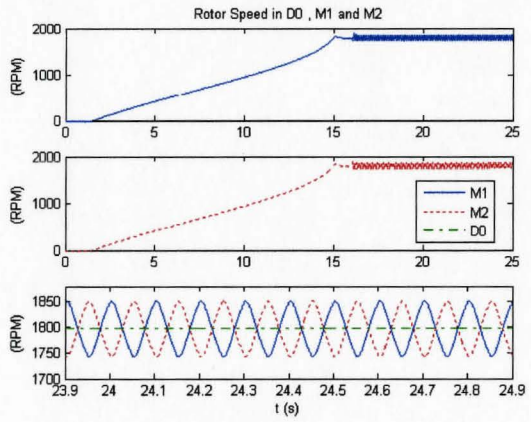

5.1(b)

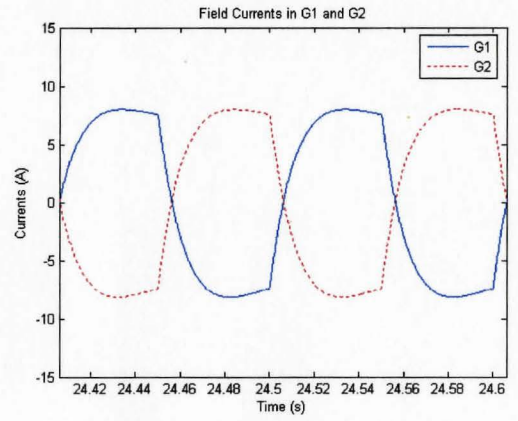

5.1(c)

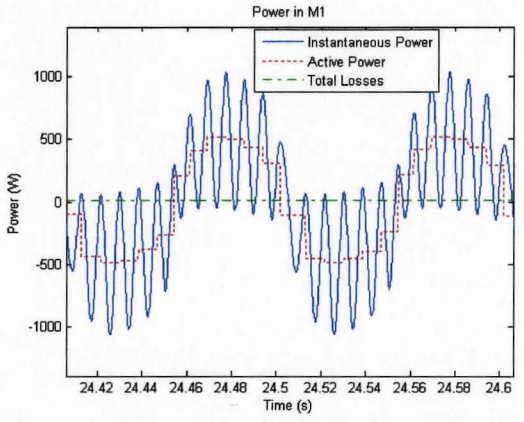

5.1(d)

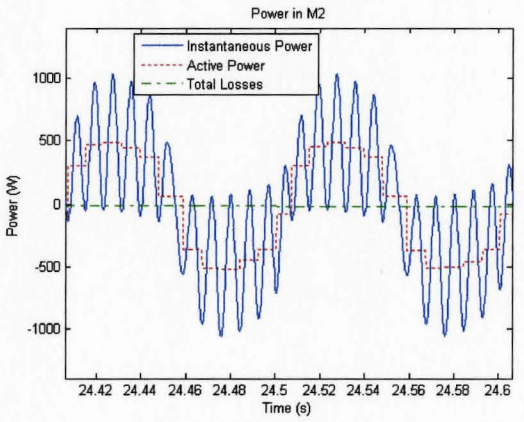

5.1(e)

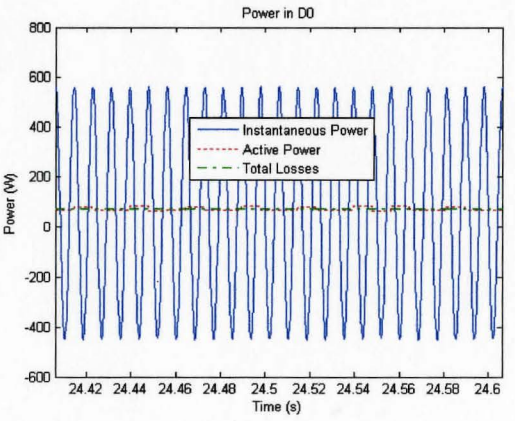

5.1(f)

Figure 5.1: *System's performance in an ideally balanced condition*

steady state is not varying. This is indeed an ideal performance desired for the system in the real world to follow; however, this is far off from the results obtained in an actual experiment. These experimental results are shown in Figure 5.2:

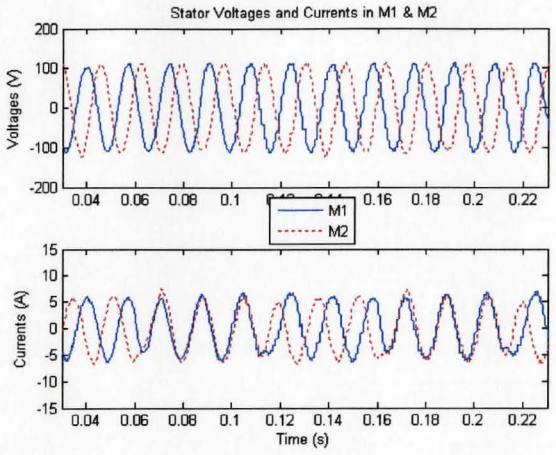

5.2(a)

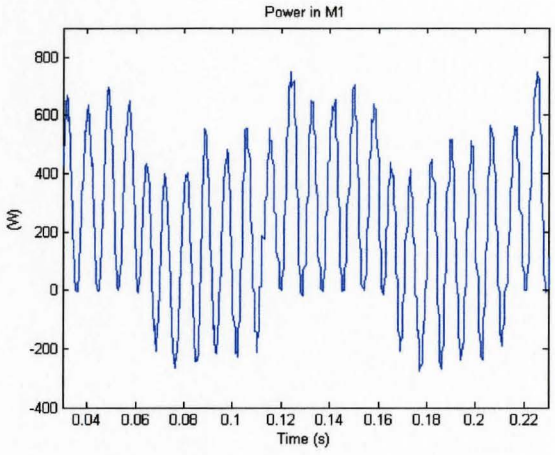

5.2(c)

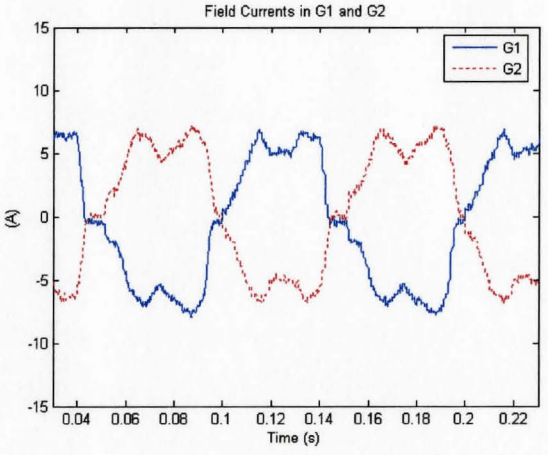

5.2(b)

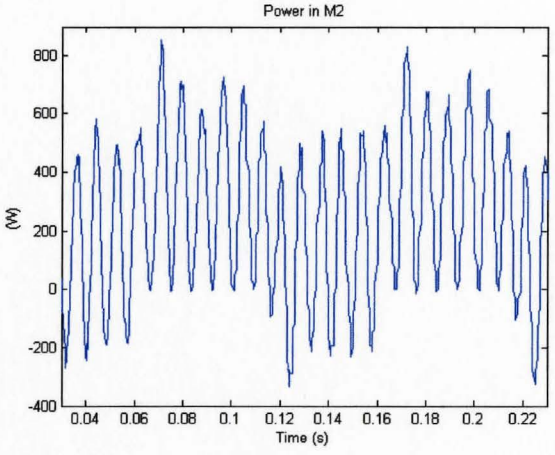

5.2(d)

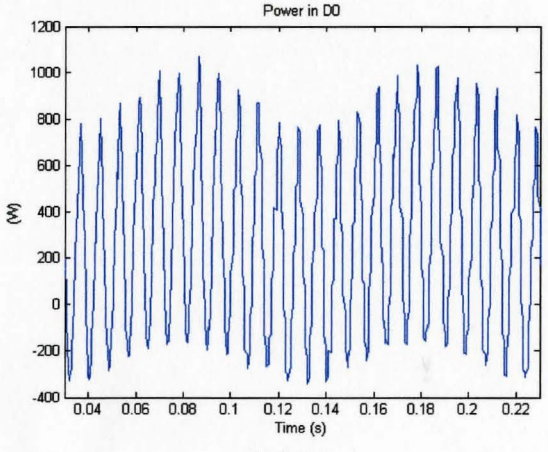

5.2(e)

Figure 5.2: *System's performance in practice*

Figure 5.2(b) shows that the excitation current waveforms are not as perfectly exponential as those appeared in Figure 5.1(c) of the simulation. This is due to a combination of the imperfection and power losses in circuit components used in the inverters. However, the test waveforms obtained are sufficiently close to the simulated results in terms of magnitude, phase and frequency. Comparing to Figure 5.1(f), the power waveform in the driver motor is no longer free of oscillation when the actual test is conducted. Figure 5.2(e) shows a 10-Hz power oscillation in D0 when the voltage applied to the direct-axis winding in each generator is modulated with a frequency of 10 Hz. As shown in Figures 5.2(c) and 5.2(d), the power waveforms in M_1 and M_2 are still in opposition of phase to each other; however, they are not as exactly symmetrical as in the simulation. This is due to imperfection in the real-world operation of power electronic components used in obtaining the data. Note that the waveforms acquired in Figure 5.2 are resulted from the minimum oscillation setting with the amplitude of the square-wave modulation voltage set at 12V and 16V for G_1 and G_2, respectively. This is amounted to 33% of voltage difference, which is required in order to force the two excitation currents in Figure 5.2(b) to be as symmetrical as possible. If the modulation voltages were not adjusted, the excitation currents in the two generators would not be as symmetrical, and the magnitude of power swing in the "driver" motor D0 would be much larger than the power waveform shown in Figure 5.2(a). Due to the lack of measurement equipments in the facility, the data for motor speeds in M_1 and M_2 were not available. Nevertheless, it was observed that M_2 reached synchronous speed much earlier than M_1. This is a very important observation for investigating the cause of power oscillation in D0.

The following sections will present investigative work being done in order to find out which of the two suggestions mentioned in chapter 1 is true, as well as what causes the waveforms between the two subsystems of G_1/M_1 and G_2/M_2 to be unsymmetrical, and what solution is suitable for minimizing the power oscillation in the driver motor.

5.2 Phase Shift Correction

As suggested in chapter 1, power oscillation in the "driver" motor D0 may have stemmed from the misalignment of electrical axes between the two generators when their shafts are connected together. The reason behind this suggestion is described next.

5.2.2 Shaft Coupling Between Generators G_1 and G_2

Assuming balanced machine properties in Systems (1) and (2) in the test system, if the shafts of generators G_1 and G_2 are coupled together with a perfect axis alignment and the applied field modulation is in opposition of phase, the d-q axis for magnetic fluxes in both generators would be directly overlapping, and the resultant flux Φ_R induced in each generator would be completely out of phase as shown in the figure below.

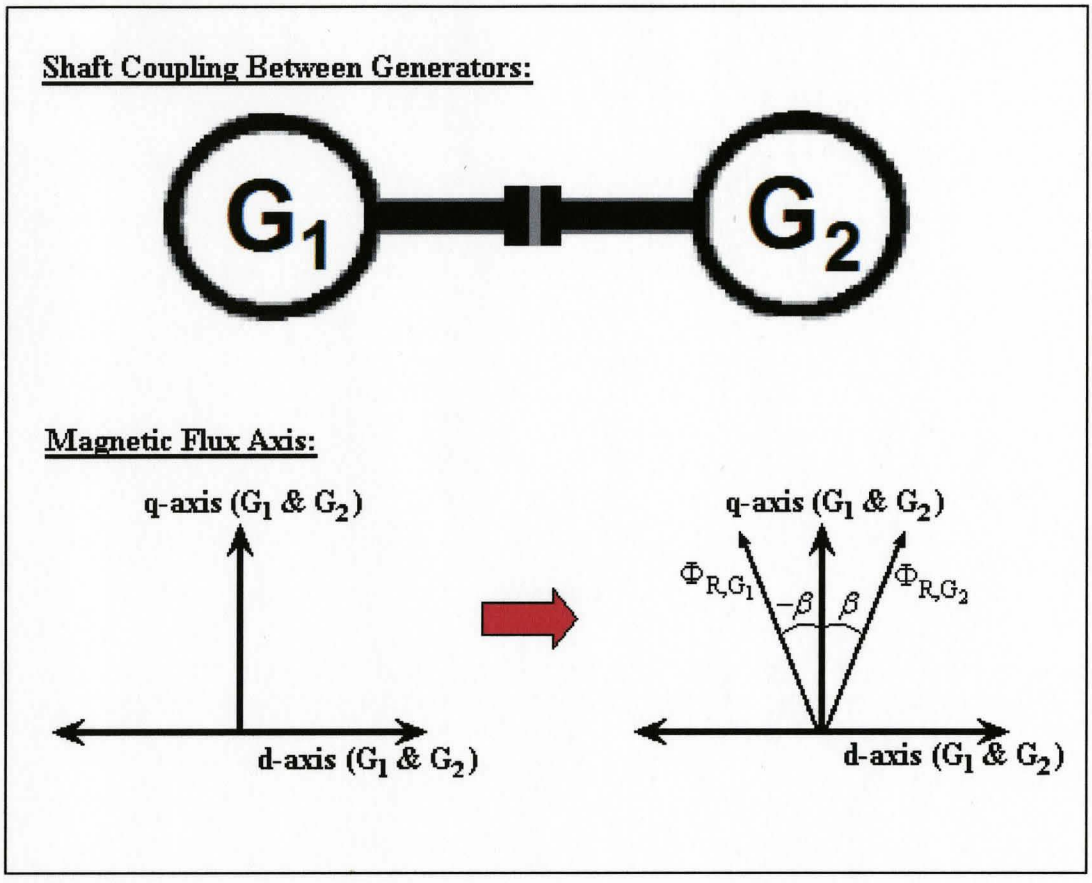

Figure 5.3: *Scenario of a perfect shaft alignment between generators G_1 and G_2*

This perfect shaft alignment will cause the power exchange between Systems (1) and (2) to be also in opposition of phase. As a result, when one system absorbs power, the other generates it, and the "driver" motor D0 will provide only the net losses of all five machines and will experience no power oscillation. However, due to physical constraint on the shaft coupler, the axis could not be aligned any better than 15° angle. For instance, if the axis alignment is within a certain angle φ, then the d-q axis in G_1 and G_2 would be out of phase by an angle φ as shown in Figure 5.4, and the resultant fluxes would no

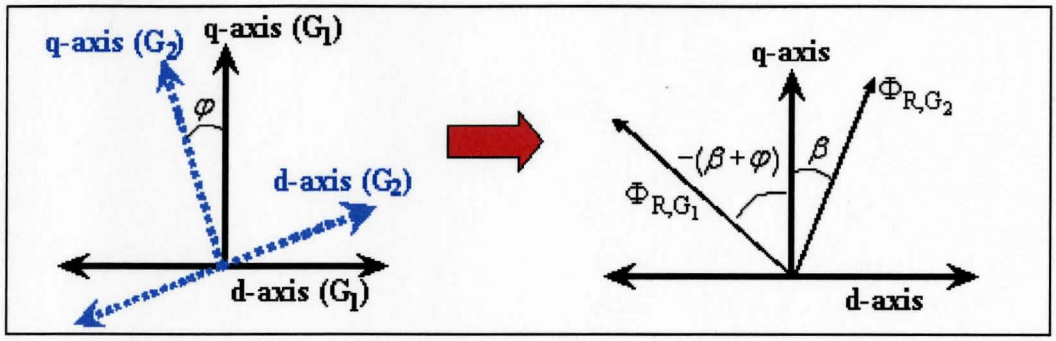

Figure 5.4: *Scenario of a shaft alignment within a certain angle φ*

longer be in a complete opposition of phase. They would be phase shifted further by an angle φ. This phase difference would cause a power mismatch between Systems (1) and (2), resulting with a power oscillation in the "driver" motor D0. Due to the misalignment between the two shafts, even if the square-wave modulation voltages v1 and v2 were applied with equal magnitudes and exact opposition of phase, the resultant fluxes in Systems (1) and (2) would not be induced with opposition of phase. Their waveforms would be further phase shifted from each other by an angle φ as shown in Figure 5.5.

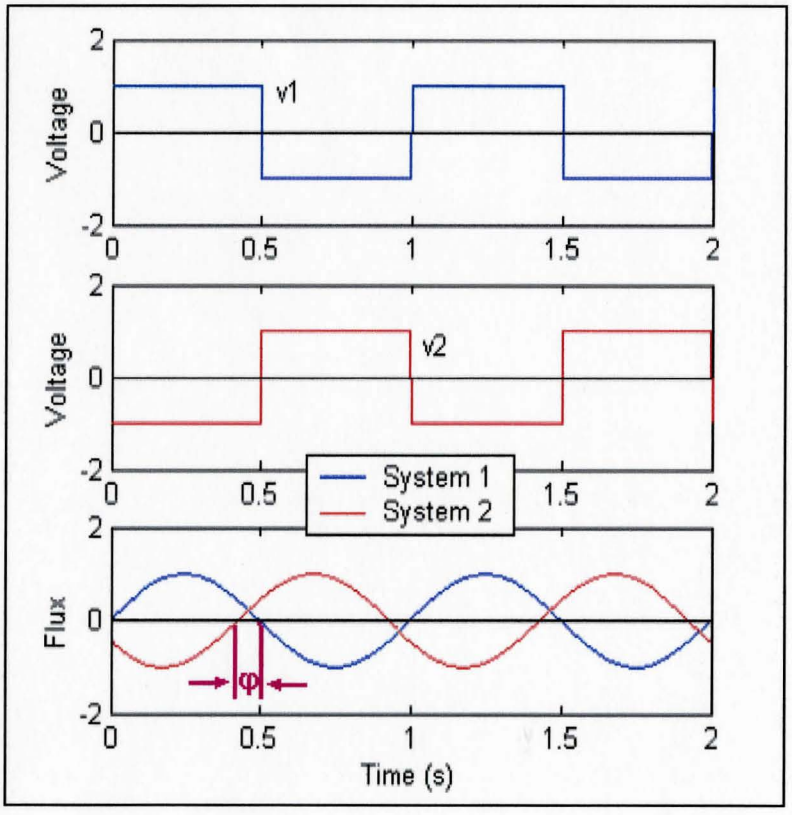

Figure 5.5: *Waveforms of the induced fluxes before correcting the phase shift*

5.2.3 The Phase Shift Correction Method

The shaft misalignment between generators G_1 and G_2 can be electrically corrected by phase shifting one square-wave modulation voltage with respect to the other along the time axis until the two resultant fluxes are completely out of phase. As shown in Figure 5.6 below, the modulation voltage v2 is phase shifted by an angle of ξ with respect to v1 in order to bring the resultant flux waveforms into a complete opposition of phase. This way of electrically correcting the shaft misalignment has been named as the phase shift correction method.

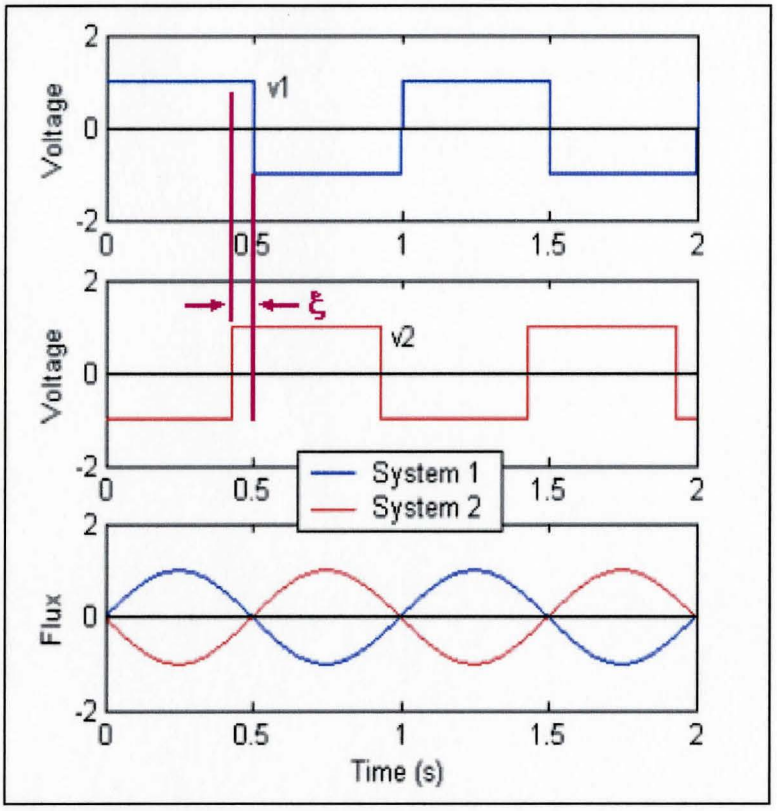

Figure 5.6: *Waveforms of the induced fluxes after correcting the phase shift*

In order to investigate whether the phase shift correction method can help suppress power oscillation in the "driver" motor D0, the shaft misalignment was emulated by introducing a phase difference between the square-wave modulation voltages applied to the two generators. The following waveforms are results obtained from simulation and experiment for the phase shift angles of 30° and 60°. Such large angles of phase shifting were chosen in order to show clearly their effects on the power oscillation in D0.

Simulation Results

30° Phase Shift

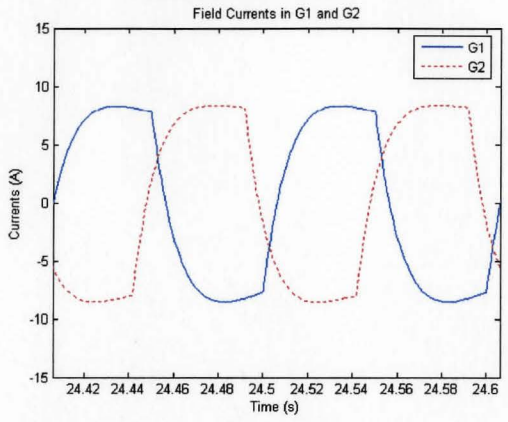

5.7(a)

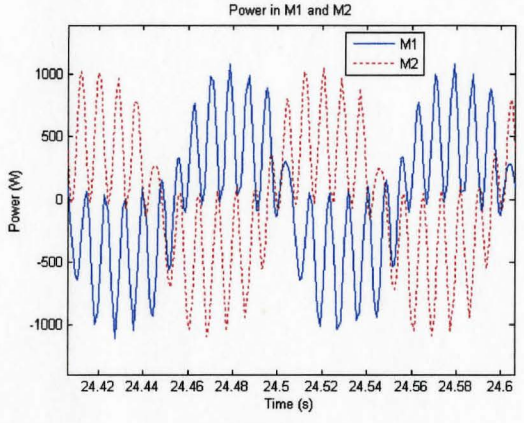

5.7(b)

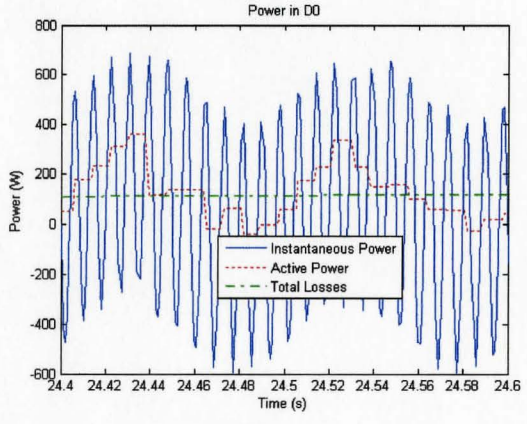

5.7(c)

60° Phase shift

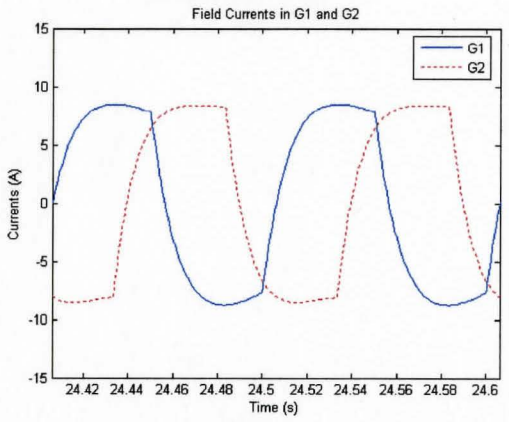

5.7(d)

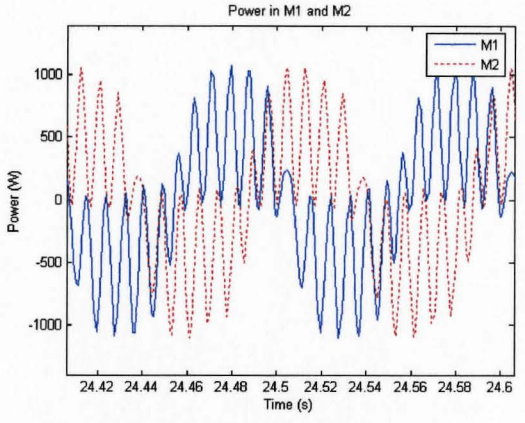

5.7(e)

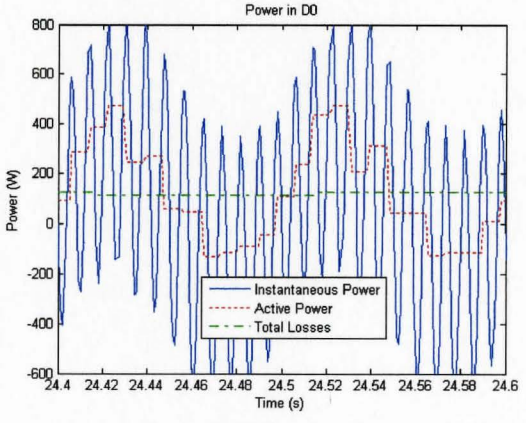

5.7(f)

Figure 5.7: *Simulated waveform comparisons between 30° and 60° phase-shifts*

Experimental Results

30° Phase Shift

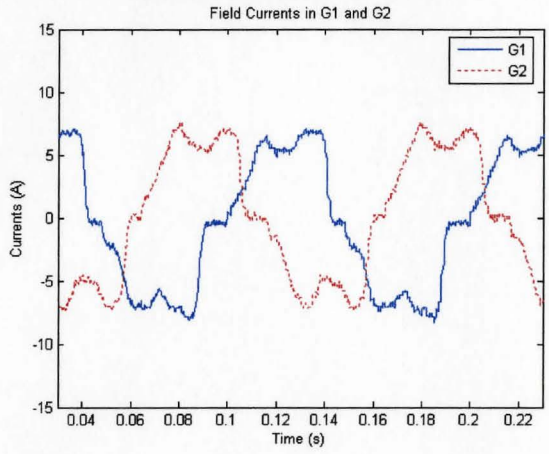

5.8(a)

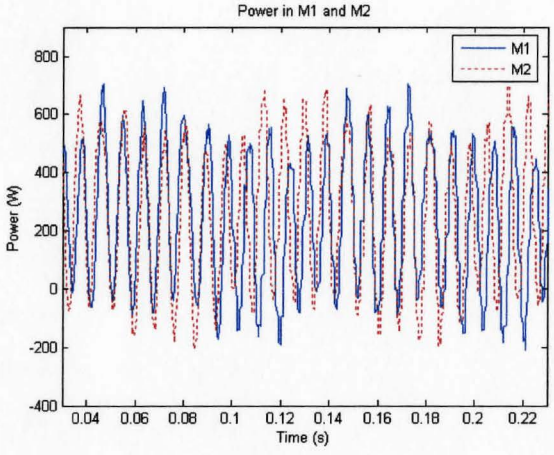

5.8(b)

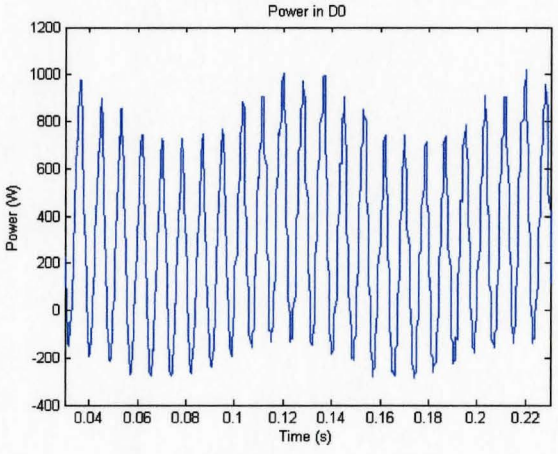

5.8(c)

60° Phase shift

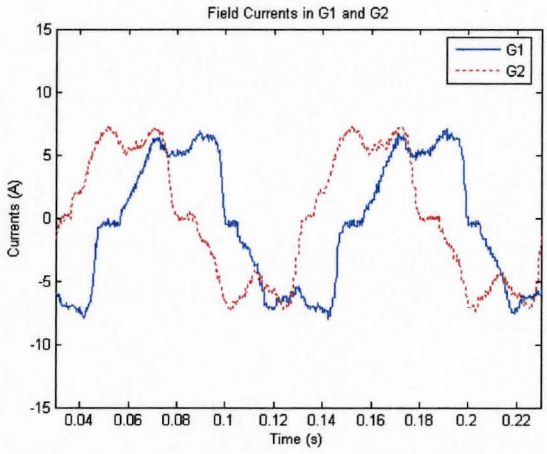

5.8(d)

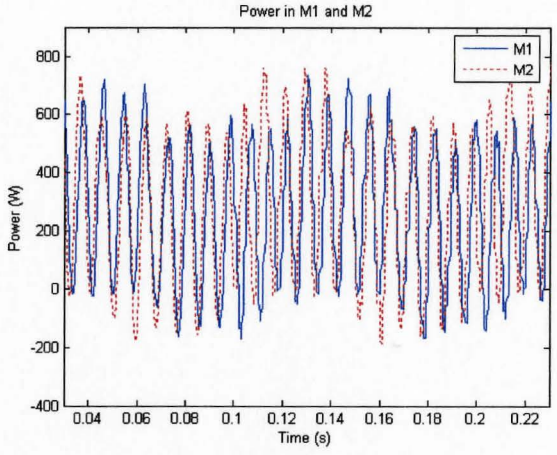

5.8(e)

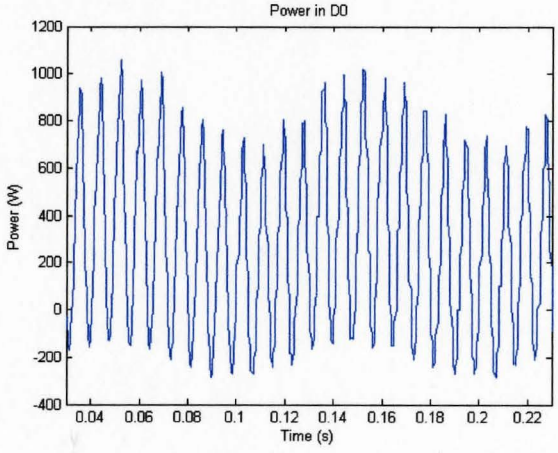

5.8(f)

Figure 5.8: *Experimental waveform comparisons between 30° and 60° phase-shifts*

As shown in Figures 5.7(a) and (d), when the "inverter-controlled" square-wave modulation voltage in G_1 was fixed in one location, while phase shifting the square-wave voltage in G_2 along the time axis, the modulated excitation currents in both generators would also be phase shifted by the same amount. Figures 5.7(b) and (e) show that when the two electrical axes are misaligned, the resulted power in M_1 and M_2 will no longer be in opposition of phase, and the power in D0 will consequently oscillate due to phase unbalance between the powers generated in the two machines. As the phase angle of misalignment increases, the magnitude of power oscillation in the driver motor would also increase (see Figures 5.7(c) and (f)). These simulated results suggest that if a *phase shifter* is used to electrically shift the "inverter-controlled" square-wave modulation voltage in one generator with respect to that of the other generator, the shaft misalignment between G_1 and G_2, in theory, would be corrected. Unfortunately, numerous experimental results could not validate such suggestion. The magnitude of power oscillation in D0 changed very slightly as the phase shift was swept from -180° to +180°. All the plots in Figure 5.8 show a typical test result in practice. Similar to the simulated results in Figures 5.7(a) and (d), the power waveforms in M_1 and M_2 got phase shifted according to the phase difference between the excited field currents in G_1 and G_2; however, the magnitude of power oscillation in D0 responded very slightly to the phase shift (see Figures 5.8(c) and (f)). This disagreement between simulation and experimental results indicates that there must be other factors with greater effect on the power oscillation in D0 than the effect caused by the axis misalignment between G_1 and G_2, and electrically correcting the phase difference caused by such misalignment is not a sufficient solution for suppressing the power oscillation in D0.

5.3 Parameter Sensitivity

As mentioned in section 5.1, it was observed in the actual experiment that the test motor M_2 reached synchronous speed well before M_1, and the magnitude of modulation voltages had to be adjusted in order to obtain symmetrical waveforms for the excitation currents in G_1 and G_2. Such experimental observation allows us to deduce that the actual machine system is far from being balanced and the values of machine parameters in M_1 are not exactly equal to those in M_2 as entered in the computer simulation. In order to

confirm property unbalance in the system, simple experiments including DC-resistance test, blocked-rotor test and no-load test were performed to approximate parameter values in each test motor. The obtained values are tabulated as follows:

Table 5.3: *Measured Parameter Values for Test Motors M_1 and M_2*

	M_1	M_2	***Difference***
R_s	0.58 Ω	0.64 Ω	10.3%
R_r	0.37 Ω	0.57 Ω	54.0%
X_{ls}	0.7 Ω	0.7 Ω	0%
X_{lr}	0.7 Ω	0.7 Ω	0%
X_m	27.72 Ω	25.89 Ω	6.71%

Since the values of X_{ls} and X_{lr} between the two machines in this test setup are equal, they will not be included in the study of parameter sensitivity here. The ones being investigated are R_s, X_m, and R_r, and the study will be conducted in the simulation by varying each of these parameters by 20% between motors M_1 and M_2, while keeping the rest of parameters in one machine equal to those in the other machine. The effects of each parameter variation will then be examined in the waveforms of excitation currents in G_1 and G_2, powers and speeds in M_1, M_2 and D0, and a general conclusion will be drawn for each finding. Since there are three machine parameters to be investigated, simulation results for three case studies will be presented in order to demonstrate the system's sensitivity to each parameter unbalance.

5.3.1 Case Study #1

In this case study, the given value of R_{s2} is greater than R_{s1} by 20%, while other parameters between the two machines are kept equal. This also means that the modulation voltages being applied to the "inverter-controlled" windings in G_1 and G_2 are equal. Note that subscripts 1 and 2 in R_s identify the test motors M_1 and M_2, respectively. As shown in the following plots of Figure 5.9, the magnitude of excitation current in G_2 is greater than that in G_1, and the power in M_2 is greater than that in M_1. Such unbalance in the value of R_s is causing the driver motor power and speed to oscillate at a frequency of 10 Hz at steady state. However, the motor speeds in M_1 and M_2 are not affected here, because Figure 5.9(d) shows that both motors reach synchronous speed simultaneously.

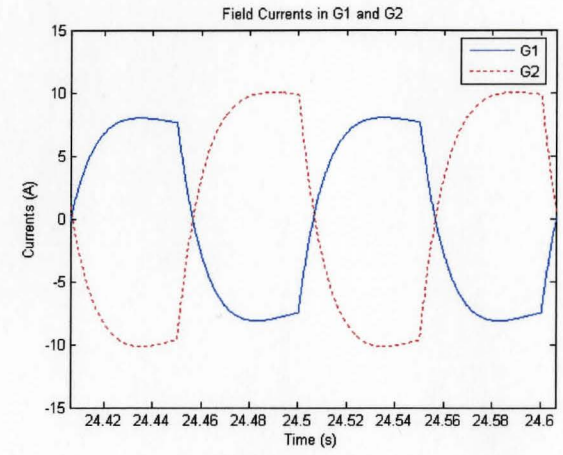

5.9(a)

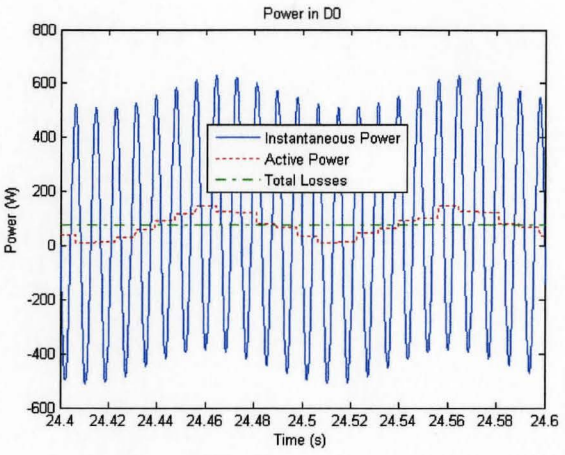

5.9(c)

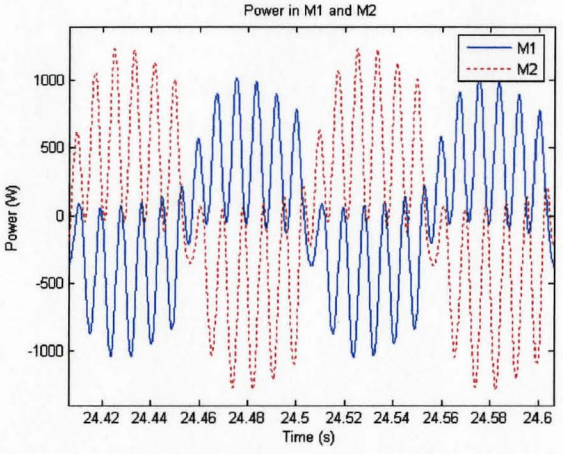

5.9(b)

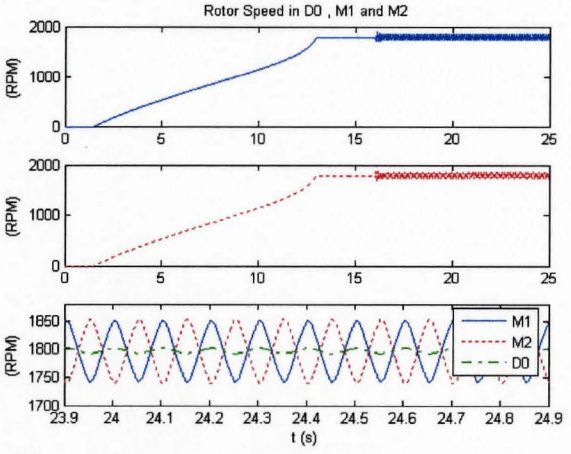

5.9(d)

Figure 5.9: *Simulated waveforms when R_{s2} is greater than R_{s1} by 20%*

5.3.2 Case Study #2

The value of X_{m2} in this case study is given to be 20% greater than X_{m1}, while other parameters between the two machines are kept equal. Similar to case study 1, the following plots in Figure 5.6 show that the excitation current in G_2 is greater than that in G_1 when the applied modulation voltages are equal between the two generators, and the power in M_2 is also greater than that in M_1. The unbalanced value of X_m in this case study is also causing a power oscillation in the driver motor at the same 10-Hz frequency as in the previous case. Comparison of waveforms between Figures 5.9(c) and 5.10(c) indicates that the oscillation amplitude is slightly larger here than that in case study 1. Unlike the case of unequal R_s, unbalanced X_m affects the order in which test motors achieve synchronous speed first. As shown in Figure 5.10(d), the test motor M_1 reaches synchronous speed well before M_2 does when the value of X_m is greater in M_2 than M_1.

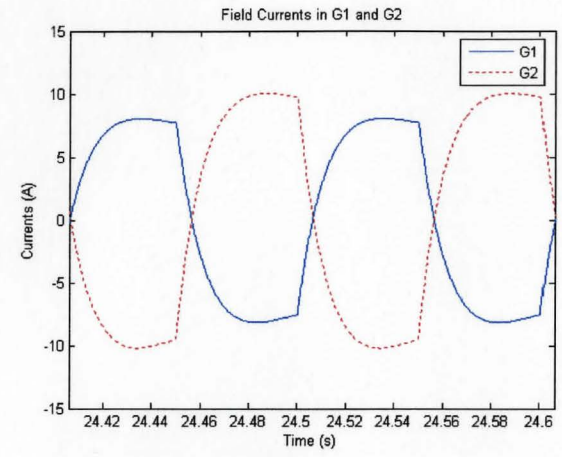

5.10(a)

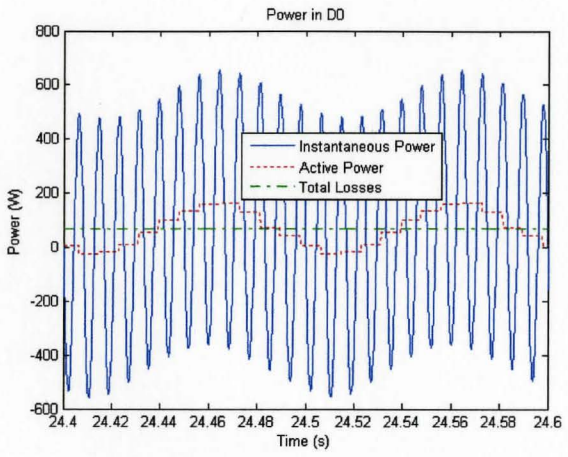

5.10(c)

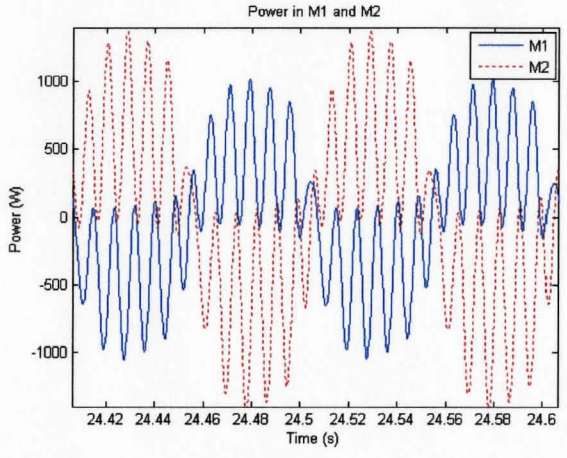

5.10(b)

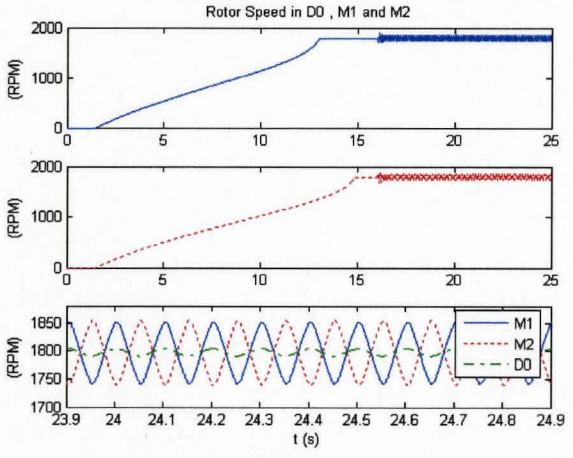

5.10(d)

Figure 5.10: *Simulated waveforms when X_{m2} is greater than X_{m1} by 20%*

5.3.3 Case Study #3

In this final case study, the value of R_{r2} is increased by 20% above R_{r1}, while other parameter values are also kept equal between the two motors. With equal modulation voltages applied to the "inverter-controlled" winding in each generator, Figures 5.11(a) and (b) show a different trend from those in Figures 5.9 and 5.10. Here, the field current in G_2 is less than that in generator G_1, and the power in M_2 is less than that in M_1. The driver motor's power is also oscillating at a frequency of 10 Hz, but with much smaller amplitude comparing to the first two case studies. Unbalanced R_r is also affecting the sequence of which test motor attains synchronous speed. Simulation result in this case shows that M_2 reaches synchronous speed earlier than M_1 (see Figure 5.11(d) below).

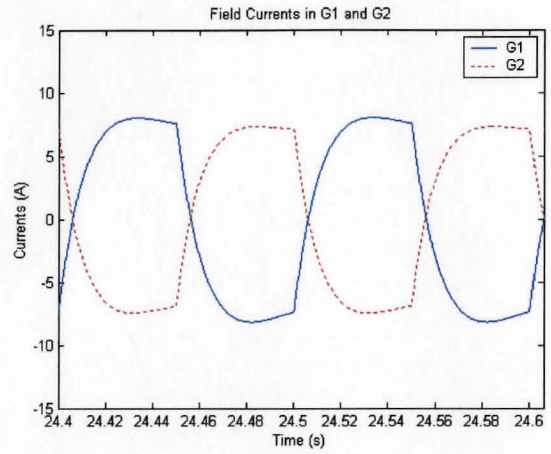

5.11(a)

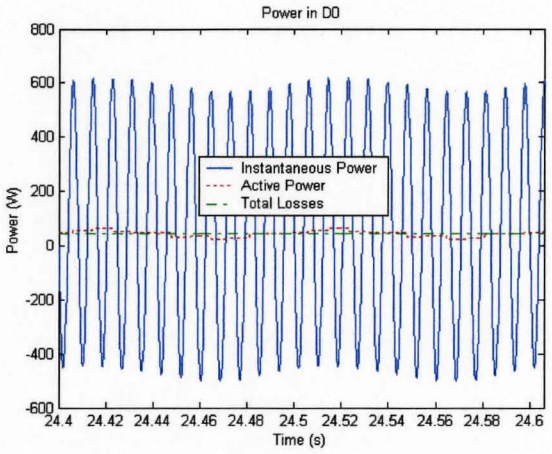

5.11(c)

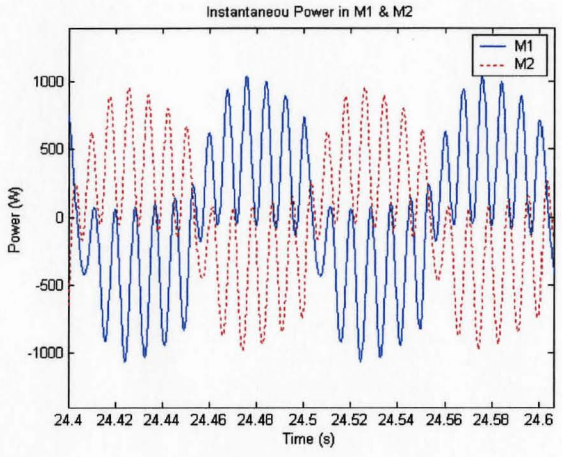

5.11(b)

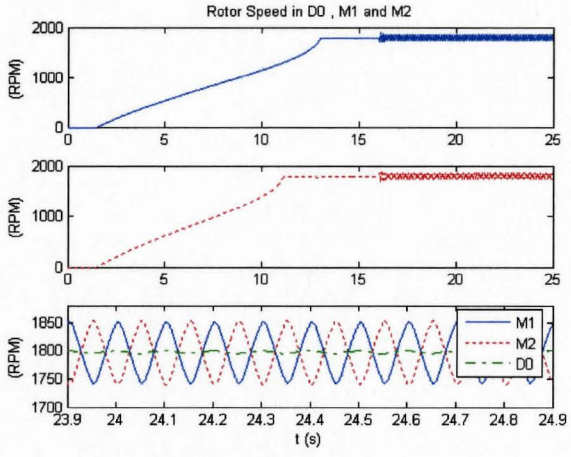

5.11(d)

Figure 5.11: *Simulated waveforms when R_{r2} is greater than R_{r1} by 20%*

5.4 System Simulation With Measured Values of Machine Parameters

After studying the effect of each parameter in the case studies, the real test setup of five interconnected machines is now simulated using the measured values of machine parameters given in Table 5.3, and their combined effects on the system are shown in Figure 5.12 on the next page.

Since the measured value of X_{m2} is less than X_{m1} by 6.71% and that of R_{r2} is 54% greater than R_{r1}, the combined effect observed in case studies 2 and 3 would cause the excitation current in generator G_2 to be less than that in G_1, and the motor speed in M_2 to reach synchronous speed before M_1. Although R_{s2} is 10.3% higher than R_{s1}, which essentially would cause the excitation current in G_2 to be greater than that in G_1 provided

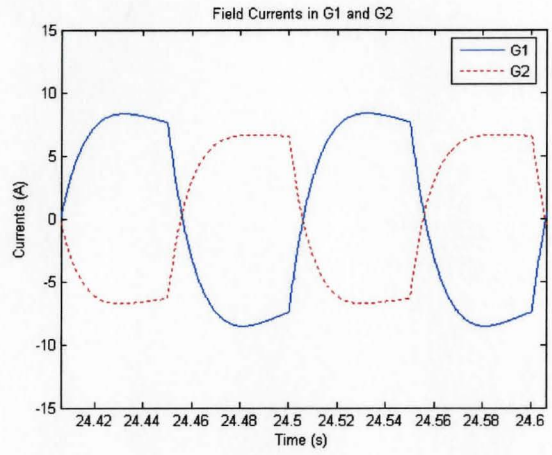

5.12(a)

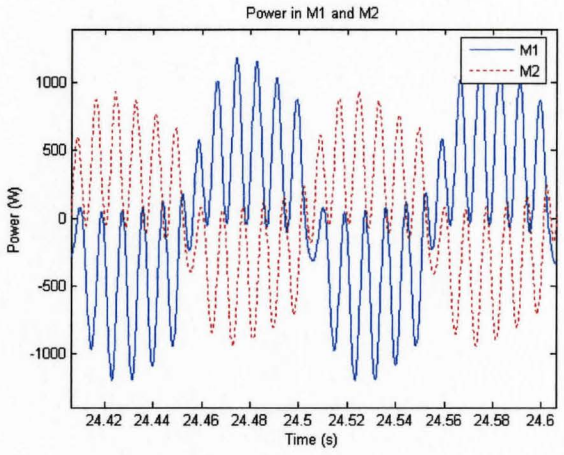

5.12(b)

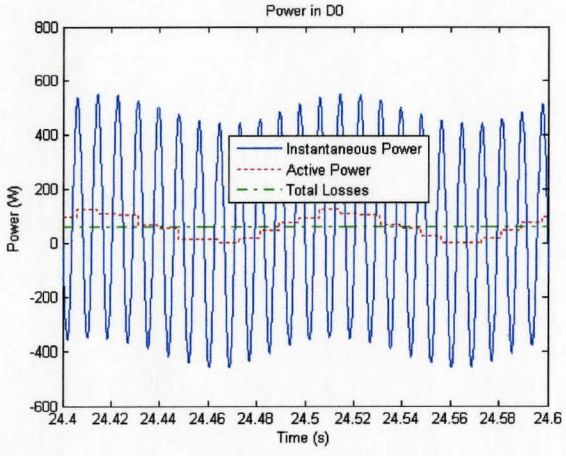

5.12(c)

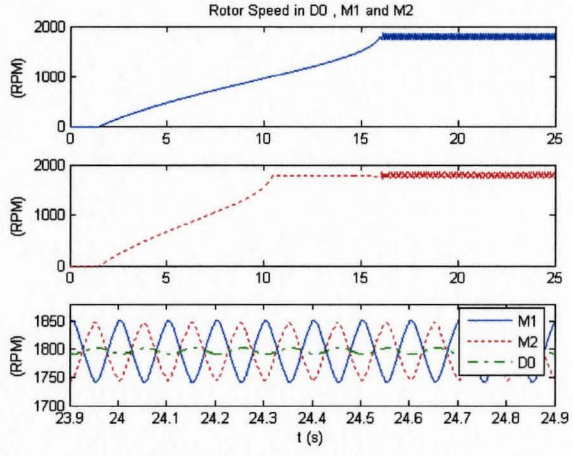

5.12(d)

Figure 5.12: *Simulated waveforms with measured parameters in the real system*

R_s is the only unbalanced parameter in the system, Figure 5.12(a) on the other hand shows that the resulted field current in G_2 remains to be less than that in G_1, indicating that the effect of unbalanced R_s in the system is not strong enough to offset the combined effect of both X_m and R_r. Consequently, as the power waveforms in M_1 and M_2 always follow the trend in excitation currents, the maximum magnitude of power in M_2 is less than that in M_1 as shown in Figure 5.12(b). As expected, the plot of motor speeds in Figure 5.12(d) shows that M_2 attains synchronous speed well before M_1, and the driver motor's power in Figure 5.12(c) is oscillating at a frequency of 10 Hz due to parameter unbalance. Thus, all the results above match perfectly with the expectation made from each case study, and the main culprit behind power oscillation in D0 in this particular system are the unbalanced values of X_m and R_r in M_1 and M_2.

5.5 Excitation Voltage Adjustment

Numerous simulations show that the power unbalance discussed in the above section can not be compensated for by adjusting the value of R_s alone between the two motors; however, it is possible to bring the system power close to being balanced by adjusting the magnitude of excitation voltage applied to the "inverter-controlled" field winding in each generator. The following plots show results of an adjusted system when

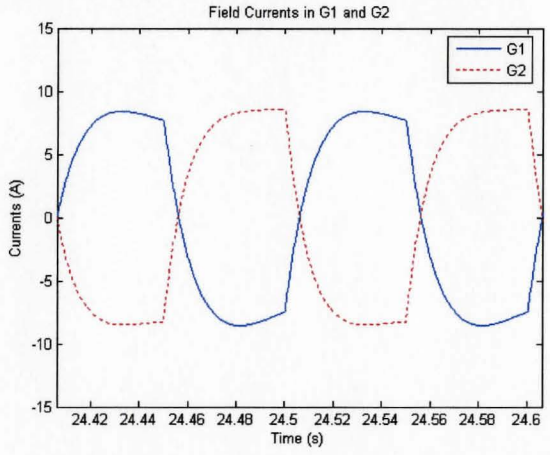

5.13(a)

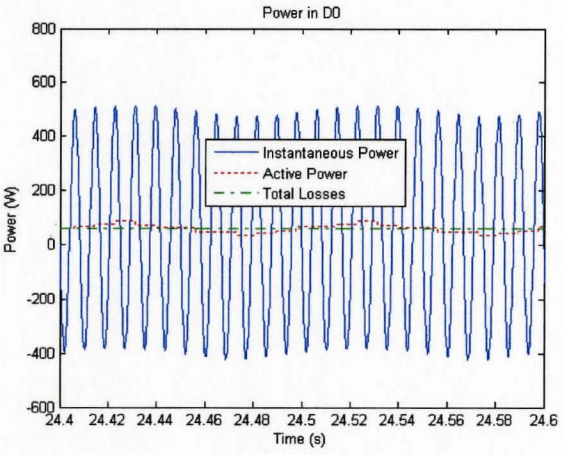

5.13(c)

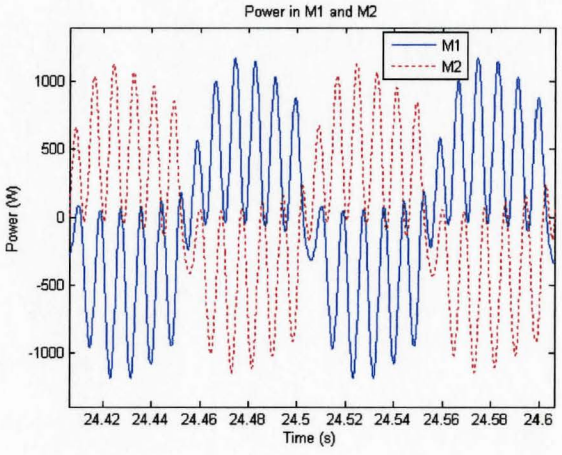

5.13(b)

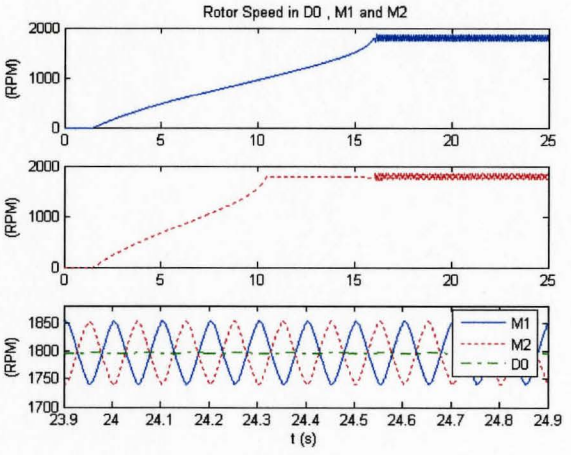

5.13(d)

Figure 5.13: *Simulated waveforms of a compensated system with modulation voltages adjusted*

the magnitude of the modulation voltage in G_2 is adjusted 25% greater than G_1. With the modulation voltages optimally fine-tuned, the waveforms of the excitation currents in Figure 5.13(a) and motor powers in Figure 5.13(b) are very close to being symmetrical,

and the power oscillation in the driver motor is almost completely eliminated (see Figure 5.13(c)). Figure 5.13(d) shows that modulation voltage adjustment has no impact on the sequence of which motor reaches synchronous speed first, because M_2 still attains synchronous speed before M_1 after the voltage adjustment is made. Note that this simulation result for the motor speeds agrees very well with the experimental observation mentioned earlier in section 5.1. Clearly, this agreement confirms that the mathematical model created in this research is a reliable one because it can closely represent the actual test setup in real life. Figure 5.14 below illustrates the difference in the driver motor's

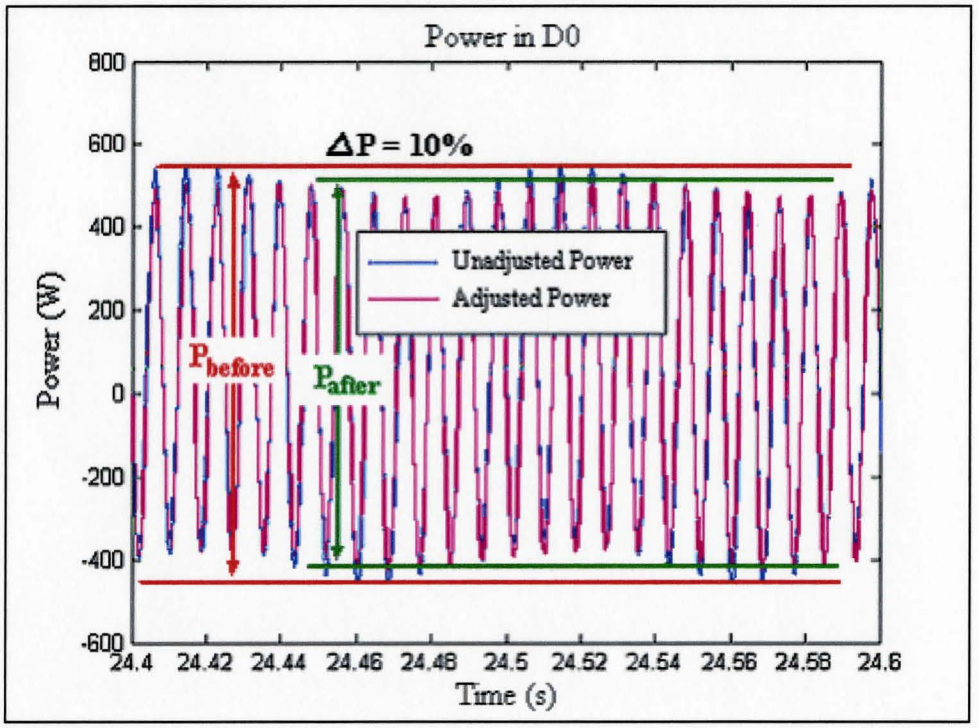

Figure 5.14: *Driver motor's power before and after modulation voltage adjustment*

power before and after the adjustment of modulation voltages was made. Clearly, the peak-to-peak amplitude of the adjusted power waveform in D0 is smaller than that of the unadjusted power by 10%. Thus, the most suitable variable for controlling power ripple in the driver motor is the magnitude of modulation voltages in G_1 and G_2.

In order to investigate how long it would take the driver motor's power to respond to the excitation voltage adjustment, a simulated plot is given in Figure 5.15 on the next page to show what happens to the driver motor's power at the instant the excitation voltages between the two generators are adjusted.

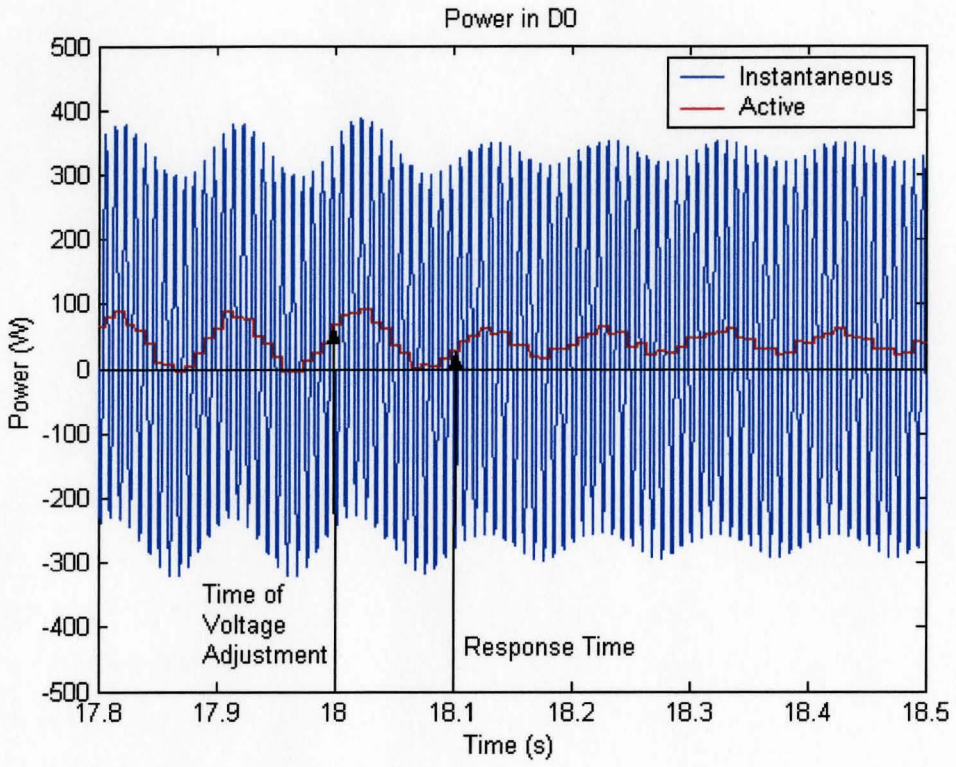

Figure 5.15: *Response time of the power in D0 due to excitation voltage adjustment*

As illustrated in the simulated plot above, the excitation voltages between the two generators are adjusted at time t = 18 second, and the response to this adjustment does not take place until t = 18.1 second, where both the active and instantaneous power waveforms in the driver motor D0 begin to settle down to smaller amplitude of oscillation. Clearly, the delay to excitation voltage adjustment here is only 0.1 second or one cycle of 10 Hz.

5.6 Discussion

The work presented in this chapter shows that the second and third research objectives outlined in chapter 1 have both been met. Case studies for machine parameter sensitivity have pointed out that the culprit behind power oscillation in the "driver" motor D0 is the unbalance of machine parameters of the two induction motors under test. As a result, the phase shift correction method showed very little improvement in reducing the power swing in D0 because the effect of parameter unbalance between the two induction motors is much greater than the effect of axis misalignment between generators G_1 and

G_2. A more effective method of minimizing power swing in the "driver" motor is by adjusting the excitation voltages applied to the direct-axis windings of the two generators. This voltage adjustment helps make the waveforms of excitation currents much more symmetrical to each other.

The simulation results for motor speeds in each case study were shown only for the purpose of demonstrating the degree of unbalance between the two machine systems in the test setup. The fact that motor M_1 reached synchronous speed before M_2 or the reverse is not relevant to the main point at all, because it only shows transient behaviors of the two induction motors under test when their machine parameters are unbalanced. What really important here are the motors' behaviors during steady state. Therefore, it is the speed oscillation in D0 at steady state that is important because it leads to power oscillation in the motor. This speed oscillation is caused by the steady-state speed mismatch between the test motors M_1 and M_2, which in turns is caused by the unbalance of their machine parameters.

Chapter 6

CONCLUSIONS AND RECOMMENDATIONS FOR FURTHER RESEARCH

6.1 Conclusions

The investigative work conducted in this research revealed that the cause of power oscillation in the "driver" motor D0 mainly originated from the unbalance of machine parameters of the two induction motors under test in the new phase modulation method. As shown in the case studies for parameter sensitivity, the unbalance in one machine parameter may cause a different effect on the power oscillation in D0 than the unbalance in another machine parameter. In this particular setup for the test system, the combined effect of unbalanced rotor resistance R_r and magnetizing inductance X_m on the power oscillation is much stronger than the effect of an unbalanced stator resistance R_s. Thus, the degree and combination of parameter unbalance dictates the magnitude of power swing between the test system and the utility source.

Due to the presence of parameter unbalance between the two induction motors, the phase shift correction method showed very little effect on suppressing power oscillation in the "driver" motor. This is because the effect of parameter unbalance is much greater than the effect of misalignment of electrical axes between generators G_1 and G_2. According to the simulation results, the phase shift correction method works effectively under a condition that the degree of parameter unbalance is minimal. This is especially true if the machine parameters in induction motors M_1 and M_2 are balanced. Unfortunately, this is rarely the case in real life because it is impossible to build two equally-rated induction machines with machine parameters of equal values. That is, there is always a certain degree of difference between the values of rotor resistance, rotor leakage inductance, stator resistance, stator leakage inductance, and magnetizing inductance in the two machines. As a result, the phase shift correction method is not a very practical way of minimizing power swing in the "driver" motor.

Since the unbalance of machine parameters is due to inherent properties in each induction motor under test, it is not possible to eliminate the power ripple in the "driver" motor completely. However, both simulation and experimental results agreed that the

most effective method of reducing this power ripple is by adjusting the magnitude of excitation voltage applied to the direct-axis rotor winding in one generator with respect to the magnitude of excitation voltage applied to the other generator until the modulated excitation currents in both generators are symmetrical to one another in their final waveforms. From this finding, one can conclude that the most suitable parameters for suppressing power oscillation in the "driver" motor are the magnitudes of excitation voltages applied to generators G_1 and G_2. These two parameters are equal only in an ideal condition where the machine parameters in motors M_1 and M_2 in the test system are equal.

Although the problem of power oscillation in the "driver" motor could not be completely resolved, the following contributions were made in this thesis research:

1. Discovered that the unbalance of machine parameters in the two induction machines under test is the main cause of power oscillation between the utility source and the test system for the new phase modulation method.
2. Developed a reliable and easy mathematical model to study the behaviors of individual machines in the test system under various operating conditions.
3. Built control hardware components to implement the new phase modulation method for synthetic loading of induction machines, and set up machines and equipments for the test system to verify the analysis from the simulation results.

6.2 Recommendations For Further Research

The method of suppressing power oscillation in the machine system created for the new phase modulation method can be improved with the following recommendations for further research:

- Introduce external resistance and inductance to each phase winding on the stator of the test motor in order to compensate for machine time constants. Each resistance and inductance should be made variable and should be connected in series with each stator winding of the induction motor. This scheme is feasible because single phase potentiometer and variable inductance are readily available off the shelf. They can also be custom built to meet the power requirement in the machine system. If this

method is successful, power loss in these external components should be taken into consideration in order to reflect the actual power loss of the test motor.

- Study the effect of the shape of excitation currents on the speed of each induction motor under test as well as the power exchange between the two parallel systems in the current test setup. If a sinusoidal modulation voltage is applied to both the quadrature-axis and direct-axis rotor windings in each generator, the resultant excitation flux is expected to have a constant magnitude with a smooth change in phase angle, which in turn will allow the generated supply frequency to vary evenly, enabling the speed of the test motor being fed by this supply to change smoothly. Applying this sinusoidal modulation voltage with opposite phase to the two parallel systems would allow a smoother power exchange and ultimately lead to smaller power oscillation in the "driver" motor. The challenge of applying such ideal modulation is to build two controlled sinusoidal voltage sources to supply the direct-axis and quadrature-axis rotor windings of each generator. This can be difficult to implement especially since large inductive values are present in the rotor field windings.

- Design a feedback controller to adjust the magnitude of excitation currents between the two parallel systems so that power ripple in the "driver" motor is minimized. As shown in Figure 5.11, when a step change was applied to the excitation voltage in one system, the system responded with a delay of only one 10-Hz cycle, proving that the system can be controlled. Thus, the controller should first be incorporated into the computer model, which has already been created in this thesis research, so that its performance can be evaluated in the simulation before deciding the feasibility of implementing it in practice.

REFERENCES

[1] A. Mihalcea, "*Equivallent Loading Methods for Determining Total Power Loss in Induction Motors*", Master's thesis, September 1999.

[2] A. E. Fitzerald, C. Kingsley and S. D. Umans, "*Electric Machinery*", 4th edition, McGraw-Hill Book Company, 1983.

[3] J. C. Andreas, "*Efficient Electric Motors*", Marcel Decker Inc. New York, 1982.

[4] J. H. Dymond, C. N. Glew and D. H. Plevin, "*Equivalent Load Test for Induction Machines – The Forward Short Circuit Test*", IEEE Transactions on Energy Conversion, Vol. 14, Issue 3, pp. 419-425, Sept. 1999.

[5] J. Hoolboom, J. Soltani and B. Szabados, "*A New Synthetic Loading for Large Induction Machines With No Feedback Into the Power System*", IEEE Transactions on Energy Conversion, Vol. 17, Issue 3, pp. 319-324, Sept. 2002.

[6] H. W. Lorenzen and A. Meyer, "*Two-Frequency Heat Run – A Method of Examination for Three-Phase Induction Motors*", IEEE Transactions on Power App. Syst., Vol. PAS-98, Issue 6, pp. 2338-2347, Nov./Dec. 1979.

[7] M. P. Romeira, "*The Superimposed Frequency for Induction Motors*", Proceedings IEEE, Vol. 36, pp. 952–953, 1948.

[8] W. Fong, "*New Temperature Test for Polyphase Induction Motors by Phantom Loading*", Proceedings IEEE, Vol. 119, Issue 7, pp.883-887, July 1972.

[9] J. Hoolboom, J. Soltani and B. Szabados, "*A New Synthetic Loading of Induction Machines Based on Phase Modulation*", in Proc. INDUSCON Conf., Porto-Alegre,. Brazil, pp. 7-11, Nov. 2000.

[10] J. Hoolboom, A. Mihalcea and B. Szabados, "*Determining Total Losses and Temperature Rise in Induction Motors Using Equivalent Loading Methods*", IEEE Transactions on Energy Conversion, Vol. 16, Issue 3, pp. 214-219, Sept. 2001.

[11] C. G. Veinott, *"Theory and Design of Small Induction Motors"*, New York: McGraw-Hill, 1959.

[12] P. C. Krause, "*Analysis of Electric Machinery*", New York: McGraw-Hill, 1986.

[13] R. H. Park, *"Two-Reaction Theory of Synchronous Machines – Generalized Method of Analysis – Part I"*, AIEE Trans., Vol. 48, July 1929, pp. 716-727.

[14] D. S. Brereton, D. G. Lewis and C. G. Young, *"Representation of Induction Motor Loads During Power System Stability Studies"*, AIEE Trans., Vol. 76, August 1957, pp. 451-461.

[15] G. Kron, *"Equivalent Circuits of Electric Machinery"*, John Wiley & Sons, Inc., New York, N. Y., 1951.

[16] J. R. Dormand, "*Numerical Methods for Differential Equations: A Computational Approach*", Florida: CRC Press, Inc., 1996.

[17] Lab-Volt Datasheet. "*The 2-kW Electromechanical Training System, Model 8013"*. Lab-Volt Systems, Inc. 2005. Retrieved October 11, 2006 from http://www1.labvolt.com/publications/Datasheets/Current2/dsa8013.pdf

[18] G. Ledwich, (1998). "*Inverter Basics*". Power Designers, 2004. Retrieved September 14, 2006 from http://www.powerdesigners.com/InfoWeb/design_center/articles/Inverters/inverters.shtm

[19] S. Lee, (June 1995). "*How to Select a Heat Sink*". ElectronicsCooling Online, 2006. Retrieved January 11, 2006 from http://www.electronics-cooling.com/Resources/EC_Articles/JUN95/jun95_01.htm

[20] Application Note 559 (February 1996). "*Tech Brief 3: Digitally Control Phase Shift*". Dallas Semiconductor: Maxim Integrated Products, 2005. Retrived February 14, 2006 from http://pdfserv.maxim-ic.com/en/an/AN559.pdf

[21] R. C. Jaeger, "*Microelectronic Circuit Design*", New York: McGraw-Hill Companies, Inc., 1997.

[22] Datasheet 5968-8152EN (May 2004). "*Agilent Technologies 54600 Oscilloscopes* ", Agilent Technologies Inc., 2004. Retrieved August 30, 2006 from http://cp.literature.agilent.com/litweb/pdf/5968-8152EN.pdf

[23] Datasheet 5968-8153EN (February 2003). "*Agilent Technologies 54600-Series Oscilloscope Probes and Accessories Selection Guide Data Sheet*", Agilent Technologies Inc., 2003. Retrieved August 30, 2006 from http://cp.literature.agilent.com/litweb/pdf/5968-8153EN.pdf

[24] B. Adkins, *"Theory of Electrical Machine"*, London: Chapman and Hall, 1957.

[25] R. T. H. Alden (December 1999), "*The Electric Machines Laboratory: Poly-phase Induction Motors",* Lab Instruction Manual. McMaster University, 1999. Retrieved October 15, 2006 from http://power.mcmaster.ca/szabados/courses/3pi4/labs/pim.pdf

[26] E. Levi, *"Polyphase Motors: A Direct Approach to Their Design"*, New York, N. Y.: Wiley, 1984.

[27] Anixter Wire & Cable Handbook, "*Electrical Characteristics*", Anixter Inc., 1996. Retrieved October 20, 2006 from http://www.anixter.com/./AXECOM/AXEDocLib.nsf/(UnID)/7B02465D0630940680256F250068807D/$file/WCTHContentsElectricalCharactersitics.pdf

[28] P. L. Alger, *"Induction Machines, Their Behaviors and Uses"*, New York: Gordon and Breach, 1970.

[29] *"IEEE Standard Test Procedures for Polyphase Induction Motors and Generators"*, IEEE Std. 112 – 1978, IEEE, Inc., New York, N. Y.

[30] C. I. Hubert, *"Electric Machines: Theory, Operation, Application, Adjustment, and Control"*, New Jersey: Prentice Hall, 2002